



INSTITUTO DE BIOINGENIERÍA

Departamento de Ciencia de Materiales, Óptica y Tecnología Electrónica

Biomateriales porosos de hidroxapatito y compuestos de HA/TCP/colágeno para regeneración ósea: obtención, caracterización y estudios experimentales in vivo.

Memoria presentada por:
José Eduardo Maté Sánchez de Val

Programa de Doctorado en Bioingeniería.

Directores:
Dra. Piedad N. De Aza Moya.
Dra. Patricia Mazón Canales.

TESIS DOCTORAL
2016



PIEDAD NIEVES DE AZA MOYA, Catedrática de Universidad de Ciencia de Materiales e Ingeniería Metalúrgica de la Universidad Miguel Hernández de Elche, y

PATRICIA MAZÓN CANALES, Profesora Contratada doctor de Ciencia de Materiales e Ingeniería Metalúrgica de la Universidad Miguel Hernández de Elche.

HACEMOS CONSTAR,

Que el presente trabajo ha sido realizado bajo nuestra dirección y recoge fielmente la labor realizada por Don José Eduardo Maté Sánchez de Val, Licenciado en Odontología, para optar al grado de Doctor. Las investigaciones reflejadas en esta Tesis se han desarrollado en la Unidad de Biomateriales del Instituto de Bioingeniería, así como en el Área de Ciencia de Materiales e Ingeniería Metalúrgica del Departamento de Ciencia de Materiales, Óptica y Tecnología Electrónica de la Universidad Miguel Hernández de Elche. La implantación en animales se ha realizado en el animalario de la Universidad de Murcia.

Esta Tesis Doctoral se enmarca dentro del siguiente proyecto

- CICYT MAT2013-48426-C2-2-R “Biomateriales cerámicos multifuncionales con estructuras jerarquizadas para regeneración ósea y/o liberación controlada de agentes bioactivos”

Así mismo, el alumno ha realizado una estancia de investigación de tres meses en la Universidad de Stony Brook, NY (EEUU), en la escuela de Medicina Dental, para la obtención de la Mención Europea en el Título de Doctor.

Fdo. Piedad N de Aza Moya
Noviembre 2015

Fdo. Patricia Mazón Canales



Eugenio Vilanova Gisbert
Director

*Avda. de la Universidad s/n, edificio Vinalopó
03202 Elche (Alicante)*

*Tel: 96 6658711 - Fax: 96 6658511
e-mail: evilanova@umh.es*

D. Eugenio Vilanova Gisbert, Director del Instituto de Bioingeniería de la Universidad Miguel Hernández:

HACE CONSTAR:

Que da su conformidad a la lectura de la tesis doctoral presentada por Don Jose Luis Calvo Guirado, titulada **“BIOMATERIALES POROSOS DE HIDROXIAPATITO Y COMPUESTOS DE HA/TCP/COLÁGENO PARA REGENERACIÓN ÓSEA: OBTENCIÓN, CARACTERIZACIÓN Y ESTUDIOS EXPERIMENTALES IN VIVO.”**, la cual ha sido desarrollada dentro del Programa de Doctorado en Bioingeniería en este Instituto, bajo la inmediata dirección y supervisión de las Dras. Piedad N. de Aza Moya y Patricia Mazón Canales.

Para que conste y surta los efectos oportunos, firma el presente certificado en Elche, a de diciembre de 2015.

PREFACIO

Este documento se ha elaborado siguiendo la normativa de la Universidad Miguel Hernández para la “Presentación de Tesis Doctorales con un conjunto de publicaciones”, y se ha dividido en las siguientes partes:

1. **Introducción**, en la que se presenta el tema de la Tesis, los antecedentes del trabajo realizado, y se defienden los objetivos perseguidos
2. **Resumen**, donde se presentan los resultados más relevantes obtenidos.
3. **Conclusiones**, finales derivadas del estudio.
4. **Anexo I**, que contiene los artículos publicados antes del depósito de la Tesis:

- Maté Sánchez de Val JE, Calvo-Guirado JL, Gómez- Moreno G, Pérez-Albacete Martínez C, Mazón P , De Aza PN. Influence of hydroxyapatite granule size, porosity and crystallinity on tissue reaction in vivo. Part A: synthesis, characterization of the materials and SEM analysis. Clin Oral Implan Res. 2015. DOI: 10.1111/clr.12722. Factor de impacto: 3.889 Puesto que ocupa / N° de revistas en el Área de conocimiento de Dentistry, Oral Surgery & Medicine 3/87.
- Maté Sánchez de Val JE, Mazón P, Calvo Guirado JL, Delgado Ruiz RA, Ramírez Fernández MP, Negri B, Abboud M, De Aza PN. Comparison of three hydroxyapatite/b-tricalcium phosphate/collagen ceramic scaffolds: An in vivo study. J Biomed Mater Res Part A 2014;102A:1037–1046. Factor de Impacto: 3.369. Puesto que ocupa / N° de revistas en el Área de conocimiento de Engineering, Biomedical. 13 /76

- Mate Sanchez de Val JE, Calvo Guirado JL, Ramirez Fernandez MP, Delgado Ruiz RA, Mazon P, De Aza PN. 2015. In vivo behavior of hydroxyapatite/ β -TCP/collagen scaffold in animal model. Histological, histomorphometrical, radiological, and SEM analysis at 15, 30, and 60 days. Clin. Oral Impl. Res. DOI: 10.1111/clr.12656. Factor de impacto: 3.889. Puesto que ocupa / N^o de revistas en el Área de conocimiento de Dentistry, Oral Surgery & Medicine 3/87

Parte de esta tesis se realizó durante una estancia de investigación en la Universidad de Stony Brook Nueva York, USA en el Departamento de Medicina Oral, lo cual posibilita la obtención de la Mención Internacional en el Título de Doctor al que se opta.

La presente memoria de tesis cumple los requisitos necesarios para la obtención de la Mención Internacional en el Título de Doctor establecidos en la normativa de enseñanzas oficiales de postgrado de la Universidad Miguel Hernández, y el Real Decreto RD1393/2007.

AGRADECIMIENTOS

A mis padres por su esfuerzo y darme todo lo necesario para poder llegar hasta aquí.
Por ser un ejemplo a seguir.

A mis hermanos por su apoyo incondicional.

A mi mujer, por soportar todas las horas que dedico a la investigación y que siempre respeta.

A mis compañeros de aventuras, *Dra. Piedad Ramírez, Dr. Carlos Pérez*; con ellos empezamos hace casi diez años y tiene visos de seguir.

A mi jefe y amigo *Dr. José Luis Calvo Guirado*, por darnos la oportunidad de trabajar a su lado y motivarnos día a día para llegar aquí. Acabamos de empezar.

A mis directoras de Tesis, *Dra. Piedad de Aza*, cuya dedicación y constancia sirven de ejemplo para cualquier investigador. *Dra. Patricia Mazón*, por su apoyo y guía.

CONTENIDOS	Páginas/ pages.
Chapter 1: Introduction	8-15
Chapter 2: Objectives / Objetivos	16-18
Chapter 3: Abstract / Resumen	19-24
Chapter 4: Materials and methods	25-35
Chapter 5: Results	36-57
Chapter 6: Discussion	58-69
Chapter 7: Conclusions / Conclusiones	70-72
Chapter 8: References	73-85
Chapter 9: Appendix I: Published papers	85
Chapter 10: Appendix II: Congress contribution	86



INTRODUCTION

1. INTRODUCTION

For decades, bone replacement materials have been used in maxillofacial surgery for filling the defects, even when the bone surface is inadequate (Daculsi et al. 2003). The most common biomaterials in use are calcium phosphate-based (Ca-P) bioceramics, which offer a composition and structure similar to the mineral phase of bone and are osteoconductive. Among the range of materials tested in recent years, tricalcium phosphate (TCP) has shown promising results in tissue cultures, animal experiments, and clinical studies (Krekmanov 2006; Calvo et al. 2012; Yang et al. 2001).

A bone substitute material should have “bimodal” behavior, which, in the early stages of differentiation, allows osteoblasts to build bridges between different sizes of grain and integrate with other osteoblasts, supporting both proliferation and differentiation. New bone formation will be stimulated by the activation of mesenchymal stem cells and their absorption into surfaces with nano-scale topographic features (Fan et al. 2007). The ultimate goal is the union of fully differentiated osteoblasts that will support bone matrix production. This requires a porous structure with nanopores, micropores, and macropores, all involved in different stages of absorption, adhesion, and bone material deposition on and within the bone substitute material (Gauthier et al. 1999).

The presence of calcium phosphate in the bone replacement material favors initial regeneration of the bone defect. Regeneration begins with the deposition of connective tissue from the defect margins, which then reaches maturation through fixing host bone minerals therein until autogenous bone consolidation is achieved.

A biomaterial must be fully compatible with the host environment and must not provoke abnormal inflammatory responses, which could be accompanied by the absence of disordered bone formation or by osteoid formation or by cicatricial connective tissue.

Commercial HA and β -TCP have been tested for their suitability as bone substitute materials in clinical situations (Ogose et al. 2006). Radiologic evaluations have revealed satisfactory osteoconductive qualities for both materials in clinical trials of implants in humans (Le Geros et al. 2003). Ceramics of higher porosity and so lower density provide more surface area for vascularization and bony ingrowth. Furthermore, the regular and uniform surface morphologies of HA and β -TCP facilitate cell proliferation and differentiation (Yuasa et al. 2005). When the ceramics are implanted into healthy bone, osteoids are produced on the biomaterial surfaces in the absence of a soft tissue interface (Giannoudis et al. 2005). In this way, HA and β -TCP act as osteoconductive scaffolds, providing a favorable environment for bone cells. (Rawlings 1993; Spector 1994; Schmitz et al. 1999; Mate et al. 2014). Moreover, synthetic ceramics need to be biodegradable in order to support the inflammation-free formation of new tissue, but HA undergoes only minimal bio-degradation (Kim et al. 2009).

Today, there are several types of commercially available calcium phosphate products for bone regeneration applications, including HA, β -TCP, and biphasic calcium phosphates (TCP/HA). With a similar composition to bone, HA ($\text{Ca}_{10}(\text{PO}_4)_6(\text{OH})_2$) is one of the most widely used chemistries for bioactive materials (Ginebra et al. 2006). Due to its ability to promote osteoconduction, the presence of HA could enhance long-term performance of orthopedic implants. The combination of hydroxyapatite with tricalcium phosphate type B gets an ideal

regeneration process material, with “bimodal” behavior; hydroxyapatite acts as a matrix for cell colonization and improves the mechanical properties of the material, with a long resorption times. Furthermore, the β -TCP act in the early stages of remodeling of the biomaterial, before being reabsorbed, and creating the ideal environment for the start of new bone medium (Mac-Millan et al. 2014). The ultimate goal was the union of fully differentiated osteoblasts that will support bone matrix production. This requires a porous structure with nanopores, micropores, and macropores, all involved in different stages of absorption, adhesion, and bone material deposition on and between the bone substitute material (Gauthier et al. 1999; Rivera-Munoz et al. 2001). Initial regeneration of the bone defect is favored by the presence of calcium phosphate in the bone replacement material (Baksh et al. 1998).

Bone substitutes based on calcium phosphates have differing physicochemical properties related to mechanical stability. They also undergo rapid degradation and have a volume instability, which does not allow new bone formation to retain the original volume (Wiltfang et al. 2002; Broggin et al. 2014).

Main advantages of using synthetic materials derived from the combination of β -TCP and hydroxyapatite are the absence of morbidity produced by obtaining autologous grafts, chemical similarity with the receiving medium and that it is fully compatible material that does not produce any anomalous inflammatory reaction during the regeneration process. Among the inconveniences, there is a lack of scientific basis related to the convergence of mechanical and physical properties between the biomaterial and the receiving area of the

graft; besides the lack of organic content in the formulation of HA/ β -TCP, which would get better adaptation to host bone (Fan et al. 2007; Dorozhkin 2009).

The use of biphasic calcium phosphates (BCP) is promising as conceptually it could overcome the disadvantages of single-phase ceramics by combining two or more ceramic phases. BCP ceramics offer controlled bioactivity and balanced biodegradation. They are osteoconductive and offer the possibility of acquiring osteoinductive properties. The conventional synthetic porous Ca-P ceramics have been composed of microscale grain size, but recent studies have focused on producing bioceramics at the nanoscale. Nano-HA can promote osteoblast cell activity and facilitate osteointegration better than microcrystalline HA and so enhance new bone tissue formation. However, the superiority of biological calcified tissues is also due to the presence of bioorganic polymers (proteins, mainly collagen type I), which give strength and partial elasticity. Therefore, the development of organic/inorganic hybrid BCP scaffolds could provide excellent possibilities for optimizing conventional bone substitutes (Huang et al. 2012; Mate-Sanchez de Val et al. 2014a,b).

The incorporation of collagen during a biphasic ceramic synthesis is a suitable option to provide the organic part of the biomaterial, solving one of the main disadvantages of the completely inorganic ceramic. This addition of collagen improves the ability of cell attachment to the biomaterial and the beginning of the process of bone remodeling. There are various studies of BCP with different weight % in the literature but little of this research has been applied clinically. This is due to the controversy in the literature concerning the optimum weight % composition, and the ideal weight % composition of BCP for clinical application remains unclear. Furthermore, research has failed to confirm the beneficial

effects of collagen coating on composite BCP scaffolds (Zheng et al. 2011; Mate-Sanchez de Val et al. 2014b).

The reconstruction of bone defects with synthetic bone substitutes requires their adaptation to the size and the location of the defects. Changes in the physicochemical properties of bone substitute materials, i.e., porosity, shape and size, are described as influencing the outcome of new bone formation and bone regeneration (Hulbert et al. 1972) and even promoting osteoinductive properties (Habibovic & de Groot 2007; Habibovic et al. 2008; Carvalho et al. 2007).

Over the years, several modifications on parameters such as sintering temperature, pH and purity of the starting products have given rise to calcium phosphates with distinct chemical and physical characteristics such as specific surface areas, surface energy, surface charge, roughness, grain size and porosity (Gauthier et al. 1999; Le Nihouannen et al. 2007; Hing et al. 2007; LeGeros et al. 2003; Julien et al. 2007). There is widespread evidence the influence of grain size in the process of integration and regeneration of biomaterials for bone regeneration. This size directly affects the absorption patterns of the materials used as well as the possibility of improving the mechanical properties of materials. Knowledge of appropriate grain size for each clinical situation and the use of treatment options to help achieve better end results in regenerative therapies.

The ability of a scaffold to enhance osteogenic signal expression and support new bone formation is largely dependent on the pore size and porosity of the scaffold. Porosity refers to the overall percentage of void space within a solid, while pore size reflects the diameter of

individual voids in the scaffold (Karageorgiou & Kaplan 2005; Mistry & Mikos 2005; Murphy et al. 2010).

The importance of scaffold porosity and pore size can be attributed to the native structure of bone which itself is a porous tissue. Cortical bone is largely a dense structure, but within it exists pores that give an overall porosity of 10% (Kim et al. 2009). Conversely, trabecular bone is a highly porous structure with typical porosity values between 50 and 90%. Porous regions of cortical bone allow for vascularization and cellular infiltration of the structure. Porosity and pore size have significant ramifications on the ability of tissue engineering scaffolds to support bone regeneration for several reasons. First, porosity and pore size have been shown to affect cell attachment efficiency which consequently impacts the cell seeding density, cell distribution and cell migration (Hollister et al. 2002; Klenke et al. 2008).

These factors have been shown to affect osteogenic differentiation through changes in signaling distances (Byrne et al. 2008). Moreover, pore size and porosity have a significant effect on the mechanical strength of a scaffold. Sufficient scaffold strength to provide mechanical support to a defect is often required of a hard tissue engineering scaffold such as bone, especially when the bone is load bearing (Kasten et al. 2008). Furthermore, porosity and pore size affect the ability of the scaffold to promote in vivo osteoconduction and vascularization. Integration of native tissue into a scaffold is fostered through growth into interconnected pores, thus both optimal and minimal pore sizes have been established to support tissue ingrowth (Karageorgiou & Kaplan 2005; Betz et al. 2010).

Finally, pore size and porosity affect in vivo and in vitro cell signaling which in turn affects osteoblastic differentiation of MSCs and the production of extracellular matrix (ECM) proteins (Yang et al. 2001). It has been established that pore sizes of at least 40 μm are required for minimal bone in growth while pore sizes of 100-350 μm are considered optimal (Moyle et al. 1973). In a study analyzing the effect of pore size and porosity on bone healing in a critical size rat cranial defect, it was shown that smaller pore sizes (100 μm) induce greater amounts of bone healing than larger pore sizes (500 μm) (Petrie Aronin et al. 2009). This study also found a link to porosity, scaffold swelling, and degradation. In this work, highly porous HA samples are subjected to an in vivo evaluation to evaluate bone recolonization and the efficiency of the mean pore and crystallinity in a new elaborated HA scaffold ceramic using polyurethane sponges as a template.



OBJETIVOS

OBJECTIVES

2. OBJECTIVES

One of the most important challenges of the XXI century in biomedicine is to obtain materials capable of stimulating the regeneration and repair of injured tissues in order to restore their function. To apply the tissue engineering to bone tissue regeneration requires a new generation of multifunctional materials that act temporarily supporting and encouraging adherence, differentiation and colonization of osteoprogenitor cells.

The aim of the Doctoral Thesis is the design, preparation, characterization and in Vivo test of materials, in the form of granules or scaffolds with high interconnected macroporosity, with controlled degradability to improve osteoinductive and / or angiogenic capacity. It is propose the design and synthesis of new biodegradable implant compositions, as well as the manufacture of hierarchical structures (granules or scaffolding) with the right features. The formulation of crystalline materials (single-phase or multiphase) will be based on the phase equilibrium diagram P_2O_5 -CaO. Such materials will be evaluated as bone substitutes. The research was conducted by clinical, histological and histomorphometric examination in various stages of time after implantation.

Materials analyzed were:

- Pure Hydroxyapatite (HA= $Ca_{10}(PO_4)_6(OH)_2$).
- Hydroxyapatite composites with different weight per cent of β -tricalcium phoshate (TCP= $Ca_3(PO_4)_3$ and collagen.

2. OBJETIVOS

Uno de los retos del siglo XXI en biomedicina es conseguir materiales capaces de estimular activamente la regeneración y la reparación de tejidos dañados, de forma que puedan restablecer su función. Para aplicar la ingeniería de tejidos a la regeneración del tejido óseo se necesita una nueva generación de materiales multifuncionales que actúen temporalmente soportando y estimulando la adhesión, diferenciación y colonización de las células osteoprogenitoras

El objetivo de la presente Tesis Doctoral es el diseño, preparación, caracterización y estudio in vivo de materiales, en forma de granulados o andamiajes, con elevada macroporosidad interconectada, que permitan el ajuste de la tasa de biorreabsorbibilidad con objeto de mejorar su capacidad osteoinductiva y/o angiogénica.. Se propone el diseño y la síntesis de nuevas composiciones para implantes biodegradables, así como la fabricación de estructuras (granulados, o andamiajes) jerárquicas con las características adecuadas. La formulación de los materiales cristalinos (monofasicos o multifasicos) se hará en base al diagrama de equilibrio de fases P2O5-CaO. Dichos materiales se evaluarán como sustitutos óseos. La investigación se ha realizado mediante un examen clínico, histológico e histomorfométrico en diversas etapas de tiempo después de la implantación.

Los materiales analizados fueron:

- Hidroxiapatito puro (HA= $\text{Ca}_{10}(\text{PO}_4)_6(\text{OH})_2$).
- Compuestos de hidroxiapatito con diferentes cantidades de β -fosfato tricálcico (TCP= $\text{Ca}_3(\text{PO}_4)_3$) y colágeno.

ABSTRACT RESUMEN

3. ABSTRACT

This research work for doctoral thesis was performed using the compendium of three articles:

Based on the phase equilibrium diagram P_2O_5 -CaO, a porous single phase of hydroxyapatite (HA) prepared in three ways (amorphous low and high crystallinity) was obtained. HA is a material highly used in clinical practice and has been used as reference material in front of composite materials also developed in this PhD thesis. HA composites were mixtures thereof with tricalcium phosphate (TCP) and collagen in the proportions 40/30/30 to 50/20/30 and 60/20/20 (in% by weight) and with different granulometry: Group I (2000-4000 microns), Group II (1000-2000 microns) and Group III (600-1000 m).

All materials have been synthesized in the laboratory and characterized from the point of view, physical, chemical, mechanical and mineralogical. After the characterization we proceeded to study its osteoinductive potential in an animal model of New Zealand rabbits by histological and histomorphometric studies at various stages of time after implantation.

The **results** show that depending on the degree of crystallinity, porosity and particle size, the reference material comprising HA, behaved differently in vivo. Thus HA material with greater porosity, low crystallinity and low grain is the one with lower stability and increased rate of resorption. The porosity and pore interconnectivity has been required for diffusion of nutrients and gases into the material and the elimination of metabolic waste from the cells which have colonized the implant outward. However, the porosity adversely affects the strength of the material, so you have to reach a suitable compromise for each specific clinical application.

All HA composites exhibit a microporous morphology in the form of aggregates of nanoparticles. Depending on their physical characteristics the in vivo behavior of the reference material has been different.

Histomorphometric analysis showed that Group A greater BIC (%) at 15, 30, and 60 days (43.12 ± 0.14 , 52.49 ± 1.08 and 67.23 ± 0.34) than Group B (38.84 ± 1.32 ; 47.64 ± 1.21 and 54.87 ± 0.32), followed by the C group (28.92 ± 2.41 , 35.94 ± 1.92 and 48.53 ± 0.31). SEM analysis showed that the group III presented numerous regions of resorption, whereas group II showed a level intermediate resorption with respect to the other two study groups. Group I showed the characteristics of smoother surface as compared to the other two groups. Also, the presence of collagen in biomaterials studied succeeded in raising the bioactivity of these materials compared with a lower proportion of collagen and especially compared with the reference material without the presence of collagen.

As a **general conclusion of** the work done in this Doctoral Thesis we can say that the data from this study show that changing the size, porosity and crystallinity of a bone substitute material based on HA can influence the integration of biomaterials at the site of implantation and new bone formation. So that we can design individualized biomaterials depending on the condition to being treated.

3. RESUMEN

Este trabajo de investigación para Tesis Doctoral fue realizado mediante el compendio de tres artículos:

En base al diagrama de equilibrio de fases P_2O_5 -CaO, se obtuvo un material sintético poroso monofásico de hidroxiapatita (HA) que se preparó en tres formas (amorfo, de baja cristalinidad y de alta cristalinidad). El HA es un material altamente utilizado en clínica y se ha utilizado como material de referencia frente a los materiales compuestos de HA también desarrollados en la presente Tesis Doctoral. Los materiales compuestos de HA fueron mezclas de éste con fosfato tricálcico (TCP) y colágeno en las proporciones 40/30/30 a 50/20/30 y 60/20/20 (en % en peso) y con distinta granulometría: Grupo I (2000 hasta 4000 micras), Grupo II (1000-2000 micras) y Grupo III (600-1000 m).

Todos los materiales han sido sintetizados en el laboratorio y caracterizados desde el punto de vista, físico, químico, mecánico y mineralógico. Una vez caracterizados se ha procedido a estudiar su potencial osteoinductivo en un modelo animal de conejos de Nueva Zelanda mediante estudios histológicos e histomorfométrico en diversas etapas de tiempo después de su implantación.

Los **resultados** ponen de manifiesto que dependiendo del grado de cristalinidad, porosidad y granulometría, el material de referencia compuesto por HA, se ha comportado in vivo de diferente forma. Así el material de HA con mayor porosidad, baja cristalinidad y baja granulometría es el que presenta menor estabilidad y la mayor tasa de reabsorción. La porosidad e interconectividad de poros ha sido necesaria para la difusión de nutrientes y gases hacia el interior del material y la eliminación de los residuos metabólicos de las células

que han colonizado el implante hacia el exterior. Sin embargo, la porosidad influye negativamente sobre la resistencia mecánica del material, de modo que hay que alcanzar un compromiso adecuado para cada aplicación clínica concreta.

En cuanto a los materiales compuestos de HA, todos ellos presentan una morfología micro porosa en forma de agregados de nanopartículas. Dependiendo de sus características físicas el comportamiento in vivo, al igual que ha pasado el material de referencia, ha sido distinto.

El análisis histomorfométrico que el Grupo A mostró un mayor BIC (%) a los 15, 30, y 60 días ($43.12 \pm 0,14$; $52,49 \pm 1.08$ y 67.23 ± 0.34) que el Grupo B (38.84 ± 1.32 ; $47.64 \pm 1,21$ y $54,87 \pm 0,32$), seguido por el Grupo C ($28,92 \pm 2,41$; $35,94 \pm 1,92$ y $48,53 \pm 0,31$). El análisis por SEM mostró que el grupo III presentó numerosas regiones de resorción, mientras que el grupo II presentó un índice de resorción intermedio con respecto a los otros dos grupos de estudio. El grupo I mostró las características de superficie más lisas, en comparación con los otros dos grupos. Así mismo, la presencia del colágeno en los biomateriales estudiados consiguió elevar la bioactividad de éstos en comparación con los materiales con menor proporción de colágeno y sobre todo en comparación con el material de referencia sin presencia alguna de colágeno.

Como **conclusión** general de los trabajos realizados en la presente Tesis Doctoral se puede afirmar que los datos de este estudio muestran que cambiando el tamaño, la porosidad y la cristalinidad de un material de sustitución ósea basado en HA se puede influir en la integración de los biomateriales en el sitio de implantación y la nueva formación de hueso.

Con lo que podemos diseñar biomateriales a la carta dependiendo del tipo de patología a tratar.





**MATERIAL &
METHODS**

4. MATERIAL AND METHODS

4.1.- Biomaterials preparation

4.1.1.-HA Graft implants preparation

The sol-gel method was used for preparing the HA slurry as follows: first, the appropriate amounts of $\text{Ca}(\text{NO}_3)_2 \cdot 4\text{H}_2\text{O}$ and P_2O_5 were separately dissolved in ethanol to form 1.67 and 0.5 mol/l solutions, respectively. The prepared solutions with Ca/P molar ratio of 10:6, which is the observed Ca/P ratio in HA, were mixed together. The mixture was then stirred at room temperature using a magnetic stirrer for 1 h. Porous scaffolds were fabricated by impregnating a polyurethane sponge with the slurry. The sponge block was dipped into the slurry and compressed slightly to remove the excess slurry on the foam. After the sponge was dried at 70 °C for 1 h, and then heat treatment at: (a) 600°C during 1 hour (b) 800°C during 1 hour and (c) 1000°C during 1 hour. From these temperatures the samples were slow cooled inside the furnace until room temperature. Finally the resultant product was ground in three different grain sizes of Group I (2000-4000 μm), Group II (1000-2000 μm) and Group III (600-1000 μm).

4.1.2 Composite implants preparation

4.1.2.1. HA synthesis

HA was synthesized by solid-state reaction from a stoichiometric mixture of calcium hydrogen phosphate anhydrous (CaHPO_4 , Sigma), and calcium carbonate (CaCO_3 , Sigma) with an average particle size of <15 μm and a Ca/P ratio of 1.72. The mixture of CaHPO_4 and CaCO_3 was heated in a platinum crucible to 1200 °C for 6 h at a heating rate of 10 °C /min followed by cooling to room temperature at a rate of 6.5 °C/min. The obtained material was

ground to an average particle size of 2 μm (Mastersizer 2000E device-Malvern) and then characterized by X-ray diffraction (XRD).

4.1.2.2. TCP synthesis

TCP was synthesized by solid-state reaction from a stoichiometric mixture of calcium hydrogen phosphate anhydrous (CaHPO_4 , Panreac) and calcium carbonate (CaCO_3 , Fluka) with an average particle size of $<15 \mu\text{m}$ and a Ca/P ratio of 1.60. The mixture of CaHPO_4 and CaCO_3 was heated in a platinum crucible to $1000 \text{ }^\circ\text{C}$ for 12 h followed by slow cooling. The obtained material was ground to an average particle size of $5 \mu\text{m}$ and then characterized by XRD.

4.1.2.3. Collagen.

Collagen type I of porcine origin (Sigma- Aldrich), a particle size of $80\text{--}120 \mu\text{m}$, was used in the study.

4.1.2.4. Ceramic scaffold preparation

The chosen constituents (Table I) were weighed out and thoroughly dry mixed in a mixing miller with partially stabilized zirconia balls. After the milling process, the powder mixture was cold isostatically pressed at 200 MPa. The pressure was maintained for 30 min, after which it was slowly depressurized to 1 atm. The whole process took 1 h.

Compound	Group A	Group B	Group C
HA	40	50%	60%
B-TCP	30	20%	20%
Collagen	30	30%	20%

Table 1. Study groups of HA/TCP/Collagen scaffolds.

4.2. Biomaterials characterization

All biomaterials have been characterized from the point of view, physical, chemical, mechanical and mineralogical before their implantation.

In order to analyze the biomaterials from mineralogical point of view, these were reduced to powder and spread over the analytical cylindrical sample holder of the X-ray diffractometer Bruker-AXS D8 Advance (XRD). XRD patterns were recorder from to 2 scans in parafofocusing Bragg-Brentano geometry with line focused copper K ($\lambda_{Cu,K1} = 1.54056\text{\AA}$) radiation from a conventional sealed tube source. The diffractometer was equipped with a scintillation detector. Scans were taken from 20 to 50° (2 θ) in 0.05° steps with counting times of 6s per step.

The crystal size of the ha samples was estimated from the XRD patterns using the Sherrer equation (Patterson 1939). According to the equation, a single crystal dimension perpendicular to the (hkl) plane (D_{hkl} ; nm) can be estimated from the peak broadening as

$$D_{hkl} = \frac{k\lambda}{B_{1/2} \cos \theta_{hkl}}$$

where k is the Scherrer constant (0.89) which depends on the crystal shape, the diffraction line indexes (Shull 1946) and the dispersion of crystallite sizes of the powder), λ is the wavelength of the Cu K ($=1.54056\text{\AA}$); $B_{1/2}$ corresponds to full width at half maximum (rad) for (hkl) reflection, θ_{hkl} is the diffraction angle (°). The line broadening of the (300) reflection corresponding to the maximum intensity peak was used to evaluate the crystal size.

In order to analyze the functional groups and structural changes of the samples were measured using Fourier Transformed Infrared Spectroscopy (FTIR- ThermoNicolet IR200, Waltham, MA, USA). The FTIR spectra were recorded between 400 and 4000 cm^{-1} at 2 cm^{-1} resolution. The pellets were prepared by mixing each sample powder with KBr matrix at a level of 1 wt%. The background data were collected for the KBr matrix and subtracted from each spectrum. All spectra were recorded at ambient temperature.

The physical characterization analyzed in terms of density and porosity: Apparent density measurement was performed on each sample using Archimedes' method by immersion in Hg. Sample mass was determined using an electronic balance and relative density (RD) was calculated with the following equation:

$$RD = \frac{\rho_a}{\rho_t} \times 100$$

where ρ_t and ρ_a are the samples' theoretical density and apparent density, respectively.

The porosity of the prepared ceramic, three samples of the foams were selected for each sintering temperature and each composition and the porosity of the bulk specimens was measured by Archimedes method. The apparent porosity, which measures the interconnected porosity, was determined by weighing the dry ceramic (W_d), and then reweighing the ceramic both when it is suspended in water (W_s) and after it is removed from the water (W_w).

$$\text{Apparent porosity} = \left[\frac{W_w - W_d}{W_w - W_s} \times 100 \right]$$

The true porosity includes both interconnected and closed pores. The true porosity, which better correlates with the properties of the ceramic, is:

$$\text{True porosity} = \left[\frac{\rho - B}{\rho} \right] \times 100$$

where

$$B = \frac{W_d}{W_w - W_s}$$

B is the bulk density and ρ is the theoretical density or specific gravity of the ceramic. The bulk density is the weight of the ceramic divided by its volume.

We used three-point bending strength (r_f) in order to study the mechanical properties of the biomaterials. The test was made using a Microtest universal testing machine set at a cross-head speed of 0.33 mm s⁻¹ and a span of 40.0 mm. Fracture toughness (K_{1c}) was also obtained in the 3-point bending test as a function of loading rate by the single edge precracked-beam method.²² Measurements were performed at room temperature using the rectangular-shaped samples (3 mm x 4 mm x 45 mm) with a notch width of <0.5 mm. The ratio between notch depth and sample thickness was 0.4. Young's modulus (E) was evaluated from the stress-strain curves obtained with the flexural strength test. Seven replicates were determined for each material and the results were expressed as mean \pm 6 standard deviation.

Finally, the microstructure of the HA graft implants and the HA/TCP/collagen composites were characterized using a scanning electron microscope (SEM, HITACHI S-3500N, Japan). Quantitative analyses were made by an Electronic Dispersive X-ray Spectroscopy (EDX) system coupled to the electron microscope (Oxford Instruments INCA 300 EDX Analytical System (Abingdon, Oxfordshire, U.K.) using ZAF (atomic number, absorption and fluorescence) correction software and Bayer standards. Microanalysis data was obtained from the mean of ten independent determinations. Every sample was embedded in an epoxy polymer with vacuum, polished with diamond paste down to 1 μ m and etched with diluted acetic acid (1.0%v/v) for 6s. Then, they were gently cleaned in an ultrasonic bath with distilled water, dried and palladium coated under an argon atmosphere using a sputtering machine (Polaron K550X Sputter Coater, Germany) for SEM-EDS observations.

4.3. Animal experimentation

Main protocol. The study protocol was approved by the Animal Ethics Committee of the University of Murcia, following Spanish Government and European Community Guidelines for animal care. Fifteen male New Zealand rabbits of 3.5–4.5 kg in weight were used. The six materials were implanted into the animals' calvariae and tibiae. General anesthesia included ketamine plus chlorbutol (5–8 mg/kg intravenously), 0.5–1 mg/kg acepromazine maleate as a coadjuvant, and 0.05 mg/kg atropine. Amoxicillin (0.1 mL/kg intramuscularly) was administered at the end of surgery.

4.3.1 HA and composite implants

Three groups of 15 rabbits were used, a total of 50 with 160 critical size defects each of cylindrical shape (6 ± 0.01 mm in diameter and 2 ± 0.01 mm in length). The sample were divided into two general groups: GROUP 1 (HA/-TCP/collagen composite) and GROUP 2: (HA pure).

GROUP 1: The ratios of three constituents HA/-TCP/collagen (in wt % varied as follows: group A: 40/30/30; group B: 50/20/30; and group C: 60/20/20). A fourth group, group D (unfilled critical size defect), acted as control.

GROUP 2: divided in 4 groups: Group I filled with hydroxyapatite granules (2000-4000 μm), Group II filled with hydroxyapatite granules (1000-2000 μm) and Group III filled with hydroxyapatite granules (600-1000 μm), Group IV empty defect, acted as control.

These were distributed randomly amongst critical size defects in rabbit calvarias and tibiae by means of random number generator software, SPSSR v.18.0. (IBM Corporation, New York, NY).

4.3.2 Surgical procedure.

Two critical defects (6 mm \emptyset) were created in each calvaria or tibia respectively. The surgical approach was in the proximal-medial area of the calvaria and in the proximal area of the tibia, several millimeters below the frontal tuberosity. Bone tissue was removed with spherical surgical drills of 6 mm in diameter at low rotation speed with constant irrigation [Fig. 1.1(a-c) & 1.2 (a-d)].

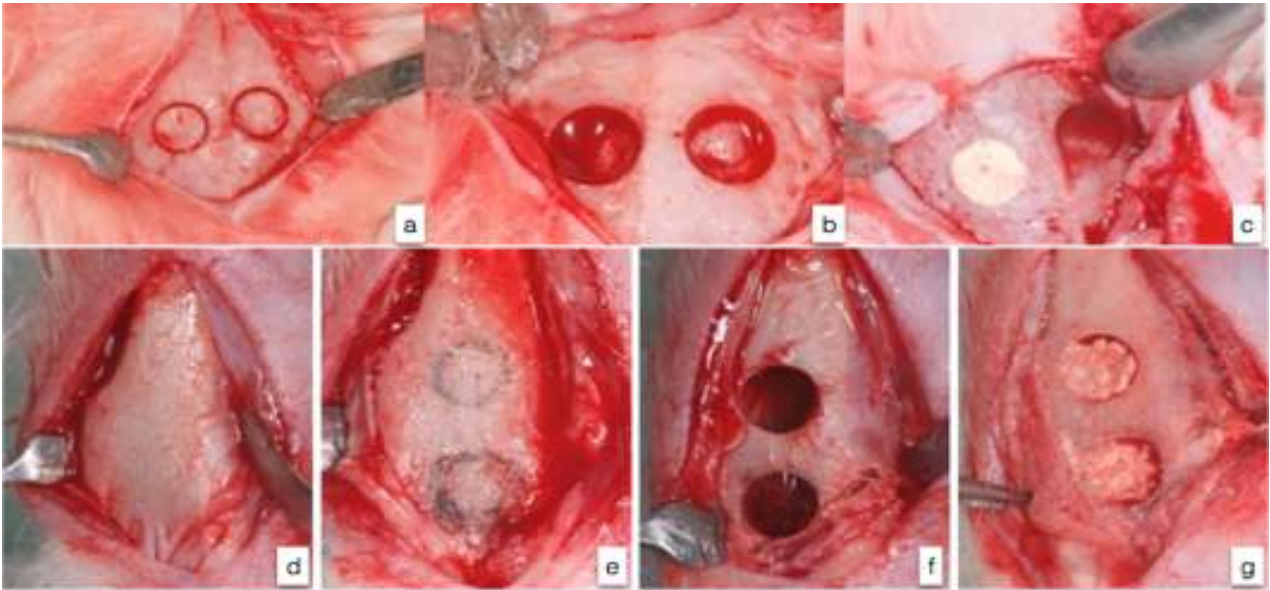


Figure 1. Surgical procedure: Calvariae: surgical approach (1a), defect preparation (1b), graft placement (1c). Tibia: surgical approach (1d), defect preparation (1e & f), graft placement (1g).

4.4. Post-mortem implant characterization

4.4.1. Histological and histomorphometric analysis

After the elapse of the 60-day implantation time, the implants together with the surrounding tissues were removed and fixed in 10% neutral buffered formalin and decalcified. The decalcification method utilized Osteomoll Merck KbaA (Germany) containing HCl (10%) and CH_2O (4%), immersing samples for 17 days and renewing the solution every 24 h. Subsequently, all samples were paraffin embedded, sectioned at 5 μm depth and stained using hematoxylin–eosin. The entire circumference of each section (containing bone, graft, and connective tissue) was traced manually to create an individual region of interest. Histomorphometric evaluations consisted of measurements of the area of graft material in relation to the total area of interest. These were carried out using Image J software

[developed by the National Institute of Health (NHS), Bethesda, MD]. Examinations were performed under a Nikon Elipse 80i microscope (Teknooptik AB, Huddinge, Sweden), equipped with an Easy Image 2000 system (Teknooptik AB) using 103 to 403 lenses for descriptive evaluation and morphometric measurement. Images were generated using a Leica Z6 APO microscope connected to a Leica DC 500 (Barcelona, Spain) digital camera, enlarged 233. After calibrating the system and digitalizing images, interactive measurements of the areas of interest were obtained using image analysis software Leica QWin V3 (Barcelona, Spain). Histomorphometric analysis produced one

4.4.2. Resorption rate and pattern of surface resorption

The image analysis program Image J (National Institutes of Health, Bethesda, MD, USA) was used to calculate the resorption rate of the different material compositions. This was performed by demarcating the area of interest as the total biomaterial at the time of implantation, measuring its perimeter, and comparing this with the residual material after 15, 30, and 60 days.

4.4.3. Scanning electron microscope study

Twenty samples of each material were studied after 15, 30, and 60 days of implantation comparing variations in the ratios of Ca/P percentages. The samples were fixed by immersion in 4% formalin solution, dehydrated in a graded ethanol series, and embedded in plastic resin (Technovit A 7210VCL; Kulzer & Co, Hanau, Germany). They were then polished using a manual grinder with 800 grit silicon carbide paper, mounted on an aluminum stub and carbon coated (using a Polaron sputter coater). Samples were examined using the SEM-

Hitachi S-3500N at a working distance of 19 mm, an acceleration voltage of 15 kv and 159 magnification, with an Oxford Instruments INCA 300 EDX System (Abingdon, Oxfordshire, UK), evaluating elemental composition of the graft material and bone in the medullary area. Areas of interest were delimited by the inner cortical walls and reached into the medullary core. Elemental mapping was performed in order to determine the chemical degradation process and changes to medullary composition in all four study groups.

4.4.4. Radiological study

Digital radiographs were taken (using a Kodak 6100, Eastman Kodak, Rochester, NY, USA) following sample removal using a custom-made acrylic support to ensure reproducibility of the technique. Exposure parameters were standardized. Each radiograph was studied using image analysis software Image J (National Institute of Health, Bethesda, MD, USA).

4.5. Statistical analysis

Statistical analysis was performed using PASW Statistics v.18.0.0 software (SPSS Inc). Values were recorded as mean \pm standard deviation and medians. Nonparametric Friedman test was applied to the comparison of medians and to quantify relationships between differences ($P < 0.05$). Equal means were regarded as the null hypothesis, whilst the existence of differences between means acted as an alternative hypothesis. As significant differences between the means existed, the null hypothesis was rejected.



RESULTS

5.1. HA Biomaterial Characterization

The XRD patterns of the HA grafts implants, sintered at a different temperatures in the range of 600°C to 1000°C is shown in Figure 2. The diffraction patterns have been identified for those belonging to the HA phase. Good agreement was found between the XRD pattern of the prepared HA powder and the stoichiometric HA [XRD JCPDS data file No. 09-0432.].

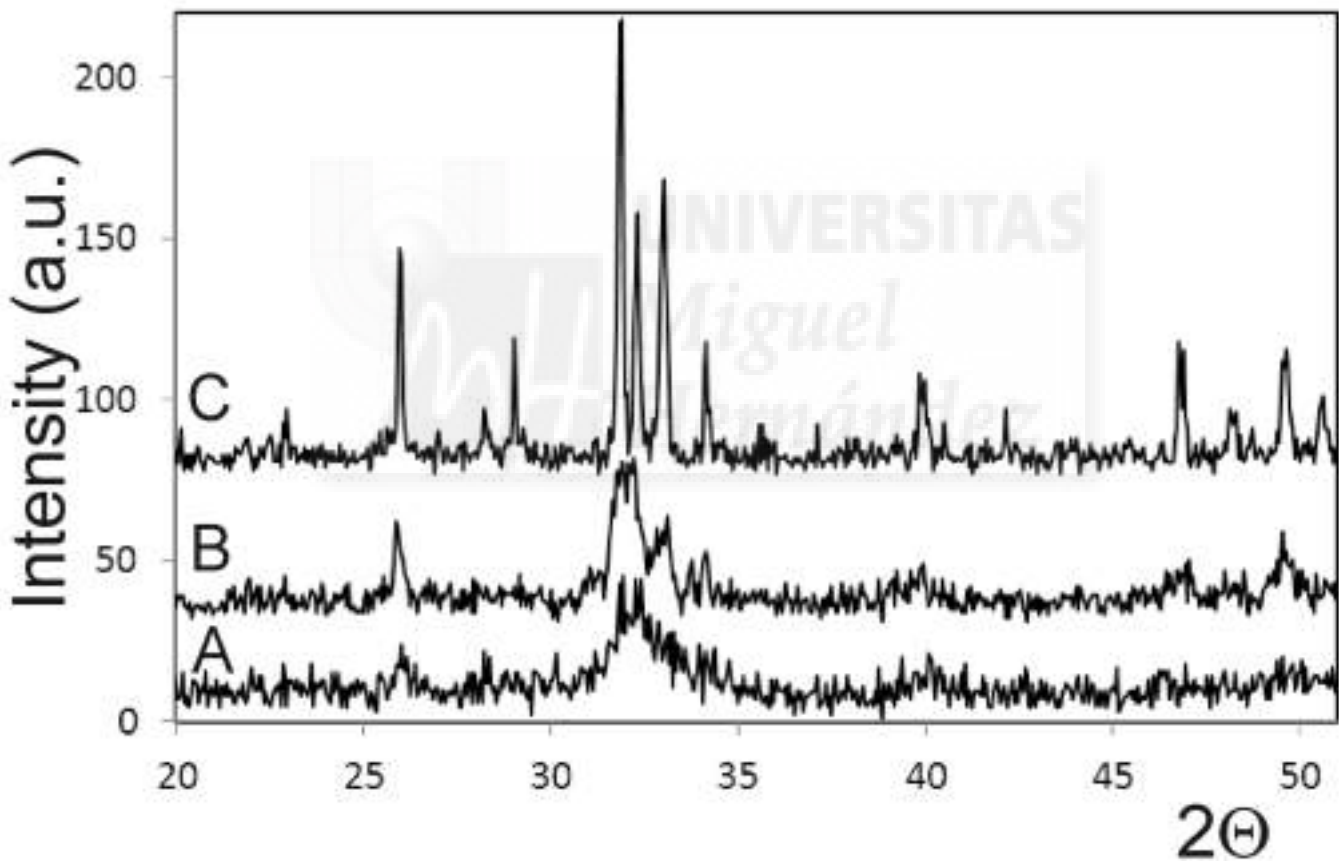


Figure 2. XRD of the HA grafts (A) at 600°C, (B) at 800°C and (C) at 1000°C.

No new phase (after sintering) is formed. The lower temperatures, 600°C and 800°C, the shift was significant suggesting a great lattice distortion. Based on XRD patterns, the crystal size of HA graft implants studied are given in Table 2. The crystal size increased with the

5. RESULTS

increasing temperature of sintering from 325 nm to 732 nm. Table 3 summarizes physical properties of HA graft as a function of sintering temperature. The sample that shows highest crystallinity and crystal size corresponding to that of group I. The differences in density are not very significant.

	Heat Treatment	Crystalline phase	Grain size (μm)
Group I	1000°C	HA	2000-4000
Group II	800°C	HA	1000-2000
Group III	600°C	HA	600-1000

Table 2. Heat treatment and the physical characteristic of the HA graft.

	Crystall size (nm)	Porous size (nm)	True Porosity (%)	Apparent Porosity (%)
Group I	325	0.5(\pm 0.1)	71 (\pm 1.9)	51(\pm 2)
Group II	458	0.5(\pm 0.1)	67(\pm 1.4)	46(\pm 1.8)
Group III	732	0.6(\pm 0.1)	65(\pm 1.8)	45(\pm 1.7)

Table 3. Physical properties of HA graft as a function of sintering temperature.

Figure 3 displays the FTIR spectra of the milled samples after thermal treatment in the range of 600–1000°C for 1h. In general, the characteristic groups of apatites are PO_4^{3-} , OH^- and HPO_4^{2-} groups which commonly appears in 4000–400 cm^{-1} region in the FTIR spectra [26,29,30]. The characteristic bands of the synthesized materials are: After 1 h of sintering, two bands were detected at 3432.2 and 1642.6 cm^{-1} as a result of the vibration of the adsorbed water in apatites. These bands shifted to 3236.5 and 1684.3 cm^{-1} , 3200.1 and 1684.5 cm^{-1} , after heating at 800, and 1000°C, respectively.

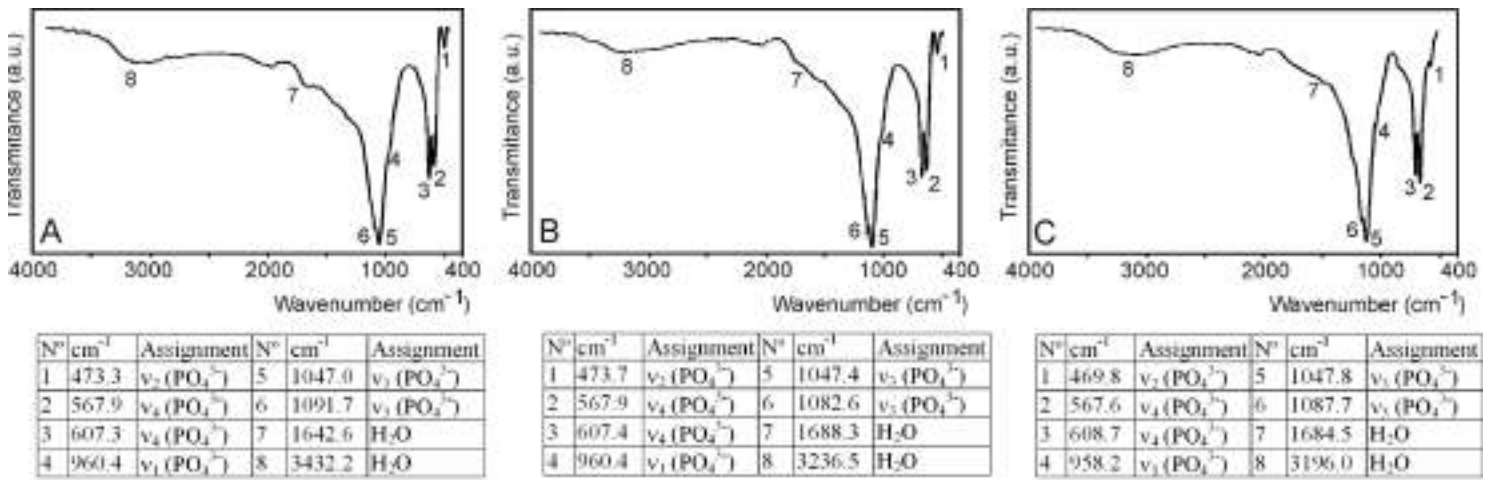


Figure 3. FTIR of the HA grafts (A) at 600°C, (B) at 800°C and (C) at 1000°C.

The intensity of these bands declined dramatically after thermal treatment especially at 1000°C. Also the PO_4^{3-} bands shifted for the annealed sample at 800°C in comparison with the heat-treated specimen at 1000°C. With an increasing of the annealing temperature, the PO_4^{3-} vibration peaks merged gradually. Figure 4 shows SEM micrographs of the HA grafts sintered at 600, 800 and 1000 °C for 1 h. SEM micrographs showed that the obtained HA grafts structure consisted of a highly spherical porous network with the pore size of 0.5 mm in average. Figure 4 shows Sem images of the samples previous to the animal implantation.

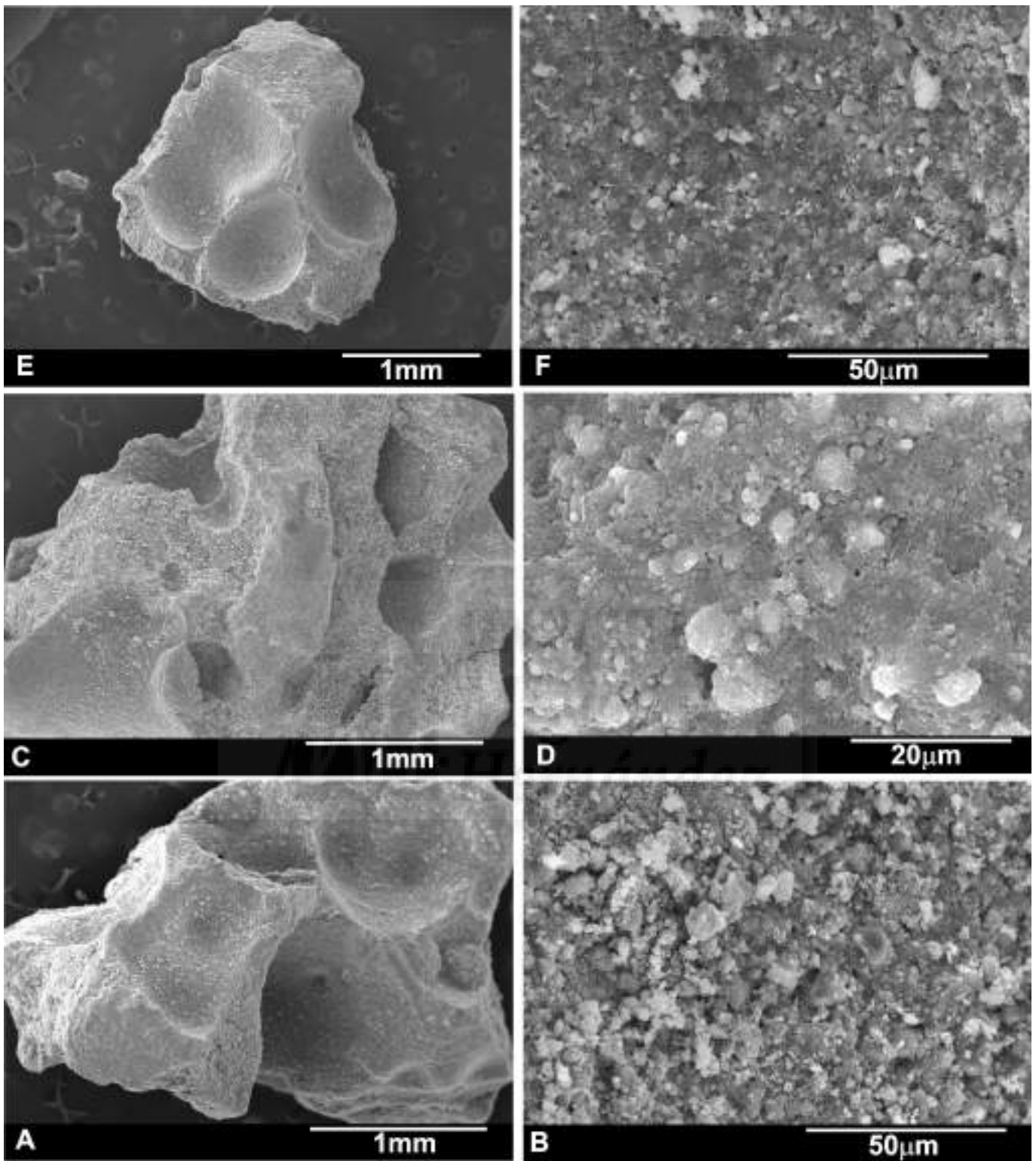


Figure 4. SEM micrographs of the HA grafts (A,B) at 600°C, (C,D) at 800°C and (E,F) at 1000°C.

5.2. HA Implant characterization

5.2.1. SEM and EDS analysis

Figure 5 presents the micrographs of the implants' cross sections after the implantation for 60 days. The SEM morphological examination showed that all the implants were well integrated into the host tissue, and developed an uneven surface caused by their gradual degradation..

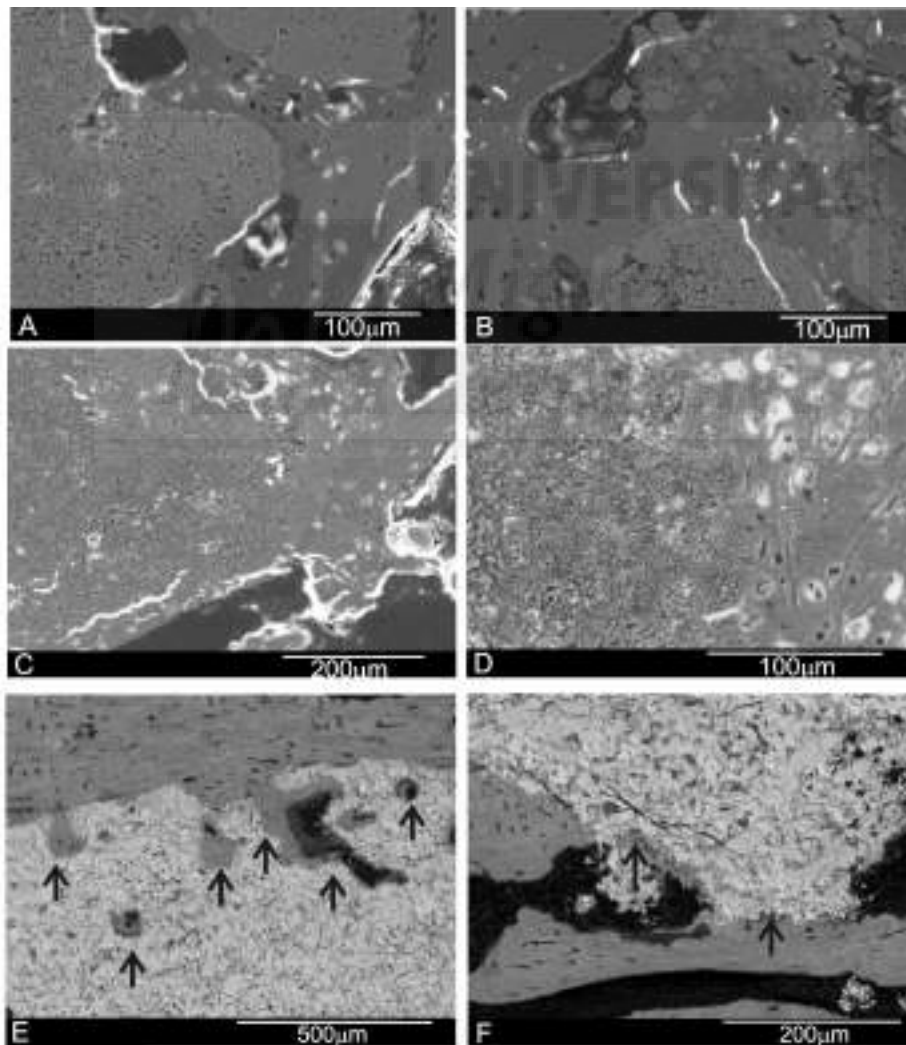


Figure 5. SEM micrographs of the 60 days HA grafts implants. (A,B) at 1000°C, (C,D) at 800°C and (E,F) at 600°C.

The group III implant showed numerous resorption regions (marked by the arrows in the Figure 5E and 5F), mainly on its surface, and also more uneven surface morphology in comparison with the other implants. The group II implant presented an average resorption rate of all the implants (Figure 5C & 5D). The group I (Figure 5A and 5B) displayed smoother surface features, in comparison with the other two implants.

According to the EDS analysis and high magnification SEM examination of the interfaces developed between all the studied implants and the surrounded tissue, the reaction zone was characterized by the intermittent presence of calcium phosphate phase, which corresponded in structure and morphology to a new bone tissue. Also The Ca/P ratio related to new bone formation level was greater in the group I implant in comparison with the other groups (Table 4)

Element	Group I		Group II		Group III	
	Weight%	Atomic%	Weight%	Atomic%	Weight%	Atomic%
<i>C K</i>	21.93	43.17	7.77	13.69	28.00	44.91
<i>O K</i>	16.14	23.86	45.07	59.61	31.32	37.71
<i>Na K</i>			0.65	0.60	9.61	5.98
<i>P K</i>	13.75	10.49	14.41	9.84	19.27	9.26
<i>Ca K</i>	32.02	18.89	30.01	15.84	11.80	2.14
<i>Pd L</i>	16.16	3.59	2.09	0.42		
Totals	100.00		100.00		100.00	
Ca/P	2.38	1.8	2.08	1.60	0.61	0.23

Table 4. EDS analysis at the interface of the HA grafts after 60 days implantation.

5.3. Preoperative composites characterization

The X-ray diffraction patterns of the synthesized powder of TCP and HA as well as the composite ceramic powder materials is shown in figure 6. It can be seen that the

polymorphic form obtained was b- TCP in the rhomboetral crystalline system with main diffraction plan [021] and corresponded to JCPDS card no. 9- 0169. On the other hand, the HA corresponded to JCPDS card no. 09-0432 and presents hexagonal system with main diffraction plan [211]. No other secondary phases were detected. The XRD patterns of the composite ceramic compositions showed peaks corresponding with b-TCP and HA.

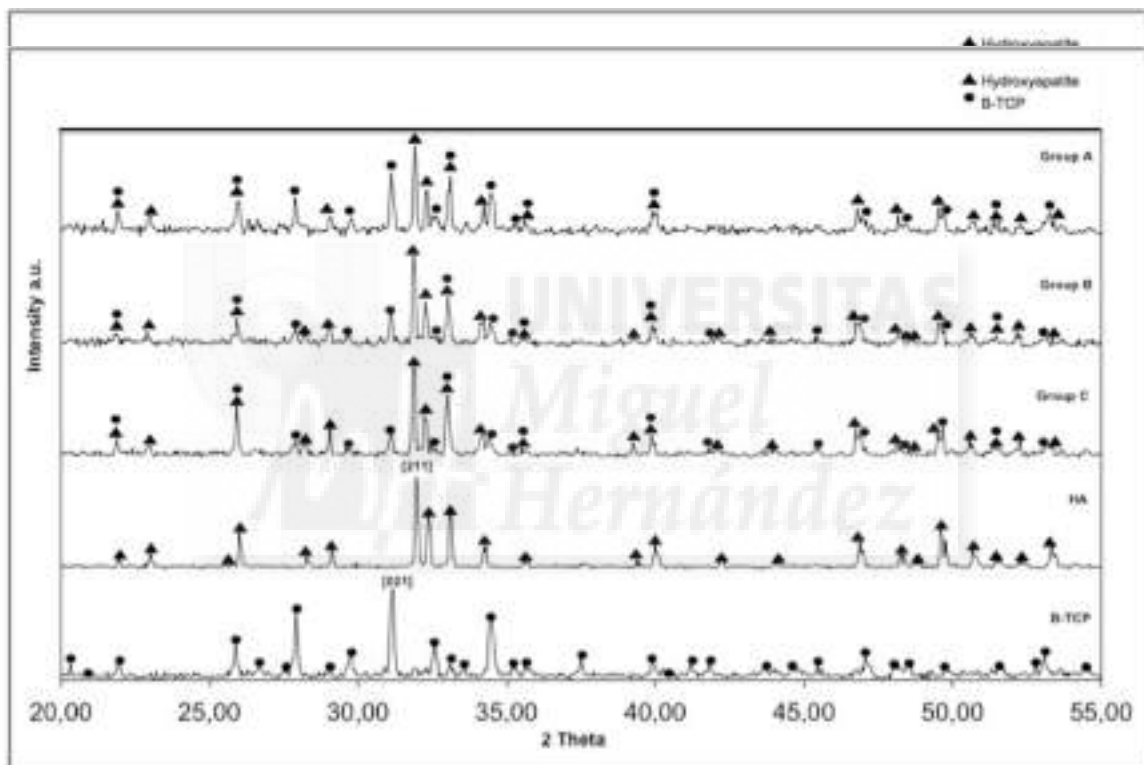


Figure 6. X-ray diffraction patterns of synthetic HA, TCP raw materials and HA/TCP/collagen compositions.

The physical and mechanical properties of the ceramic scaffolds are reported in Table 5. As the collagen content increased (from 20 to 30 wt%), the porosity increased by about 4% for group B composition to about 9% for Group A. Bending strengths ranged between 7.76 and 8.21 MPa. Although there was almost no difference between the composites, it was obvious that the addition of collagen produced various responses among the different ratios in

relation with porosity and mechanical properties of the compounds. Fracture toughness, the material's resistance to crack propagation, is an important parameter for assessing a material's susceptibility to failure. In general, toughness was seen to increase for Group B and decrease for Group A with the addition of collagen. When each group was compared, significant differences were recorded (to facilitate comparison, the properties of sintered HA, b-TCP, cortical, and cancellous bone are also included).

	Crystalline phases	Porosity (%)	Density (g cm⁻³)	RD (%)	Bending strength, σ_t (MPa)	Young's modulus, E (GPa)	Fracture toughness, K_{Ic} (MPam^{1/2})
Group A	HA/ β -TCP	32 \pm 1.23	2.18 \pm 0.56	76.25 \pm 2.34	7.76 \pm 1.02	3.15 \pm 1.12	0.34 \pm 0.03
Group B	HA/ β -TCP	27 \pm 1.07	2.20 \pm 0.67	78.12 \pm 2.56	8.21 \pm 0.99	3.18 \pm 0.89	0.40 \pm 0.12
Group C	HA/ β -TCP	23 \pm 0.98	2.35 \pm 0.38	85.25 \pm 3.01	7.92 \pm 1.76	3.16 \pm 1.02	0.37 \pm 0.07
Sintered HA	HA		99.2 \pm 0.98		115-200	80-110	1.0
Sintered TCP	β -TCP		99.7 \pm 0.87		140-154	33-90	
Cortical bone	CHA	5-12		1.8-2.0	60-147	11-19	2-11
Cancellous bone	CHA	46-95		0.09-1.0	0.5-8.0	0.06-1.5	

Table 5. Physical and mechanical properties of the materials studied. For comparative purposes the mechanical properties of sintered HA, sintered TCP and cortical and cancellous bone are also included.

Table 6 shows the results of the specific surface on the nanostructured powders after milling b-TCP, HA, and the ceramic composites. The results show higher values for the HA matrix, getting to 10.4 m²/g. Also the HA powder present a morphology formed by clustered nanoparticles smaller in size by 50 nm, and the b-TCP powder shows nano-particles bigger to those found for HA. The results found for the b-TCP, and HA nano-structured powder after

the mill shows a change of the nanoparticles surface, generated by the process in the attrition mill. This superficial change of the nanoparticles has already been identified by other authors that have used the high-energy method of attrition milling in the development of ceramic powders (Camargo et al. 2012, 2014).

	B-TCP	HA	Group A	Group B	Group C
Superficial Area (m ² /g)	8,7 ±0,5	10,4±0,5	8,6±0,5	8,8±0,5	9,3±0,5

Table 6. Specific surface of the presintered materials as well as the composites.

Fig. 7 shows surface morphology of the three composites. If the micrographs obtained on the different composites are comparable, it is possible observe that the materials revealed a microporous morphology formed by aggregated nanoparticles independently of the composition of the composite. The particles present an average diameter of ~50– 60 nm. In addition, dense powder aggregates with sizes of ~2–5 μ m were observed.

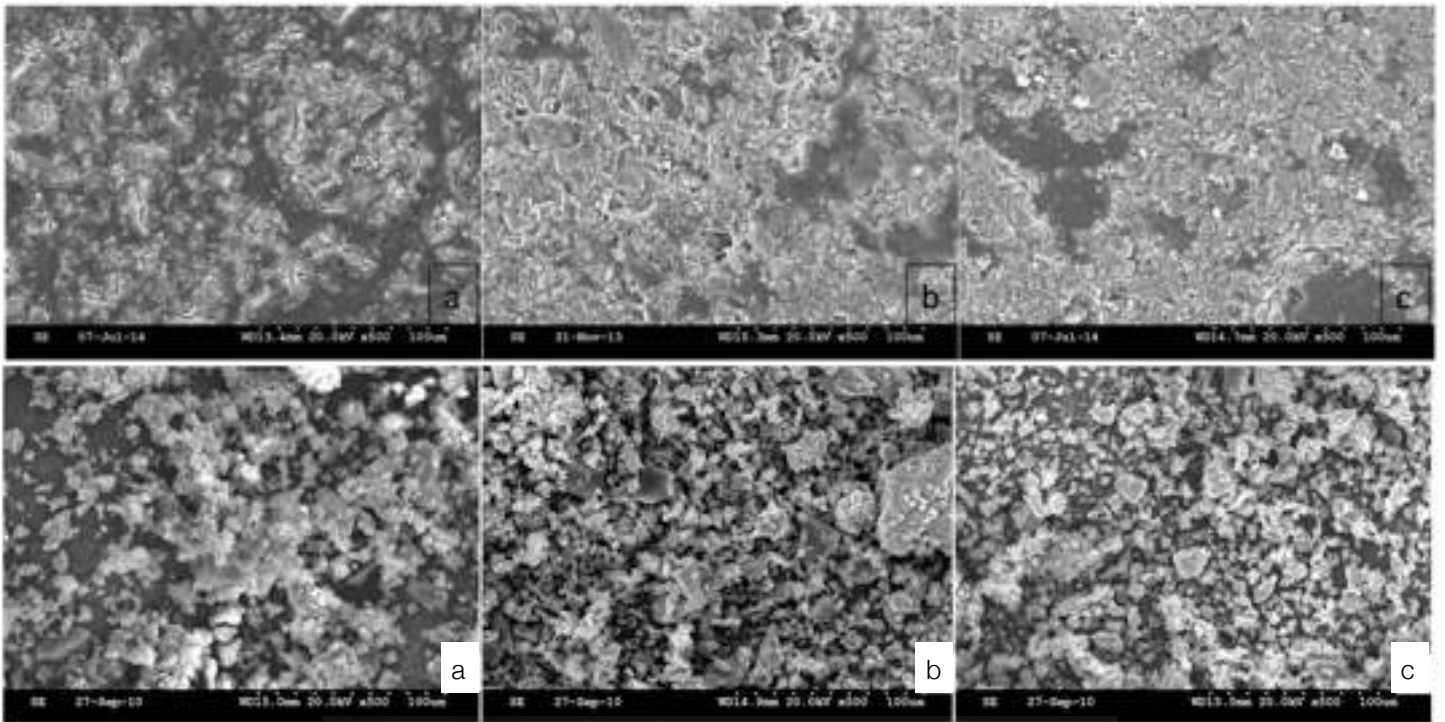


Figure 7. SEM images of materials obtained: (3a) Group A, (3b) Group B, (3c) Group C. (100 microns).

5.4. Composite implants characterization.

5.4.1. Histological and resorption analysis

Analysis of the histological sections of each of the three materials was performed at 60 days post implantation. None of the grafted materials elicited a significant inflammatory reaction. In all samples, woven bone was identified around and in close contact with the material and, as might be expected in rabbit calvarial bone, small marrow spaces were observed in the peri-material bone, which had reached maturity over 60 days. The volume of the graft block in group A decreased progressively as bone formation increased at the periphery and within the block, leading to its virtual disappearance and almost complete closure of the cortex at 60 days. In group C, graft blocks showed slower resorption than the other groups;

histological results showed that after implantation, changes to residual block content, peripheral bone resorption, new bone formation, and closure of the cortex were minimal in comparison with the other graft compositions (Fig. 8). In calvariae treated with group B blocks, there was intermediate block stability, much greater resorption than in group C, but lower than in group A and an intermediate rate of neoformation. In the control group, no spontaneous closure of the defect was seen, as might be expected of a critical defect [Fig. 8(a)]. The resorption pattern was variable across the groups. Group A samples [Fig. 8(b)] showed numerous resorption foci on block surfaces, which produced a much more irregular surface compared with other samples (peaked resorption pattern). Group B samples [Fig. 8(c)] presented intermediate behavior showing a moderate resorption pattern, with fewer unfilled regions and less irregularity, after a wavy resorption type across the surface. Finally, in group C, a linear pattern was observed with few resorption foci that were more regular and less active [Fig. 8(d)].

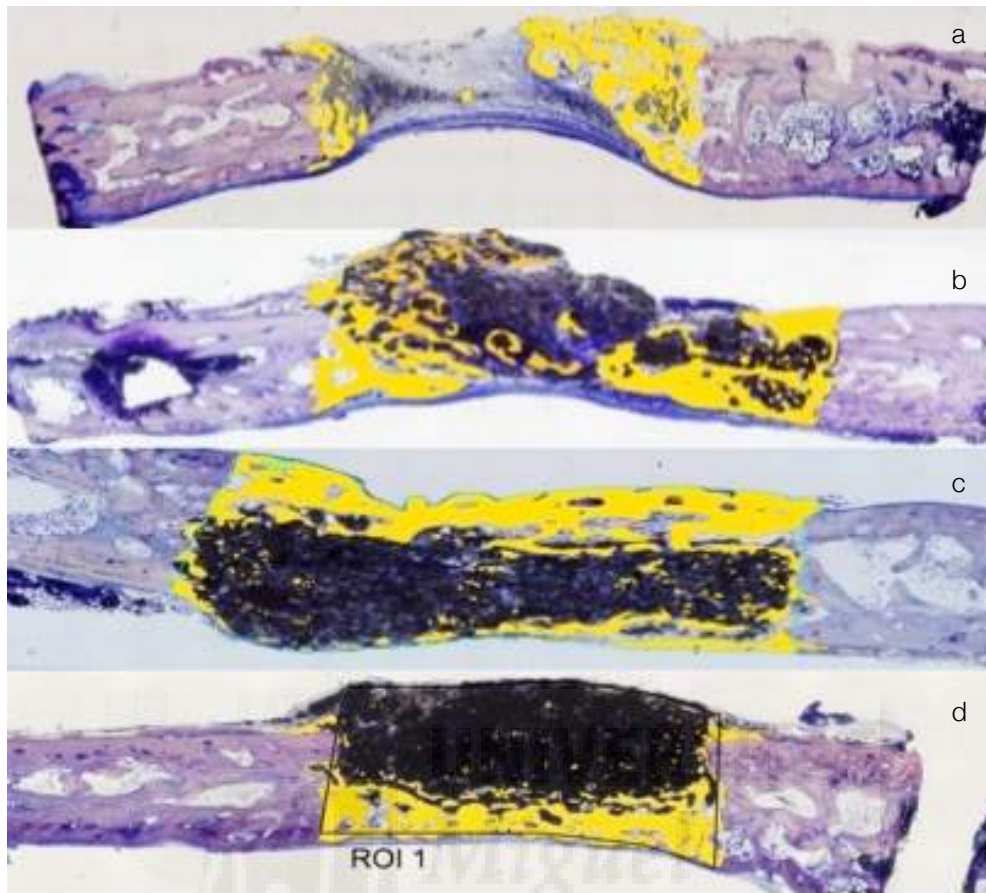


Figure 8. Analyses of histological sections were performed at 60 days for each of the three materials: Control (a), Group A (b), Group B (c) and Group C (d). Black: residual material. Yellow: bone remodeling site. (resorption foci). (200x).

In tibiae, analysis of the histological sections of each of the three materials was performed at 15, 30, and 60 days post-implantation. None of the grafted materials elicited a significant inflammatory reaction. In all samples, woven bone was identified around and in close contact with the material and, as might be expected in rabbit tibia bone, small marrow spaces were observed in the peri-material bone, which had reached maturity over 60 days. The volume of the graft block in Group A decreased progressively during the time of study, starting with minimal signs at 15 days until the material reabsorbed at 60 days and increased new bone formation surrounding and inside the biomaterials; bone formation increased at the periphery and within the block, leading to its

virtual disappearance and almost complete closure of the cortex at 60 days. In Group C, graft blocks showed slower resorption than the other groups; histological results showed that following implantation, changes to residual block content, peripheral bone resorption, new bone formation and closure of the cortex were minimal in comparison with the other graft compositions (Fig. 9).

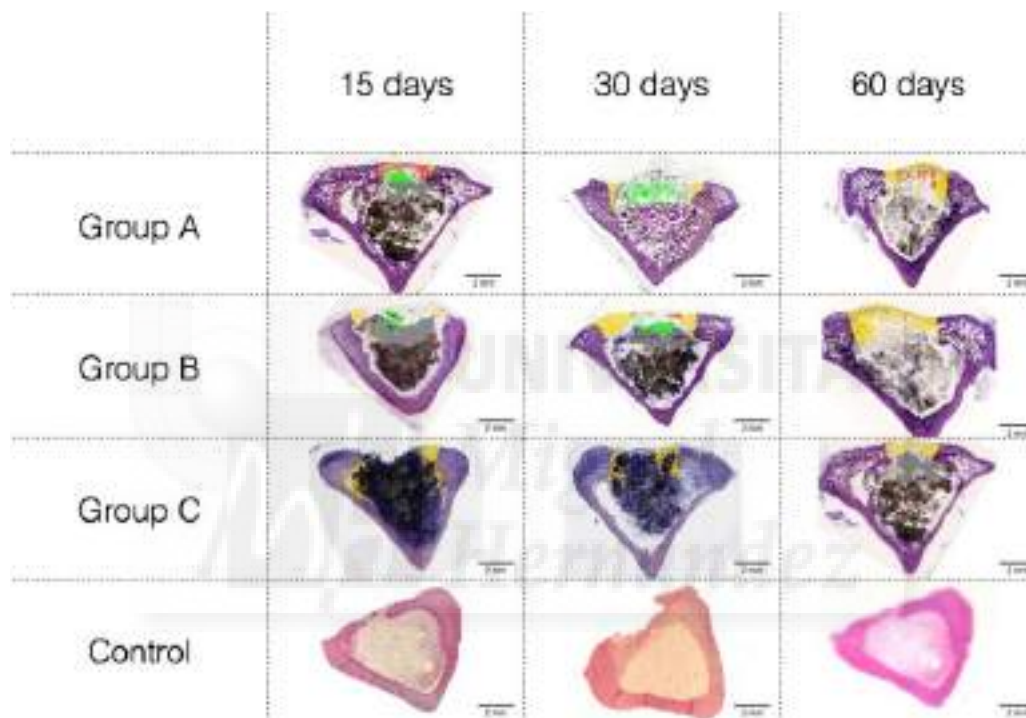


Figure 9: Histologic results at 15, 30 & 60 day implantation. Group A (40/30/30), Group B (50/20/30), Group C (60/20/20) and control. Detailed images of biomaterials with ROI. (Magnification 50x).

In tibiae treated with Group B blocks, there was intermediate block stability, much greater resorption than in Group C, less than Group A, and an intermediate rate of neoformation. In the control group, no spontaneous closure of the defect was seen, as might be expected of a critical defect. The resorption pattern was variable across the groups being observed a progressive

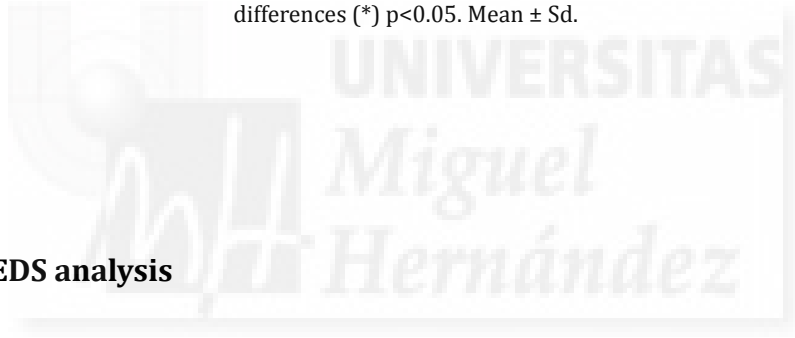
resorption during the time of study to achieve greater resorption at 60 days. Thus, 15 days there is a partial resorption, being higher for group A, followed by group B and group C where finally reabsorption is partial. Similarly to 30 days resorption rates are higher with respect to the 15-day study and lower than those found at 60 days for the three study groups. Group A samples showed numerous resorption foci on block surfaces, which produced a much more irregular surface compared with other samples (peaked resorption pattern). Group B samples presented intermediate behavior showing a moderate resorption pattern, with fewer light areas and less irregularity, following a wavy resorption type across the surface. Finally, in Group C, a linear pattern was observed with few resorption foci that were more regular and less active (linear resorption pattern).

5.4.2. Histomorphometric analysis

Histomorphometric analysis was carried out to establish BIC values for the three materials, with Group A showing best BIC (%) at 15, 30 and 60 days (43.12 ± 0.14 ; 52.49 ± 1.08 and 67.23 ± 0.34) (without empty spaces) than Group B (38.84 ± 1.32 ; 47.64 ± 1.21 and 54.87 ± 0.32), followed by Group C (28.92 ± 2.41 ; 35.94 ± 1.92 and 48.53 ± 0.31), in which close contact between bone and graft was significantly less. Moreover, new bone ingrowth, defect closure, and residual biomaterial were recorded and analyzed, showing better values for Group A samples in comparison with the other groups (Table 7).

Time (days)	Group A			Group B			Group C			Control		
	15	30	60	15	30	60	15	30	60	15	30	60
BIC (%)	43.12 ± 0.14	52.49 ± 1.08 *	67.23 ± 0.34 *	38.84 ± 1.32	47.64 ± 1.21 *	54.87 ± 0.32 *	28.92 ± 2.41	35.94 ± 1.92	48.53 ± 0.31 *	0.00 ± 0.00	0.00 ± 0.00	0.00 ± 0.00
New bone ingrowth	39.32 ± 3.01	58.38 ± 2.14 *	78.23 ± 2.65 *	34.73 ± 10.65	56.03 ± 1.74 *	74.12 ± 2.83 *	29.75 ± 1.10	68.48 ± 3.01 *	72.52 ± 2.49 *	24.84 ± 0.05	29.84 ± 2.13	37.38 ± 3.97
Defect Closure	18.64 ± 1.13	37.43 ± 2.41 *	63.34 ± 3.43 *	16.32 ± 2.01	34.63 ± 3.21 *	59.54 ± 3.32 *	19.94 ± 2.01	32.24 ± 0.64	60.46 ± 3.01 *	10.21 ± 0.32	23.98 ± 3.10	34.21 ± 2.34 *
Residual Biomaterial	78.32 ± 1.09 *	65.09 ± 0.94 *	59.34 ± 2.95	80.09 ± 1.05 *	72.52 ± 0.98 *	63.43 ± 2.90	83.32 ± 2.31 *	74.34 ± 0.64	79.39 ± 2.98	0.00 ± 0.00	0.00 ± 0.00	0.00 ± 0.00
Resorption rate	21.68 ± 2.18	34.91 ± 3.21 *	40.66 ± 3.10 *	19.91 ± 0.39	27.48 ± 2.43 *	36.57 ± 2.64 *	16.68 ± 1.22	25.66 ± 1.18 *	20.61 ± 3.01	0.00 ± 0.00	0.00 ± 0.00	0.00 ± 0.00

Table 7. Histomorphometric analysis to evaluate BIC for the three materials. Non Parametric Friedmann Test. Significant differences (*) p<0.05. Mean ± Sd.



5.4.3. SEM and EDS analysis

SEM images showed complete integration of all specimens, without significant differences between the groups. In all cases, the cell growth was observed to be orderly and structured; there was cell attachment to the biomaterial and the establishment of an interface between the biomaterial and the old bone (Fig. 10). Examining the details of each panoramic image, group A showed integration of the graft in the calvarial bone [Fig. 10(a)], as well as cellular arrangement over the graft block [Fig. 10(b)]. In group B, integration existed in the surrounding

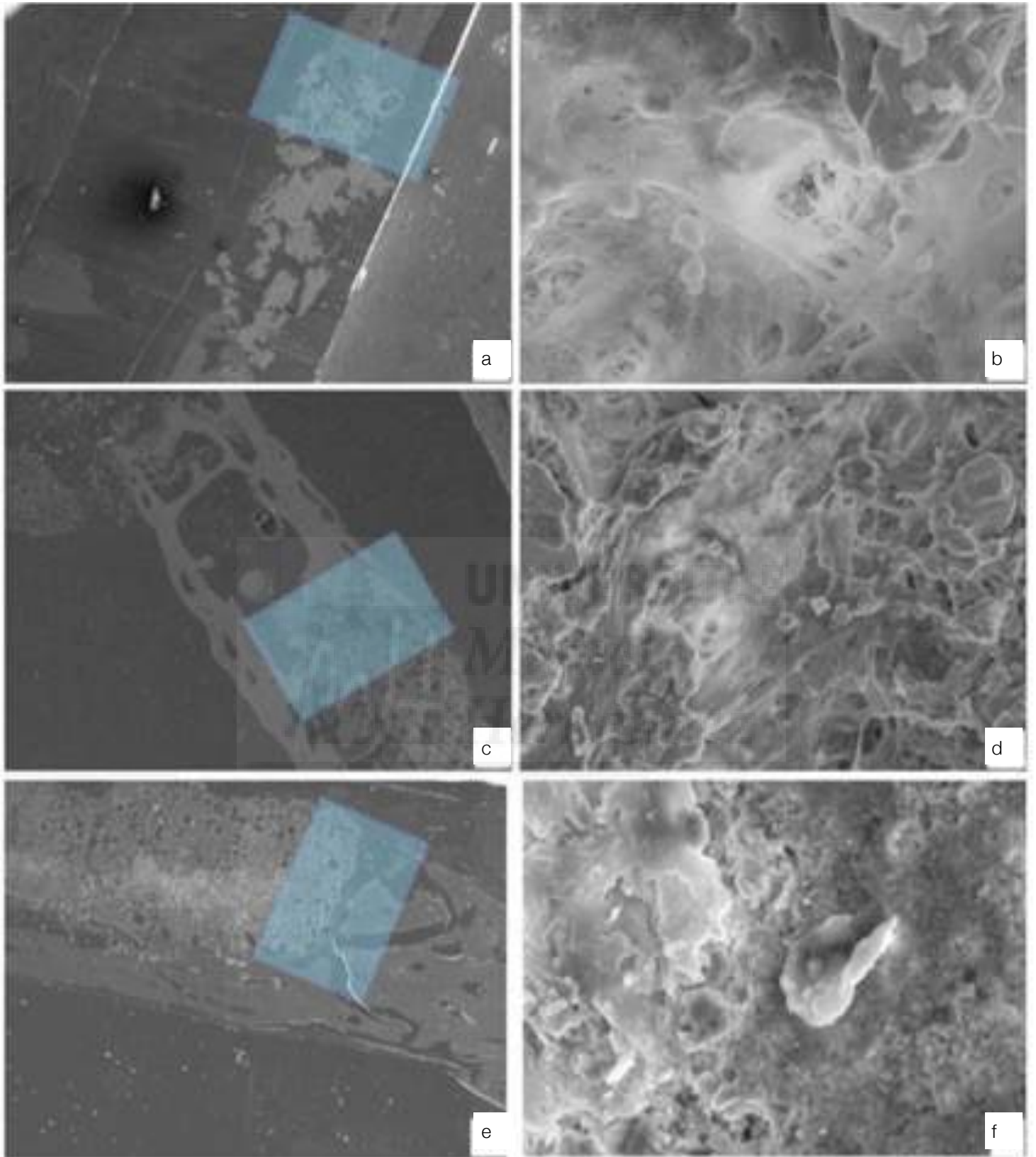


Figure 10. Post-extraction SEM images of samples in calvariae. Group A: panoramic and detailed (a, b); Group B: panoramic and detailed (c, d); and Group C: panoramic and detailed (e, f)

bone [Fig. (c)] and an equally cellular arrangement and growth over the graft [Fig. (d)]. In group C, a higher percentage of residual graft material was observed at 60 days

[Fig. (e)], as well as cellular surface growth and integration. The interrelation with the peripheral bone was worse in comparison with the other two composites [Fig. (f)]. EDS analysis showed higher content of Ca and P in the new bone region for the composites of higher collagen content.

In tibiae, SEM images showed complete integration of all specimens, without significant differences between the groups. In all cases, the cell growth was observed to be orderly and structured; there was cell attachment to the biomaterial and the establishment of an interface between the biomaterial and the old bone (Fig. 11). Examining the details of each panoramic image, Group A showed integration of the graft in the tibial bone (a), as well as cellular arrangement over the graft block (b). In Group B, integration existed in the surrounding bone (c) and an equally cellular arrangement and growth over the graft (d). In Group C, a higher percentage of residual graft material was observed at 60 days (e), as well as cellular surface growth, but integration arranged on the surface. The interrelation with the peripheral bone was worse in comparison with the other two composites (f). EDS analysis showed higher content of Ca and P in the new bone region for the composites of higher collagen content. The best results were recorded for Group A. The Ca/P ratio at the interface was best for Group A, as listed in Table 8.

Ca/P Ratio	New Bone			Residual Biomaterial			Interface		
	Group A	Group B	Group C	Group A	Group B	Group C	Group A	Group B	Group C
15 days	2.13 ± 0.23	2.19 ± 1.02	2.43 ± 0.10 *	2.22 ± 1.2	2.06 ± 1.43	2.44 ± 0.45 *	2.34 ± 0.99	2.23 ± 1.25	2.42 ± 0.59 *
30 days	2.23 ± 0.16	2.20 ± 0.65	2.46 ± 0.61 *	2.19 ± 1.02	2.12 ± 0.54	2.48 ± 1.01 *	2.29 ± 0.67	2.30 ± 1.11	2.41 ± 0.27
60 days	2.26 ± 0.64	2.23 ± 0.93	2.49 ± 1.23 *	2.23 ± 0.88	2.08 ± 0.43	2.45 ± 0.98 *	2.70 ± 1.02 *	2.06 ± 1.10	2.20 ± 0.75

Table 8: EDS analysis with content of Ca and P in the new bone region, interface and residual biomaterial for the composites at 15, 30 & 60 days. Non Parametric Friedmann Test. Significant differences (*) p<0.05. Mean ± Sd.

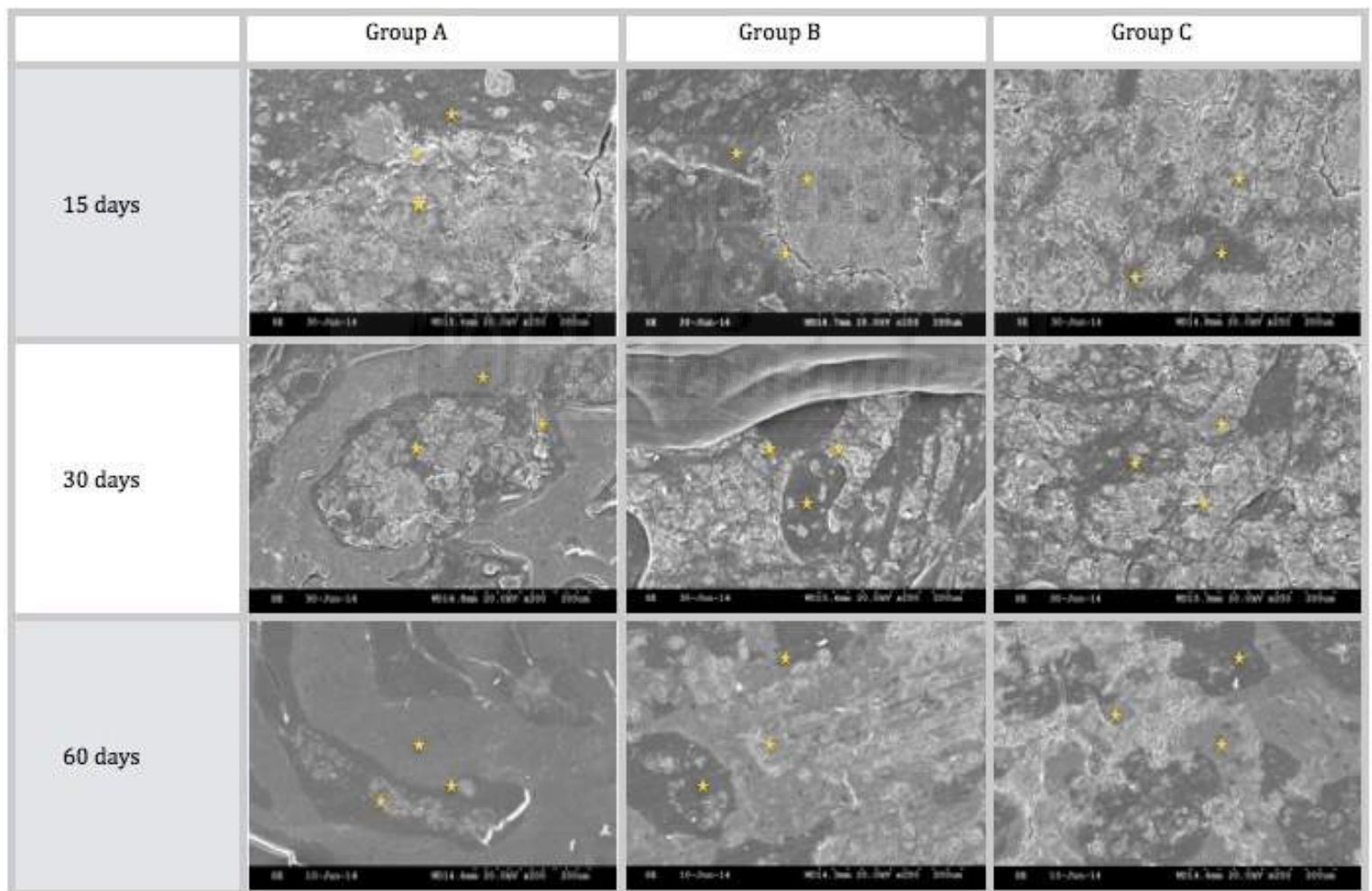


Figure 11: SEM analysis of samples in tibiae after 15, 30 & 60 days implantation showing biomaterials, interface and new bone; Group A (40/30/30), Group B (50/20/30) and Group C (60/20/20), images show correct integration of the implant and the absence of peripheral gaps surrounding the materials. (Original magnification: 50x; 200 μm).

The BSE imaging was used to highlight contrasts between resin, bone, and biomaterial. EDX was used to identify and evaluate the relative concentrations of all chemical elements present in the tissues, using point analysis to determine mineral distribution. EDX spectra were collected at discrete points in each biopsy (* from Fig. 11). Elemental composition (atomic %) of the graft materials and bone were calculated from the spectra.

In BSE images, particles of HA/TCP/ collagen implant were seen to be a white-gray color due to low organic content and a relatively high Ca/P ratio (atomic %), whereas newly formed bone had a darker gray color because of the presence of collagen, marrow, and fat. SEM-BSE evaluation confirmed that the residual graft particles were surrounded by newly formed bone, which presented characteristics of mature bone with well-organized lamellae and numerous small osteocytic lacunae (Fig. 11).

The bone-to-biomaterial interface was characterized by small numbers of projections of newly formed bone reaching into the graft particles. In many areas, much bigger regions containing exposed and partly loose parent implant particles were present, as a result of the material degradation in the physiological environment.

After 15 days of implantation, the implant was already well integrated into the host tissue, forming an irregular surface boundary caused by gradual degradation of the material, Fig. 11. The interface developed between the implant and the surrounded tissue was characterized by intermittent presence of calcium phosphate phase, which corresponded in structure and morphology to new bone tissue. The EDS analysis and histological studies backed up these findings. In many areas, much bigger regions containing exposed and partly

loose parent implant particles were present, as a result of the material degradation in the physiological environment. At 30 days, the outside surface of the implant presented active regions, where the degradation process of the material originated. These observations led to the conclusion that interfacial activities at 60 days were already well in progress, remodeling the chemistry and morphology of the interface.

5.4.4. Radiological study

Radiographs were obtained after sample extraction, observing integration with the host bone in all study groups. The radiographic density varied with the chemical content of the samples, with group A showing correct integration and partial resorption that corresponded to the histological findings [Fig. 12(a)]; group B behaved similarly and was seen to be fully integrated with the surrounding bone [Fig. 12(b)]; group C showed a greater presence of residual biomaterial and correct integration [Fig. 12(c)]. There was no spontaneous closure of the defect, as expected for a critical defect [Fig. 12(d)].

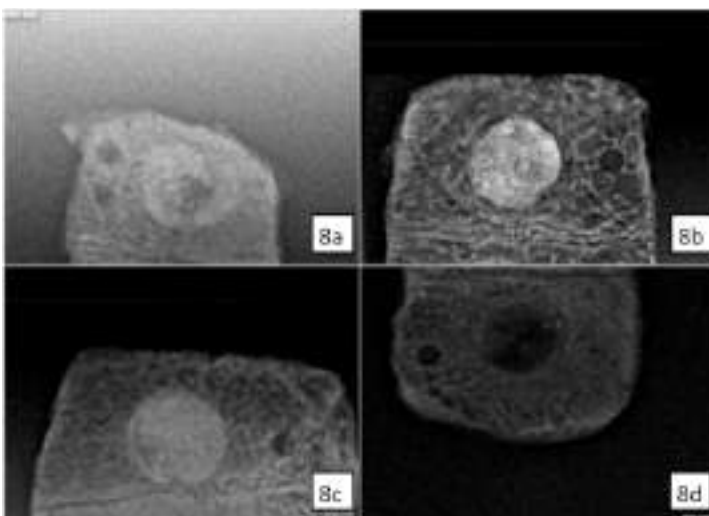


Figure 12. Radiological analysis of the implanted samples. Radiographic density: Group A (6a), Group B (6b), Group C (6c) and Control (6d).

In tibiae, radiographs were made following sample extraction, observing integration with the host bone in all study groups (Fig. 13). The radiographic density varied with the chemical content of the samples, with Group A showing correct integration and partial resorption that corresponded to the histological findings; Group B behaved similarly and was seen to be fully integrated with the surrounding bone; Group C showed a greater presence of residual biomaterial and correct integration. There was no spontaneous closure of the defect, as could be expected for a critical defect.

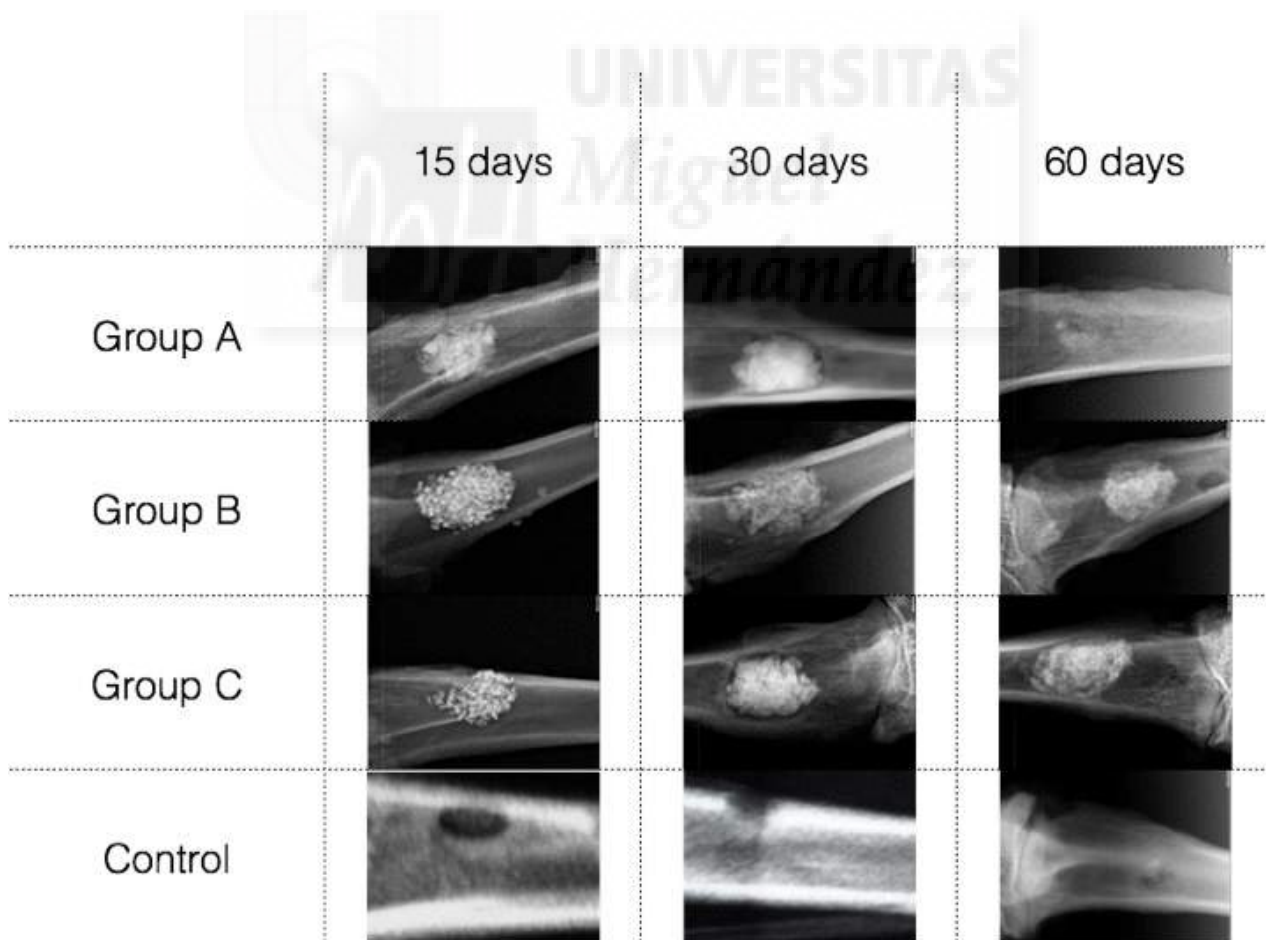


Figure 13: Radiological images of samples after 15, 30 & 60 days implantation showing remaining materials and control.



UNIVERSITAS
Miguel
ALEMÁN

DISCUSSION

6. DISCUSSION

Porous calcium-phosphate ceramic scaffolds were tested for their bone-healing capacity and osteoinductivity. Critical-sized calvarial wing defects were used to compare bone formation following the implantation of ceramics. For bone tissue engineering, the design of calcium phosphate scaffolds should mimic the structure and properties of the bone extracellular matrices and this study set out to produce and test scaffolds with physical and biological properties similar to natural bone. (Zheng et al. 2011).

Different composition ratios of HA/TCP/Collagen can also produce different biological responses and so an ideal balance between these two phases should improve the physical, mechanical properties as well as the biological behavior of calcium-phosphate scaffolds. The effect of collagen can be understood as a facilitator of the early stages of cell anchorage to the biomaterial and as a vehicle to allow the action of bone cells to initiate biomaterial and new bone substitution. Currently, several synthetic routes have been utilized for the preparation of calcium-phosphate ceramic powders with different composition ratios. In this study, a solid-state reaction followed by cold isostatic pressing was used successfully for preparation of porous calcium-phosphate ceramic scaffolds. This technique is simple and economical.

Brodie *et al.* 2006, reported that collagen coating increases the strength of HA/TCP 50/50 (wt%), whereas it weakens HA/TCP 25/75 (wt%) and pure TCP discs. These inconsistent mechanical behaviors are in accordance with our results.

All the materials in this study were found to offer biocompatibility, sufficient mechanical strength and did not produce any adverse inflammatory reactions at the insertion site. The fact that they are absorbable allowed their rapid replacement by the new bone without causing any reactions to foreign bodies. The fastest resorption rate of the material in Group

A> Group B> Group C (Study 1) was related to the percentage of HA in each material and also collagen in the composition. There were no inflammatory reactions either near the grafts or the controls. Rapid replacement by new bone allows a bone matrix to become established within the material, giving the host area physical properties similar to the bone (Ono et al. 2011).

A significant difference in resorption time and in the stability of the material was found in Group C, which showed greater stability and less resorption than the other groups.

The HA/ β -TCP scaffold in cylinder form allows a precise evaluation of resorption, dimensional stability and replacement by new bone (Ebrahimi et al. 2010). It is known that an appropriate concentration of collagen in this biomaterial acts as an integration stimulant, promoting bone matrix and ion exchange with the implant environment.

According to Araujo *et al.* 2010, who studied an *in vivo* experimental model, the material produced appropriate bone replacement, cell differentiation and stimulated osteoblasts, the authors observing increased amounts of mineralized bone and osteoblast activity.

Despite the New Zealand rabbit's rapid metabolic activity, other studies have established its validity as an experimental model for testing biomaterials used for bone replacement. (Calvo et al 2012) In view of this, the results in this study were enhanced through the creation of critical defects of 6 mm diameter, which will not close spontaneously and therefore demonstrate the regenerative potential of the biomaterials under observation.

Resorption patterns in the groups containing the highest percentage of collagen and less HA were more active than in the groups with lower percentages, which showed more irregular

shapes and became smoother as the collagen content was reduced. This corresponds to collagen's proven osteogenic capacity, increasing foci of resorption and new bone formation. In the study of bone-to-implant contact, all the materials showed appropriate percentages of integration. The presence of collagen in group A produced higher bone-to-implant contact values, with a much larger pattern of interdigitation in comparison with the other two groups. The addition of 30 wt% of collagen and the reduction in the HA content with higher presence of more soluble TCP also improved the rate of new bone formation at the implant periphery. The percentage of new bone formation for Group A samples was significantly higher than in the other groups; the presence of collagen allows internal replacement of the material by new bone within a favorable time span, as demonstrated by the presence of new bone within the material and at its periphery. (Maté et al. 2014).

The results obtained from the x-ray diffractometry on the ceramic composites powders show the presence of representative peaks from the β -TCP and HA phases for all the powder compositions, where only a slight variation in the intensities of the peaks between the compositions, which is related to the presence of the concentration of phases in % in each two phase powder composition.

The presence of a larger concentration of the matrix HA in the composites was prepared, which lead to a slight reduction of the specific surface for these compositions, if these results are associated to the HA matrix. This small variation in the specific surface between the compositions can be explained by the slight variation of the morphological characteristics, previously observed through the micrographs represented by figures 3a, 3b and 3b, (study 2) where there is a thin morphology of nanoparticles for the HA matrix. Morphological

characterization has shown that the powder HA has a morphology that is more refined than the powder β -TCP. It has been observed that this fine morphology of the powder HA has also influenced the values of the superficial area obtained by BET, showing slightly superior superficial area, for the compositions with a larger concentration of the matrix HA. These fine morphologies found can be a potential in the development of biomaterials for bone replacement and leads to innovative results in the microstructural level of microporosity and of surface grains and microporos. The literature shows that the developments of β -TCP-HA nanostructured powders and biphasics compositess have two basic targets: improve physical characteristics as open porosity, superficial area of grains and microporus, and biomaterial solubility.

In this paper (Study 2) three different compositions of the combination of hydroxyapatite, β -TCP and collagen are formulated. The differences in the proportions of the three synthesized materials must produce different reactions in vivo in animals which are implanted; as these variations of the composition will provide different resorption times, different mechanical, physical properties and therefore a different in vivo behavior of the tested biomaterials. (Keaveny et al. 1993)

The adaptation of the properties of the biomaterial to the receiving area in relation to the physical, mechanical properties, their structure and biological behavior directly affects the remodeling process. So the greater convergence is achieved between the biomaterial and the receiving area, the better it will behave the biomaterial. The effect of collagen can be understood as facilitating the early stages of cell anchorage to the biomaterial and as a vehicle allowing the action of bone cells to initiate biomaterial substitution by new bone.

Currently, several synthetic routes have been utilized for the preparation of calcium-phosphate ceramic powders with different composition ratios. In this study, a solid-state reaction followed by cold isostatic pressing was used successfully for preparation of porous calcium-phosphate ceramic scaffolds. This technique is simple and economical. (Dorozhkin et al. 2009).

The surface roughness of biomaterials directly influences the possibility to create a zone of facilitated cell anchorage. This synthesis process achieves a highly rough and irregular surface appearance with some micro-cracks, creating a favorable environment for the initial attachment of cells and the beginning of the process of bone remodeling. Studies of the effects of collagen on the behavior of ceramic composite scaffolds have not found any significant differences in physical-mechanical properties arising from different ratios of collagen content (Maté et al. 2014). Therefore, other factors such as porosity and density must play a major role in determining the physical, mechanical properties and biological behavior of HA/TCP/collagen ceramic scaffolds. When the present study data was compared with human bone (Table 2), the materials' Young's moduli were quite different from that of cortical bone but were closer to cancellous bone (Keaveny et al. 1993).

Brodie *et al.* 2007 reported that collagen coating increases the strength of HA/TCP 50/50 (wt%), whereas it weakens HA/TCP 25/75 (wt%) and pure TCP discs. These inconsistent mechanical behaviors are in accordance with our results.

One of the main disadvantages of the cold isostatic method is the poor mechanical strength of the materials for load bearing applications (Table 2). Although a highly porous scaffold is preferred, as it will favor bone cell adhesion and regeneration, this is achieved at the expense

of mechanical strength and resistance. However, the method can be improved by incorporating collagen into the composite material to achieve improved mechanical strength and optimum physicobiological properties.

Multiple light microscopy and SEM evaluations of the implant-bone interface show how the same structure is represented differently according to the examination method selected. The precision and reliability of a histomorphometric study of newly formed bone depends upon the correct identification and ultra structural characterization of all the cellular components that might play a role in the osseointegration process. Optical microscopy lacks the resolving power required for detailed structural analysis (Orsini et al. 2005; Wierzchos et al. 2008; Jasty et al. 1989).

SEM analysis of the samples studied, revealed intimate contact between biomaterials and bone receptor areas, with significant absences spaces that could lead to the conclusion that it is wrong the integration of biomaterials used. The three compositions behaved in a similar way, an increased mineral content observed in those samples where the hydroxyapatite content is higher (60%).

Elemental analysis of the bone tissue demonstrated the presence of calcium and phosphorus, pointing to the presence of mineralized bone tissue. This observation suggests that the graft surface may provide an optimal stratum for bone tissue ingrowth (Skedros et al. 1993; Ramirez et al. 2012). The highest concentrations of calcium in the interface region were recorded for group A, indicating the highest levels of new bone formation, due to the faster ion exchange rate in the interface area. The presence of extracellular Ca^{2+} resulting from resorption activity might be involved in the stimulation of osteoblasts.

Groups A and B had a high degree of porosity facilitating the implants' resorption process as the external and internal surface areas of the pores were exposed to the medium over the several microns distance beyond the graft body (as the results from the elemental mapping indicated), in turn facilitating osteoconduction. Analysis was carried out at a selection of different points, taking different points of interest from the middle and from the periphery of the samples to detect changes to Ca/P ratios. This element mapping revealed an increase in the areas of Ca and P reaching from within the biomaterial graft towards its periphery. It could be that this ion increases areas of biological apatite on the agglutinated Ca and P deposits and crystals, which in turn facilitate osteoconduction. In all cases, a decrease in the percentage of Ca and P was found in the residual biomaterial, with respect to the initial composition, while a gradual increase in the percentages of Ca and P ratio was found at the interface, suggesting an increase in the osteoinductive capacity of the material and replacement by new bone at its periphery.

In agreement with an earlier study of the mineral degradation process of β -tricalcium phosphate using the SEM-BSE technique (Calvo et al. 2012), the present study found a release of Ca and P ions, which was seen to promote new bone growth; it is possible that high levels of Ca and P stimulate osteogenesis due to their effects on osteoblast gene expression, as described by Lazary *et al.* 2007 [34]. In normal calcified bone, the Ca/P molar ratio increases with increasing calcification.

The three compositions studied were completely biocompatible with perfect mechanical properties to accommodate the environment in which they were implanted. All were gradually reabsorbed without producing any abnormal inflammatory reaction. This process

of partial and progressive resorption, allowed to create an ideal location for the gradual replacement by new bone. The fastest resorption rate of the material was in Group A > Group B > Group C and was related to the percentage of HA in each material and also collagen in the composition. (Ebrahimi et al. 2012). A significant difference in resorption time and in the stability of the material was found in Group C, which showed greater stability and less resorption than the other studied groups during 15, 30 and 60 days.

Thus the pattern of resorption and the grain size are two of the factors that will affect the handling and use of a biomaterial for bone regeneration and their potential clinical applications. Secondary surface porosity is established to start the resorption process on the surface of the material and the change of initial porosity to the final stage of the process of resorption, is directly related to the grain size and the ease of the cells to bind to the biomaterial surface. A completely resorbable ceramic has been the goal of several studies; however, a high rate of resorption or solubilization can interfere with bone formation as the biomaterial may degrade faster than the rate of bone formation. This phenomena leads to a change in the bioceramic's physical structure, i.e., loss of the concavity in the macropore and the mechanical stability of the surface, which will interfere with cell attachment (Yuan et al. 2001]. Moreover, the release of high concentrations of calcium to the microenvironment results in a change of the pH, promotes a mild inflammatory response and favors fibrous tissue formation (Chou et al. 2005). Furthermore, higher calcium ion levels have been shown to effect osteoclastic activity, varying from its inhibition to its stimulation or no effects (Berger et al. 2001; Zaidi et al. 2004).

The present study (study 3) has demonstrated that none of the HA granules used induced any toxic tissue reaction, i.e. necrosis or a severe inflammatory response. These findings reveal the purity of

the granules used and underline data which established a correlation between the presence of granule fragments within lymphatic nodes and their non purity (Yang et al. 2001). SEM and EDS analysis revealed a close relation between the newly formed bone matrix and the graft surface. The increase of surface porosity in the three study materials suggest that there is a rapid remodeling of the material surface due to the cellular action, increasing the size and number of the pores on the surface and thus enabling the arrival and anchor cell and bone resorption and replacement by new bone in the recipient area. Group III material with lower grain size is the fastest undergoes remodeling and thus a further increase in the secondary porosity, so it can be considered as the most active in terms of resorption and new bone formation. Elemental analysis of the bone tissue demonstrated the presence of calcium and phosphorus, pointing to the presence of mineralized bone tissue. This observation suggests that the graft surface may provide an optimal stratum for bone tissue ingrowth (Ramírez-Fernández et al. 2013). The highest concentrations of calcium in the interface region were recorded for group III, indicating the highest levels of new bone formation, due to the faster ion exchange rate in the interface area. The presence of extracellular Ca^{2+} resulting from resorption activity might be involved in the stimulation of osteoblasts.

Yamaguchi et al. showed that moderately high extracellular Ca^{2+} is a chemotactic and proliferating signal for osteoblasts and stimulates pre-osteoblast differentiation (Yamaguchi et al. 2010). Groups II and III had a small grain size, so improve the surface resorption and increase the surface porosity, facilitating the implants' resorption process as the external and internal surface areas of the pores were exposed to the medium over the several microns distance beyond the graft body (as the results from the elemental mapping indicated), in turn facilitating osteoconduction.

Analysis was carried out at a selection of different points, taking different points of interest from the middle and from the periphery of the samples to detect changes to Ca/P ratios. This element mapping revealed an increase in the areas of Ca and P reaching from within the biomaterial graft towards its periphery. It could be that this ion increases areas of biological apatite on the agglutinated Ca and P deposits and crystals, which in turn facilitate osteoconduction. In all cases, a decrease in the percentage of Ca and P was found in the residual biomaterial, with respect to the initial composition, while a gradual increase in the percentages of Ca and P ratio was found at the interface, suggesting an increase in the osteoinductive capacity of the material and replacement by new bone at its periphery.

In agreement with an earlier study of the mineral degradation process of β -tricalcium phosphate using the SEM-BSE technique (Calvo-Guirado et al. 2012; Lazáry et al. 2007), our study found a release of Ca and P ions, which was seen to promote new bone growth; it is possible that high levels of Ca and P stimulate osteogenesis due to their effects on osteoblast gene expression, as described by Lazáry et al. (Lazáry et al. 2007)) In normal calcified bone, the Ca/P molar ratio increases with increasing calcification.

All the materials in this study were found to offer biocompatibility, sufficient mechanical strength and did not produce any adverse inflammatory reactions at the insertion site. The fact that they are absorbable allowed their replacement by new bone without causing any reactions to foreign bodies. The fastest resorption rate of the material was in Group III > Group II > Group I and was related to the granulometry of each material. There were no inflammatory reactions near either the grafts or the controls. Rapid replacement by new bone allows a bone matrix to become established

within the material, giving the host area physical properties similar to the bone (Ebrahimi et al. 2012).

A significant difference in resorption time and in the stability of the material was found in Group I, which showed greater stability and less resorption than the other groups.





CONCLUSIONS

7. CONCLUSIONS

- Ceramic synthetic biomaterials of HA / β -TCP can be used as bone substitutes in situations of bone regeneration process. Due of its high safety, dimensional stability and its bimodal behavior, offers an effective alternative to other graft materials. Biomaterials proved to be biocompatible, bioresorbable and osteoconductive.
- The inclusion of collagen in the composition of the biomaterial provides a medium to accelerating bone regeneration, since it allows the prompt arrival cell and replacing it with new bone material.
- The cold isostatic method was used successfully for fabricating HA/TCP/Collagen ceramic scaffolds of desired shape and high porosity.
- SEM and elemental analysis revealed that newly formed bone was closely attached to the synthetic material, there was a gradual diffusion of Ca ions from the biomaterial into the newly forming bone at the interface.
- Changes in the size, porosity and crystallinity of one HA-based bone substitute material can influence the integration of the biomaterials within the implantation site and the new bone formation. High porosity led to cell and fiber in-growth within the center of the bone substitute, while lowering the porosity gave the material “place holder” properties. The HA with high porosity, low crystallinity and low granule size present low stability and high resorption rate.
- This study demonstrates that variations in the physical properties of a bone substitute material clearly influence in the tissue reaction. As a consequence, biomaterials can be designed to demand depending on the needs of resorption, dimensional stability and handling needed for each case.

7. CONCLUSIONES

- Los biomateriales compuestos, sintéticos cerámicos de HA / β -TCP pueden utilizarse como sustitutos óseos en regeneración ósea. Debido a su alta seguridad, estabilidad dimensional y su comportamiento bimodal, ofrece una alternativa eficaz a otros materiales de injerto. Se ha demostrado que son materiales biocompatibles, bioabsorbibles y osteoconductivos.
- La inclusión de colágeno en la composición del material compuesto de HA/TCP proporciona un medio de acelerar la regeneración ósea, ya que permite a la célula un medio de actuación rápido y formar nuevo material óseo.
- El estudio por SEM y el análisis elemental, reveló que el hueso recién formado se encuentra estrechamente unido al material sintético, produciéndose una difusión gradual de iones de Ca desde el biomaterial a la interfase neoformada.
- Los cambios en el tamaño, la porosidad y la cristalinidad de un material de sustitución ósea basada en HA pueden influir en la integración de los biomateriales. El material poroso de HA con alta porosidad, baja cristalinidad y baja granulometría disminuye la estabilidad y aumenta la tasa de reabsorción del mismo.
- Este estudio demuestra que las variaciones en las propiedades físicas de un material de sustitución ósea influyen claramente en la reacción de los tejidos. Como consecuencia, los biomateriales pueden ser diseñados a demanda en función de las necesidades de la reabsorción, estabilidad dimensional y manipulación necesarios para cada caso.



REFERENCES

8. REFERENCES

Araujo MG, Liljenberg B, Lindhe J. Dynamics of Bio-Oss Collagen incorporation in fresh extraction wounds: An experimental study in the dog. *Clin Oral Impl Res* 2010;21:55–64.

Baksh D, Davies JE & Kim S. Three dimensional matrices of calcium polyphosphates support bone growth in vitro and in vivo. *Journal Material Science Material Medicine* 1998; 9: 743–748.

Berger CE, Rathod H, Gillespie JJ, Horrocks BR & Datta HK. Scanning electrochemical microscopy at the surface of bone-resorbing osteoclasts: Evidence for steady-state disposal and intracellular functional compartmentalization of calcium. *Journal of Bone and Mineral Research* 2001; 16: 2092-2102.

Betz MW, Yeatts AB, Richbourg WJ, Caccamese JF, Coletti DP, Falco EE & Fisher JP. Macroporous Hydrogels Upregulate Osteogenic Signal Expression and Promote Bone Regeneration. *Biomacromolecules* 2010; 11: 1160-1168.

Brodie JC, Merry J & Grant MH. The mechanical properties of calcium phosphate ceramics modified by collagen coating and populated by osteoblasts. *Journal Material Science Materials Medicine* 2006; 17: 43–48.

Broggini N, Bosshardt DD, Jensen SS, Bornstein MM, Wang CC & Buser D. Bone healing around nanocrystalline hydroxyapatite, deproteinized bovine bone mineral, biphasic calcium phosphate, and autogenous bone in mandibular bone defects. *Journal Biomedical Materials Research B: Appl Biomaterials* 2014; 103(7): 1478-87

Byrne EM, Farrell E, McMahon LA, Haugh MG, O'Brien FJ, Campbell VA, Prendergast PJ & O'Connell BC. Gene expression by marrow stromal cells in a porous collagen-glycosaminoglycan scaffold is affected by pore size and mechanical stimulation. *Journal of Materials Science: Materials in Medicine* 2008; 19: 3455–3463.

Calvo JL, Delgado RA, Ramirez MP, Mate JE, Ortiz A, Abboud M. Histomorphometric and mineral degradation study of Ossceram: A novel biphasic B-tricalcium phosphate, in critical size defects in rabbits. *Clin Oral Implants Res* 2012;23:667–675.

Carvalho AL, Faria PE, Grisi MF, Souza SL, Taba MJ, Palioto DB, Novaes AB, Fraga AF, Ozyegin LS, Oktar FN & Salata LA. Effects of granule size on the osteoconductivity of bovine and synthetic hydroxyapatite: a histologic and histometric study in dogs. *Journal of Oral Implantology* 2007; 33: 267-76.

Chou YF, Huang W, Dunn LC, Miller TA & Wu BM. The effect of biomimetic apatite structure on osteoblast viability, proliferation and gene expression. *Biomaterials* 2005; 26: 285-295.

Daculsi G, Laboux O, Malard O, Weiss P. Current state of the art of biphasic calcium phosphate bioceramics. *J Mater Sci Mater Med* 2003; 14:195–200.

Dorozhkin SV. Calcium orthophosphate-based biocomposites and hybrid biomaterials. *J Mater Sci* 2009; 44:2343–2387.

Ebrahimi M, Pripatnanont P, Monmaturapoj N, Suttapreyasri S. Fabrication and characterization of novel nano hydroxyapatite/ b-tricalcium phosphate scaffolds in three different composition ratios. *J Biomed Mater Res A* 2012;100(9):2260–2268.

Fan H, Ikoma T, Tanaka J, Zhang X. Surface structural biomimetics and the osteoinduction of calcium phosphate biomaterials. *Nanosci Nanotechnol* 2007; 7:808–813.

Gauthier O, Bouler JM, Aguado E, Legeros RZ, Pilet P, Daculsi G. Elaboration conditions influence physicochemical properties and in vivo bioactivity of macroporous biphasic calcium phosphate ceramics. *J Mater Sci Mater Med* 1999; 10:199–204.

Giannoudis PV, Dinopoulos H & Tsiridis E. Bone substitutes: an update. *Injury* 2005; 36: 20–27.

Ginebra MP, Traykova T & Planell JA. Calcium phosphate cements as bone drug delivery systems: a review. *Journal Control Release*. 2006; 113: 102–110.

Habibovic P & de Groot K. Osteoinductive biomaterials--properties and relevance in bone repair. *Journal of Tissue Engineering and Regenerative Medicine* 2007; 1: 25-32.

Habibovic P, Krzyt MC, Juhl MV, Clyens S, Martinetti R, Dolcini L, Theilgaard N & van Blitterswijk, C.A. Comparative in vivo study of six hydroxyapatite-based bone graft substitutes. *Journal of Orthopaedic Research* 2008; 26: 1363-1370.

Hing KA, Wilson LF & Buckland T. Comparative performance of three ceramic bone graft substitutes. *The Spine Journal* 2007; 7: 475-490.

Hollister SJ, Maddox RD & Taboas JM. Optimal design and fabrication of scaffolds to mimic tissue properties and satisfy biological constraints. *Biomaterials* 2002; 23: 4095-4103.

Huang Y, Zhou G, Zheng L, Liu H, Niu X & Fan Y. Micro-/nano sized hydroxyapatite directs differentiation of rat bone marrow derived mesenchymal stem cells towards an osteoblast lineage. *Nanoscale* 2012; 4: 2484–2490.

Hulbert SF, Morrison SJ & Klawitter JJ. Tissue reaction to three ceramics of porous and non-porous structures. *Journal of Biomedical Materials Research* 1972; 6: 347-374.

Jasty M, Bragdon CR, Schutzer S, Rubash H, Haire T, Harris WH. Bone ingrowth into porous coated canine total hip replacements. Quantification by backscattered scanning electron microscopy and image analysis. *Scanning Microsc* 1989; 3:1051-1057.

Julien M, Khairoun I, LeGeros RZ, Delplace S, Pilet P, Weiss P, Daculsi G, Bouler JM & Guicheux J. Physico-chemical-mechanical and in vitro biological properties of calcium phosphate cements with doped amorphous calcium phosphates. *Biomaterials* 2007; 28: 956-965.

Karageorgiou V & D Kaplan. Porosity of 3D biomaterial scaffolds and osteogenesis. *Biomaterials* 2005; 26: 5474-5491.

Kasten P, Beyen I, Niemeyer P, Luginbühl R, Böhner M & Richter W. Porosity and pore size of beta-tricalcium phosphate scaffold can influence protein production and osteogenic differentiation of human mesenchymal stem cells: an in vitro and in vivo study. *Acta Biomaterialia* 2008; 4: 1904-1915.

Keaveny TM & Hayes WC. Mechanical Properties of Cortical and Trabecular Bone. *Bone Growth*, 1993; 285-344. Boca Raton, FL: CRC Press.

Kim K, Dean D, Mikos AG & Fisher JP. Effect of initial cell seeding density on early osteogenic signal expression of rat bone marrow stromal cells cultured on cross-linked poly(propylene fumarate) disks. *Biomacromolecules* 2009; 10: 1810-1817.

Klenke FM, Liu Y, Yuan H, Hunziker EB, Siebenrock KA & Hofstetter W. Impact of pore size on the vascularization and osseointegration of ceramic bone substitutes in vivo. *Journal of Biomedical Materials Research Part A* 2008; 85: 777-786.

Krekmanov L. The efficacy of various bone augmentation procedures for dental implants: A Cochrane systematic review of randomized controlled clinical trials. *Int J Oral Maxillofac Implants* 2006; 21:696-710.

Lazary A, Balla B, Kosa JP, Bacsi K, Nagy Z. & Takacs I. Effect of gypsum on proliferation and differentiation of MC3T3-E1 mouse osteoblastic cells. *Biomaterials* 2007; 28: 393-399.

LeGeros RZ, Lin S, Rohanizadeh R, Mijares D & LeGeros JP. Biphasic calcium phosphate bioceramics: Preparation, properties and applications. *Journal of Materials Science: Materials in Medicine* 2003; 14: 201-209.

Le Nihouannen D, Duval L, Lecomte A, Julien M, Guicheux J, Daculsi G & Layrolle P. Interactions of total bone marrow cells with increasing quantities of macroporous calcium

phosphate ceramic granules. *Journal of Materials Science: Materials in Medicine* 2007; 18: 1983-1990.

MacMillan AK, Lamberti FV, Moulton JN, Geilich BM & Webster TJ. Similar healthy osteoclast and osteoblast activity on nanocrystalline hydroxyapatite and nanoparticles of tri-calcium phosphate compared to natural bone. *International Journal Nanomedicine* 2014; 9: 5627–5637.

Maté-Sánchez de Val JE, Calvo-Guirado JL, Delgado-Ruiz RA, Gomez-Moreno G, Ramirez-Fernandez MP & Romanos GE Bone neo-formation and mineral degradation of 4Bone. Part I: material characterization and SEM study in critical size defects in rabbits. *Clinical Oral Implants Research* 2014; 26 (10) :1165-9.

Mate-Sanchez de Val JE, Mazon P, Guirado JL, Ruiz RA, Ramirez Fernandez, MP, Negri B, ,Abboud M & De Aza PN. Comparison of three hydroxyapatite/b-tricalcium phosphate/collagen ceramic scaffolds: an in vivo study. *Journal Biomedical Materials Research A*. 2014; 102: 1037– 1046.

Mistry AS & Mikos AG. Tissue engineering strategies for bone regeneration. *Advances in Biochemical Engineering/Biotechnology* 2005; 94: 1-22.

Moyle DD, Klawitter JJ & Hulbert SF. Mechanical properties of the bone-porous biomaterial interface: elastic behavior *Journal of Biomedical Materials Research* 1973; 7: 363-382.

Murphy CM, Haugh MG & O'Brien FJ. The effect of mean pore size on cell attachment, proliferation and migration in collagen-glycosaminoglycan scaffolds for bone tissue engineering. *Biomaterials* 2010; 31: 461-466.

Ogose A, Kondo N, Umezu H, Hotta T, Kawashima H, Tokunaga K, Ito T, Kudo N, Hoshino M, Gu W & Endo N. Histological assessment in grafts of highly purified beta-tricalcium phosphate (OSferion) in human bones. *Biomaterials* 2006; 27: 1542-1549.

Ono D, Jimbo R, Kawachi G, Ioku K, Ikeda T & Sawase T. Lateral bone augmentation with newly developed b-tricalcium phosphate block: an experimental study in the rabbit mandible. *Clinical Oral Implants Research* 2011; 22: 1366-1371.

Orsini G, Traini T, Scarano A, Degidi M, Perrotti V, Piccirilli M, Piatelli A. Maxillary sinus augmentation with Bio-Oss particles: A light, scanning, and transmission electron

microscopy study in man. *J Biomed Mater Res Part B: Appl Biomater* 2005; 74:448–457.

Petrie Aronin CE, Sadik KW, Lay AL, Rion DB, Tholpady SS, Ogle RC & Botchwey EA. Comparative effects of scaffold pore size, pore volume, and total void volume on cranial bone healing patterns using microsphere-based scaffolds. *Journal of Biomedical Materials Research Part A* 2009; 89: 632-641.

Ramirez MP, Calvo JL, Mate JE, Delgado RA, Negri B, Barona C. Ultrastructural study by backscattered electron imaging and elemental microanalysis of bone-to-biomaterial interface and mineral degradation of porcine xenografts used in maxillary sinus floor elevation. *Clin Oral Implants Res* 2013; 24:523–530.

Rawlings CE. Modern bone substitutes with emphasis on calcium phosphate ceramics and osteoinductors. *Neurosurgery* 1993; 33: 935–938.

Rivera-Munoz E, Diaz JR, Rogelio Rodriguez J, Brostow W, Castano VM. Hydroxyapatite spheres with controlled porosity for eye ball prosthesis: Processing and characterization. *J Mater Sci Mater Med* 2001; 12: 305–311.

Schmitz JP, Hollinger JO & Milam SB. Reconstruction of bone using calcium phosphate bone cements: a critical review. *Journal of Oral & Maxillofacial Surgery* 1999; 57: 1122–1126.

Skedros JG, Bloebaum RD, Bachus KN, Boyce TM, Constantz B. Influence of mineral content and composition on gray levels in backscattered electron images of bone. *J Biomed Mater Res* 1993; 27:57–64.

Spector M. Anorganic bovine bone and ceramic analogs of bone mineral as implants to facilitate bone regeneration. *Clinics in Plastic Surgery* 1994; 21: 437–444.

Wierzchos J, Falcioni T, Kiciak A, Wolinski J, Koczorowski R, Chomiccki P, Porembaska, M., Ascaso, C. Advances in the ultrastructural study of the implant–bone interface by backscattered electron imaging. *Micron* 2008; 39:1363–1370.

Wiltfang J, Merten HA, Schlegel KA, Schultze-Mosgau S, Kloss FR, Rupprecht S, et al. Degradation characteristics of alpha and beta tricalcium-phosphate (TCP) in minipigs. *J Biomed Mater Res* 2002; 63:115–121.

Yamauchi K, Takahashi T, Funaki K, Hamada Y, Yamashita Y, Histological and histomorphometrical comparative study of b-tricalcium phosphate block grafts and periosteal expansion osteogenesis for alveolar bone augmentation. *Int J Oral Maxillofac Surg* 2010; 39:1000–1006.

Yuan H, de Bruijn JD, Li Y, Feng J, Yang Z, de Groot K & Zhang X. Bone formation induced by calcium phosphate ceramics in soft tissue of dogs: A comparative study between porous alpha-TCP and beta-TCP. *Journal of Materials Science: Materials in Medicine* 2001; 12: 7-13.

Yang S, Leong KF, Du Z & Chua CK. The design of scaffolds for use in tissue engineering. Part I. Traditional factors. *Tissue Engineering* 2001; 7: 679-689.

Yuasa T, Miyamoto Y, Kon M, Ishikawa K, Takeuchi M, Momota Y, Tatehara S, Takano H, Mimamiguchi S & Nagayama M. Proliferation and differentiation of cultured MC3T3-E1 osteoblasts on surface-layer modified hydroxyapatite ceramic with acid and heat treatments. *Dental Materials Journal* 2005; 24: 207–212.

Zaidi M, Moonga BS & Huang CL. Calcium sensing and cell signaling process in the local regulation of osteoclastic bone resorption. *Biological reviews of the Cambridge Philosophical Society* 2004; 79: 79-100.

Zheng L, Yang F, Shen H, Hu X, Mochizuki C, Sato M, Wang S & Zhang Y. The effect of composition of calcium phosphate composite scaffolds on the formation of tooth tissue from human dental pulp stem cells. *Biomaterials* 2011; 32: 7053–7059.





APPENDIX I

Published Papers

José E. Maté Sánchez de Val
José L. Calvo-Guirado
Gerardo Gómez-Moreno
Carlos Pérez-Albacete
Martínez
Patricia Mazón
Piedad N. De Aza

Influence of hydroxyapatite granule size, porosity, and crystallinity on tissue reaction *in vivo*. Part A: synthesis, characterization of the materials, and SEM analysis

Authors' affiliations:

José E. Maté Sánchez de Val, International Research Cathedra, UCAM, Universidad Católica San Antonio, Murcia, Spain

José L. Calvo-Guirado, International Research Cathedra, UCAM, Universidad Católica San Antonio, Murcia, Spain

Gerardo Gómez-Moreno, Periodontology and Implant Dentistry, Pharmacological Research in Dentistry Group, Special Care in Dentistry, Faculty of Dentistry, University of Granada, Granada, Spain

Carlos Pérez-Albacete Martínez, Murcia University, Murcia, Spain

Patricia Mazón, Departamento de Materiales, Óptica y Tecnología Electrónica, Universidad Miguel Hernández, Avda. Universidad s/n, Elche (Alicante), Spain

Piedad N. De Aza, Instituto de Bioingeniería, Universidad Miguel Hernández, Avda. Universidad s/n, Elche (Alicante), Spain

Corresponding author:

José E. Maté-Sánchez de Val
Plaza los Luceros nº 15 Bajo izq.
Zip Code: 03004
Alicante
Spain
Tel.: +00 + 34 + 637 477 932.
Fax: +965145695
e-mail: jemate@ucam.edu

Key words: characterization, hydroxyapatite, *in vivo*, SEM, synthesis

Abstract

Objective: The aim of this study was the synthesis and analysis of the tissue reaction to three different Hydroxyapatite (HA)-based bone substitute materials differing only in granule size, porosity, and crystallinity through an animal experimental model at 60 days.

Materials and methods: Three different HA-based biomaterials were synthesized and characterized by X-ray diffraction, SEM, and EDS analysis, the resultant product was ground in three particle sizes: Group I (2000–4000 μm), Group II (1000–2000 μm), and Group III (600–1000 μm). Critical size defects were created in both tibias of 15 rabbits. Four defects per rabbit for a total of 60 defects were grafted with the synthesized materials as follows: Group I (15 defects), Group II (15 defects), Group III (15 defects), and empty (15 defects control). After animals sacrifice at 60 days samples were obtained and processed for SEM and EDS evaluation of Ca/P ratios, elemental mapping was performed to determine the chemical degradation process and changes to medullary composition in all the four study groups.

Results: The tendency for the density was to increase with the increasing annealing temperature; in this way it was possible to observe that the sample that shows highest crystallinity and crystal size corresponding to that of group I. The SEM morphological examination showed that group III implant showed numerous resorption regions, group II implant presented an average resorption rate of all the implants. The group I displayed smoother surface features, in comparison with the other two implants.

Conclusion: The data from this study show that changing the size, porosity, and crystallinity of one HA-based bone substitute material can influence the integration of the biomaterials within the implantation site and the new bone formation.

The reconstruction of bone defects with synthetic bone substitutes requires their adaptation to the size and the location of the defects. Changes in the physico-chemical properties of bone substitute materials, i.e., porosity, shape, and size, are described as influencing the outcome of new bone formation and bone regeneration (Hulbert et al. 1972) and even promoting osteoinductive properties (Habibovic & de Groot 2007; Habibovic et al. 2008); (Carvalho et al. 2007).

Calcium phosphate ceramics have been widely applied as bone substitutes, coatings, cements, drug delivery systems, and tissue engineering scaffolds due to their resemblance to the mineral portion of the bone tissue, relative ease in processing and good cell attachment (Gauthier et al. 1999; Barrère

et al. 2006; Le Nihouannen et al. 2007; Khan et al. 2008). Its biocompatibility, safety, predictability, unlimited availability, lower morbidity for the patient, and cost effectiveness represent important advantages over autografts and allografts (Schawartz et al. 1999; Le Nihouannen et al. 2007) and make them a good choice for reconstructive surgery, orthopedics, dentistry, maxillo and craniofacial surgeries, spinal arthrodesis, and neurosurgery (Schawartz et al. 1999; Le Nihouannen et al. 2007; Schindler et al. 2008).

Over the years, several modifications on parameters such as sintering temperature, pH and purity of the starting products have given rise to calcium phosphates with distinct chemical and physical characteristics such as specific surface areas, surface energy, surface

Date:
Accepted 8 October 2015

To cite this article:

Maté Sánchez de Val JE, Calvo-Guirado JL, Gómez-Moreno G, Martínez CP-A, Mazón P, De Aza PN. Influence of hydroxyapatite granule size, porosity, and crystallinity on tissue reaction *in vivo*. Part A: synthesis, characterization of the materials, and SEM analysis. *Clin. Oral Impl. Res.* 00, 2015, 1–8
doi: 10.1111/clr.12722

charge, roughness, grain size, and porosity (Gauthier et al. 1999; LeGeros et al. 2003; Hing et al. 2007; Julien et al. 2007; Le Nihouannen et al. 2007). There is widespread evidence the influence of grain size in the process of integration and regeneration of biomaterials for bone regeneration. This size directly affects the absorption patterns of the materials used as well as the possibility of improving the mechanical properties of materials. Knowledge of appropriate grain size for each clinical situation and the use of treatment options to help achieve better end results in regenerative therapies.

The ability of a scaffold to enhance osteogenic signal expression and support new bone formation is largely dependent on the pore size and porosity of the scaffold. Porosity refers to the overall percentage of void space within a solid, whereas pore size reflects the diameter of individual voids in the scaffold (Karageorgiou & Kaplan 2005; Mistry & Mikos 2005; Murphy et al. 2010). The importance of scaffold porosity and pore size can be attributed to the native structure of bone which itself is a porous tissue. Cortical bone is largely a dense structure, but within it exists pores that give an overall porosity of 10% (Kim et al. 2009). Conversely, trabecular bone is a highly porous structure with typical porosity values between 50 and 90%. Porous regions of cortical bone allow for vascularization and cellular infiltration of the structure. Porosity and pore size have significant ramifications on the ability of tissue engineering scaffolds to support bone regeneration for several reasons. First, porosity and pore size have been shown to affect cell attachment efficiency which consequently impacts the cell seeding density, cell distribution, and cell migration (Hollister et al. 2002; Klenke et al. 2008). These factors have been shown to affect osteogenic differentiation through changes in signaling distances (Byrne et al. 2008). Moreover, pore size and porosity have a significant effect on the mechanical strength of a scaffold. Sufficient scaffold strength to provide mechanical support to a defect is often required of a hard tissue engineering scaffold such as bone, especially when the bone is load bearing (Kasten et al. 2008). Furthermore, porosity and pore size affect the ability of the scaffold to promote *in vivo* osteoconduction and vascularization. Integration of native tissue into a scaffold is fostered through growth into interconnected pores, thus both optimal and minimal pore sizes have been established to support tissue ingrowth (Alsberg et al. 2001; Karageorgiou & Kaplan 2005; Sundelacruz & Kaplan 2009; Betz et al. 2010). Finally, pore

size and porosity affect *in vivo* and *in vitro* cell signaling which in turn affects osteoblastic differentiation of MSCs and the production of extracellular matrix (ECM) proteins (Yang et al. 2001). It has been established that pore sizes of at least 40 μm are required for minimal bone in growth, whereas pore sizes of 100–350 μm are considered optimal (Moyle et al. 1973). In a study analyzing the effect of pore size and porosity on bone healing in a critical size rat cranial defect, it was shown that smaller pore sizes (100 μm) induce greater amounts of bone healing than larger pore sizes (500 μm) (Petrie Aronin et al. 2009). This study also found a link to porosity, scaffold swelling, and degradation. In this work, highly porous HA samples are subjected to an *in vivo* evaluation to evaluate bone recolonization and the efficiency of the mean pore and crystallinity in a new elaborated HA scaffold ceramic using polyurethane sponges as a template.

The aim of this study was the synthesis and analysis of the tissue reaction to three Hydroxyapatite (HA) with different particle size-based bone substitute materials differing only in granule size, porosity, and crystallinity through an animal experimental model at 60 days.

Material and methods

Animal experimentation

The experimental protocol was approved by the Ethical Committee of the University of Murcia (Spain) following the local and European regulations. Fifteen male New Zealand rabbits of 3.5–4.5 Kg in weight were used. General anesthesia included ketamine plus chlorbutol (5–8 mg/Kg intravenously), 0.5–1 mg/Kg acepromazine maleate as a coadjuvant, and 0.05 mg/Kg atropine. Amoxicillin (0.1 ml/Kg intramuscularly) was administered at the end of surgery. Two defects were performed in each tibiae for a

total of 60 defects and four groups were created – Group I filled with hydroxyapatite granules (2000–4000 μm), Group II filled with hydroxyapatite granules (1000–2000 μm), Group III filled with hydroxyapatite granules (600–1000 μm), and Group IV empty defect.

Surgical procedure

Two critical defects (6 mm \varnothing) were created in each tibia. The surgical approach was in the proximal–medial area of the tibiae, several millimeters below the frontal tuberosity. Bone tissue was removed with spherical surgical drills of 6 mm in internal diameter at low rotation speed with constant irrigation (Fig. 1a, b & c). Distance between defects was of 5 mm.

Graft implants preparation

The sol–gel method was used for preparing the HA slurry as follows: first, the appropriate amounts of $\text{Ca}[\text{NO}_3]_2 \cdot 4\text{H}_2\text{O}$ and P_2O_5 were separately dissolved in ethanol to form 1.67 and 0.5 mol/l solutions, respectively. The prepared solutions with Ca/P molar ratio of 10 : 6, which is the observed Ca/P ratio in HA, were mixed together. The mixture was then stirred at room temperature using a magnetic stirrer for 1 h. Porous scaffolds were fabricated by impregnating a polyurethane sponge with the slurry. The sponge block was dipped into the slurry and compressed slightly to remove the excess slurry on the foam. After the sponge was dried at 70°C for 1 h, and then heat treatment at: (a) 600°C during 1 h, (b) 800°C during 1 h, and (c) 1000°C during 1 h. From these temperatures the samples were slow cooled inside the furnace until room temperature. Finally the resultant product was ground in three different grain sizes of Group I (2000–4000 μm), Group II (1000–2000 μm), and Group III (600–1000 μm).

Graft implants characterization

To analyze the HA graft implants; these were reduced to powder and spread over the ana-

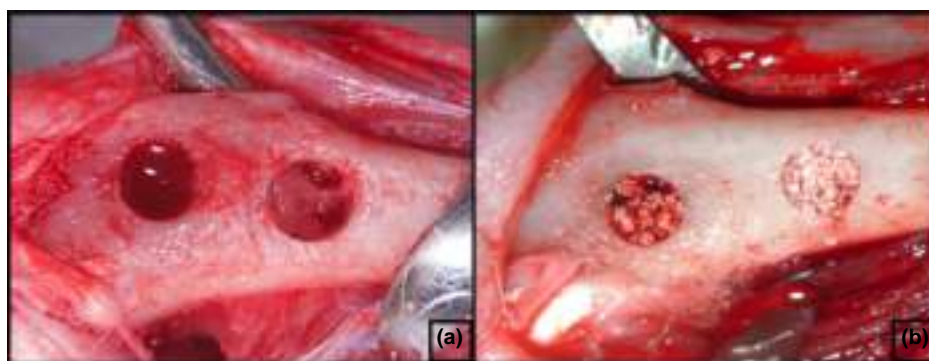


Fig. 1. Detail of surgical procedure. The surgical approach was in the proximal–medial area of the tibiae.

lytical cylindrical sample holder of the X-ray diffractometer Bruker-AXS D8 Advance (XRD). XRD patterns were recorded from θ to 2θ scans in parafocusing Bragg-Brentano geometry with line focused copper $K\alpha$ (λ_{Cu} , $k\alpha1 = 1.54056\text{\AA}$) radiation from a conventional sealed tube source. The diffractometer was equipped with a scintillation detector. Scans were taken from 20 to 50° (2θ) in 0.05° steps with counting times of 6s per step.

The crystal size of the HA samples was estimated from the XRD patterns using the Scherrer equation (Patterson 1939). According to the equation, a single crystal dimension perpendicular to the (hkl) plane (D_{hkl} , nm) can be estimated from the peak broadening as

$$D_{hkl} = \frac{k\lambda}{B_{1/2} \cos\theta_{hkl}}$$

where k is the Scherrer constant (0.89) which depends on the crystal shape, the diffraction line indexes (Shull 1946), and the dispersion of crystallite sizes of the powder, λ is the wavelength of the Cu $K\alpha$ ($\lambda = 1.54056\text{\AA}$); $B_{1/2}$ corresponds to full width at half maximum (rad) for (hkl) reflection, and θ_{hkl} is the diffraction angle ($^\circ$). The line broadening of the (300) reflection corresponding to the maximum intensity peak was used to evaluate the crystal size.

To determine the porosity of the prepared ceramic, three samples of the foams were selected for each sintering temperature and each composition and the porosity of the bulk specimens was measured by Archimedes method. The apparent porosity, which measures the interconnected porosity, was determined by weighing the dry ceramic (W_d), and then reweighing the ceramic both when it is suspended in water (W_s) and after it is removed from the water (W_w).

$$\text{Apparent porosity} = \left[\frac{W_w - W_d}{W_w - W_s} \times 100 \right]$$

The true porosity includes both interconnected and closed pores. The true porosity, which better correlates with the properties of the ceramic, is given by the following equation:

$$\text{True porosity} = \left[\frac{\rho - B}{\rho} \times 100 \right]$$

where

$$B = \frac{W_d}{W_w - W_s}$$

B is the bulk density and r is the theoretical density or specific gravity of the ceramic. The bulk density is the weight of the ceramic divided by its volume.

The functional groups and structural changes in the samples were measured using Fourier-transformed infrared spectroscopy (FTIR-ThermoNicolet IR200, Waltham, MA, USA). The FTIR spectra were recorded between 400 and 4000/cm at 2/cm resolution. The pellets were prepared by mixing each sample powder with KBr matrix at a level of 1 wt%. The background data were collected for the KBr matrix and subtracted from each spectrum. All spectra were recorded at ambient temperature.

The microstructure and the composition of the HA graft implants were characterized using a scanning electron microscope (SEM, HITACHI S-3500N, Japan). Quantitative analyses were made by an electronic dispersive X-ray spectroscopy (EDX) system coupled to the electron microscope (Oxford Instruments INCA 300 EDX Analytical System (Abingdon, Oxfordshire, UK) using ZAF (atomic number, absorption, and fluorescence) correction software and Bayer standards. Microanalysis data were obtained from the mean of 10 independent determinations. Every sample was embedded in an epoxy polymer with vacuum, polished with diamond paste down to $1\ \mu\text{m}$, and etched with diluted acetic acid (1.0%v/v) for 6 s. Then, they were gently cleaned in an ultrasonic bath with distilled water, dried and palladium coated under an argon atmosphere using a sputtering machine (Polaron K550X Sputter Coater, Germany) for SEM-EDS observations.

Scanning electron microscopy

Fifteen samples of each material were studied before and 60 days after implantation comparing variations in Ca/P ratios. The samples were fixed by immersion in 4% formalin solution,

dehydrated in a graded ethanol series, and embedded in plastic resin (Technovit A 7210VCL; Kulzer & Co, Hanau, Germany). They were then polished using a manual grinder with 800 grit silicon carbide paper, mounted on an aluminum stub, and carbon coated (using a Polaron sputter coater). Samples were examined using the above-mentioned SEM-EDS at a working distance of 19 mm, an acceleration voltage of 15 kv and $15\times$ magnification. The areas of interest were outlined by the inner cortical walls and reached into the medullary core. Elemental mapping was performed to determine the chemical degradation process and changes to medullary composition in all four study groups.

Statistical analysis

Statistical analysis was performed using PASW Statistics v.22.0.0 software (SPSS Inc, IBM, New Orchard Road, Armonk, NY, USA). Values were recorded as means \pm standard deviation and medians. Friedman test was applied for the comparison of the medians, assuming level of significance of 95% ($P < 0.05$).

Results

Material characterization

Fig. 2 shows the XRD patterns of the HA graft implants, sintered at a different temperatures in the range of 600°C to 1000°C . The diffraction patterns have been identified for those belonging to the HA phase. Good agreement was found between the XRD pattern of the prepared HA powder (Fig. 2) and the stoichiometric HA [XRD JCPDS data file No. 09-0432.]. No new phase (after sintering) is formed. The lower temperatures, 600°C and 800°C , the shift was significant suggesting a great lattice distortion. Based on XRD patterns, the crystal

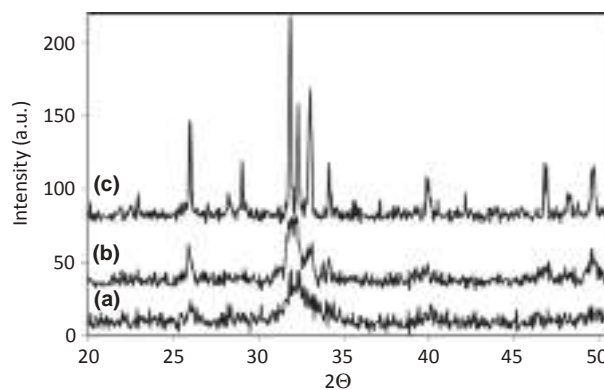


Fig. 2. XRD of the HA grafts (a) at 600°C , (b) at 800°C , and (c) at 1000°C .

size of HA graft implants studied are given in Table 1. The crystal size increased with the increasing temperature of sintering from 325 nm to 732 nm. Table 2 summarizes physical properties of HA graft as a function of sintering temperature. The sample that shows highest crystallinity and crystal size corresponding to that of group I. The differences in density are not very significant.

Fig. 3 displays the FTIR spectra of the milled samples after thermal treatment in the range 600–1000°C for 1 h. In general, the characteristic groups of apatites are PO₄³⁻, OH⁻, and HPO₄²⁻ groups which commonly appears in 4000–400/cm region in the FTIR spectra (Klenke et al. 2008; Mistry & Mikos 2005; Moyle et al. 1973). The characteristic bands of the synthesized materials are: After 1 h of sintering, two bands were detected at 3432.2 and 1642.6/cm as a result of the vibration of the adsorbed water in apatites. These

bands shifted to 3236.5 and 1684.3/cm, 3200.1 and 1684.5/cm, after heating at 800, and 1000°C, respectively. The intensity of these bands declined dramatically after thermal treatment especially at 1000°C. Also the PO₄³⁻ bands shifted for the annealed sample at 800°C in comparison with the heat-treated specimen at 1000°C. With an increasing of the annealing temperature, the PO₄³⁻ vibration peaks merged gradually.

Fig. 4 shows SEM micrographs of the HA grafts sintered at 600, 800, and 1000°C for 1 h. SEM micrographs showed that the obtained HA grafts structure consisted of a highly spherical porous network with the pore size of 0.5 mm in average.

SEM and EDS analysis

Fig. 5 presents the micrographs of the implants' cross sections after the implantation for 60 days. The SEM morphological examination showed that all the implants were well integrated into the host tissue, and developed an uneven surface caused by their gradual degradation. The group III implant showed numerous resorption regions (marked by the arrows in the Fig. 5e, F), mainly on its surface, and also more uneven surface morphology in comparison with the other implants. The group II implant presented an average resorption rate of all the implants.

The group I (Fig. 5a, b) displayed smoother surface features, in comparison with the other two implants.

According to the EDS analysis and high magnification SEM examination of the interfaces developed between all the studied implants and the surrounded tissue, the reaction zone was characterized by the intermittent presence of calcium phosphate phase, which corresponded in structure and morphology to a new bone tissue. Also the Ca/P ratio related to new bone formation level was greater in the group I implant in comparison with the other groups (Table 3).

Discussion

Crystallite size is an indication of the crystallinity of the material and can be defined as the average size of a domain within a material that has a coherently diffracting the monocrystalline structure. By increasing the sintering temperature, the XRD patterns of the HA graft exhibited an increase in peak height and a decrease in peak width, thus indicating an increase in crystallinity and crystallite size. The crystal size is inversely proportional to the peak width. The broadening of the peaks was evident at lower sintering temperatures,

Table 1. Heat treatment and the physical characteristic of the HA graft

	Heat Treatment	Crystalline phase	Grain size (µm)
Group I	1000°C	HA	2000-4000
Group II	800°C	HA	1000-2000
Group III	600°C	HA	600-1000

Table 2. Physical properties of HA graft as a function of sintering temperature. Friedman test was applied for the comparison of the medians, assuming level of significance of 95% (p < 0.05)

	Crystal size (nm)			Porous size (mm)			True Porosity (%)			Apparent Porosity (%)		
	Mean ± SD	Median	P-value	Mean ± SD	Median	P-value	Mean ± SD	Median	P-value	Mean ± SD	Median	P-value
Group I	325	325	0.16	0.5 ± 0.1	0.5	0.21	71 ± 1.9*	71	0.01	51 ± 2*	51	0.03
Group II	458	458	0.13	0.5 ± 0.1	0.5	0.17	67 ± 1.4	67	0.21	46 ± 1.8	46	0.14
Group III	732*	732	0.00	0.6 ± 0.1*	0.6	0.02	65 ± 1.8	65	0.11	45 ± 1.7	45	0.09

*Significant differences.

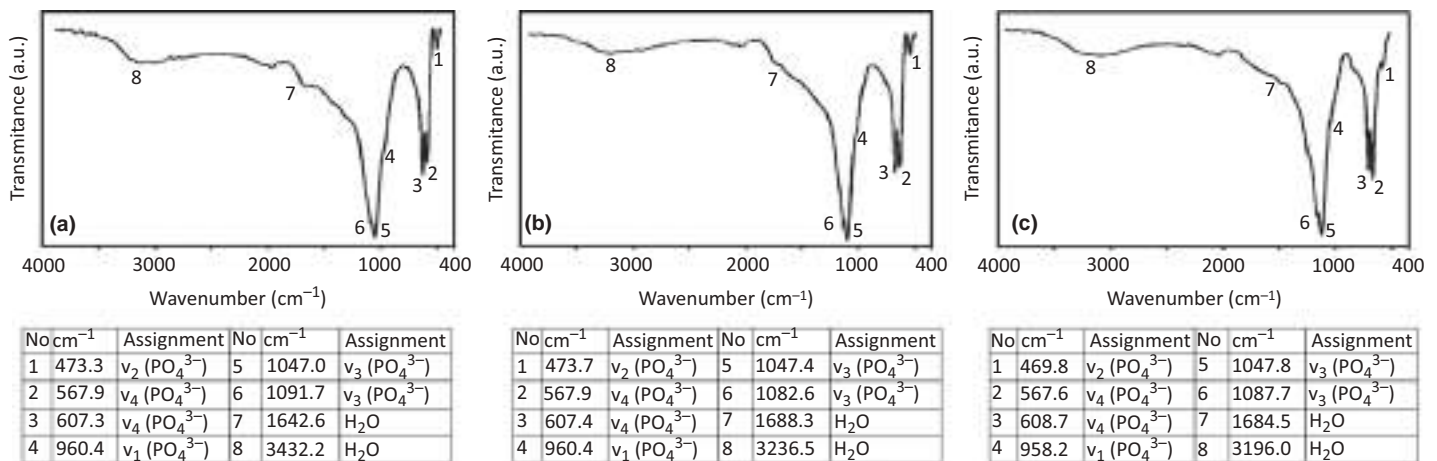


Fig. 3. FITR of the HA grafts (a) at 600°C, (b) at 800°C, and (c) at 1000°C.

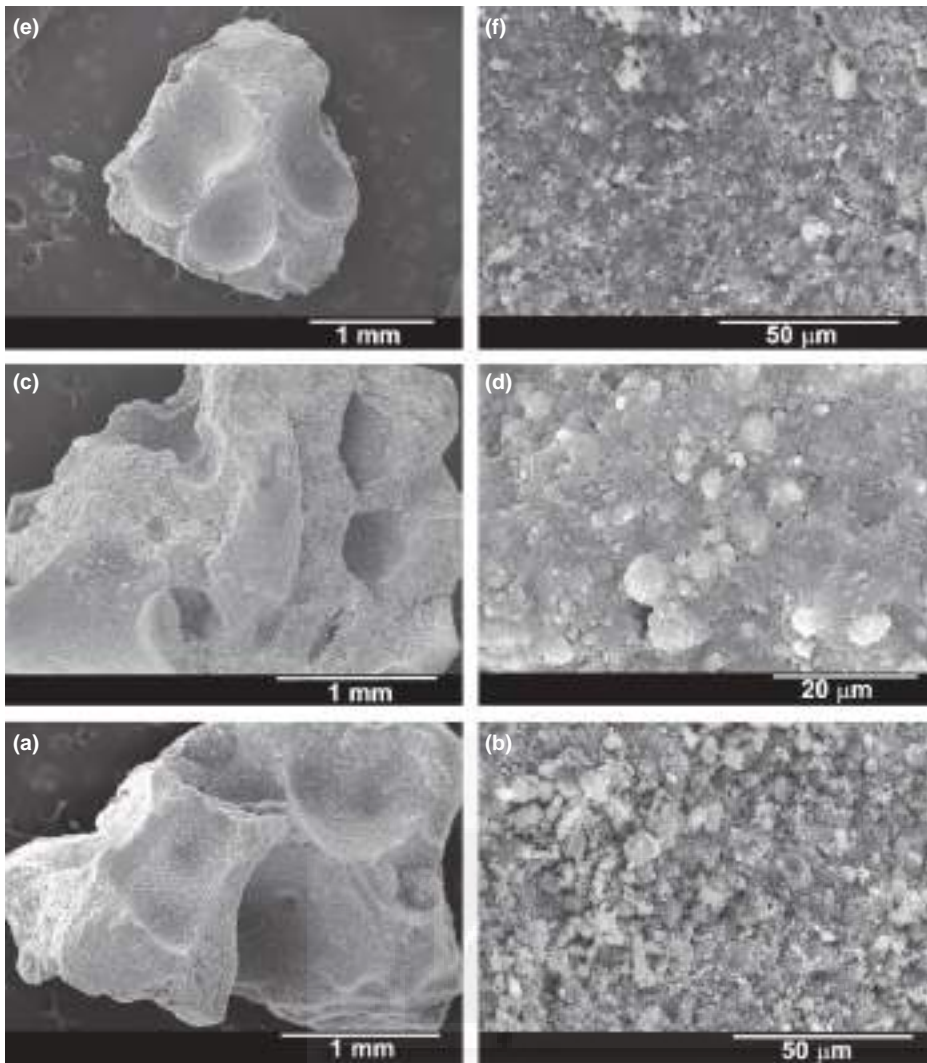


Fig. 4. SEM micrographs of the HA grafts (a,b) at 600°C, (c,d) at 800°C, and (e,f) at 1000°C.

indicating the initial state of crystal formation. At higher sintering temperatures, the growth of the crystal was evidenced by the sharpening to the peaks. Related with physical properties, the tendency for the density was to increase with the increasing annealing temperature.

In agreement with an earlier study of the mineral degradation process of β -tricalcium phosphate using the SEM-BSE technique (Calvo-Guirado et al. 2012; Lazáry et al. 2007), our study found a release of Ca and P ions, which was seen to promote new bone growth; it is possible that high levels of Ca and P stimulate osteogenesis due to their effects on osteoblast gene expression, as described by Lazáry et al. (Lazáry et al. 2007)) In normal calcified bone, the Ca/P molar ratio increases with increasing calcification.

The fact that they are absorbable allowed their replacement by new bone without causing any reactions to foreign bodies. The fastest resorption rate of the material was in Group III > Group II > Group I and was

related to the granulometry of each material. There were no inflammatory reactions near either the grafts or the controls. Rapid replacement by new bone allows a bone matrix to become established within the material, giving the host area physical properties similar to the bone (Ebrahimi et al. 2012). A significant difference in resorption time and in the stability of the material was found in Group I, which showed greater stability and less resorption than the other groups.

According to Araújo et al. (Araújo et al. 2010), who studied an *in vivo* experimental model, the material produced appropriate bone replacement, cell differentiation, and stimulated osteoblasts, the authors observing increased amounts of mineralized bone and osteoblast activity. A completely resorbable ceramic has been the goal of several studies; (Carvalho et al. 2007), however, a high rate of resorption or solubilization can interfere with bone formation as the biomaterial may

degrade faster than the rate of bone formation. This phenomena leads to a change in the bioceramic's physical structure, i.e., loss of the concavity in the macropore and the mechanical stability of the surface, which will interfere with cell attachment (Yuan et al. 2001). Moreover, the release of high concentrations of calcium to the microenvironment results in a change of the pH, promotes a mild inflammatory response and favors fibrous tissue formation (Chou et al. 2005). Furthermore, higher calcium ion levels have been shown to effect osteoclastic activity, varying from its inhibition to its stimulation or no effects. In the same way, element Na K in group I is not present, whereas in group II it represents (0.65) weight % and in group III represents (9.61) weight %. Previous studies demonstrated that inhibition of Na-dependent phosphate transport in the osteoclast led to reduced ATP levels and diminished bone resorption. (Berger et al. 2001; Yang et al. 2001; Zaidi et al. 2004). SEM and EDS analysis revealed a close relation between the newly formed bone matrix and the graft surface. Group III material with lower grain size is the fastest undergoes remodeling and thus a further increase in the secondary porosity, so it can be considered as the most active in terms of resorption and new bone formation. Elemental analysis of the bone tissue demonstrated the presence of calcium and phosphorus, pointing to the presence of mineralized bone tissue. This observation suggests that the graft surface may provide an optimal stratum for bone tissue ingrowth (Ramírez-Fernández et al. 2013). The highest concentrations of calcium in the interface region were recorded for group III, indicating the highest levels of new bone formation, due to the faster ion exchange rate in the interface area. The presence of extracellular Ca^{2+} resulting from resorption activity might be involved in the stimulation of osteoblasts.

Yamaguchi et al. showed that moderately high extracellular Ca^{2+} is a chemotactic and proliferating signal for osteoblasts and stimulates pre-osteoblast differentiation (Yamauchi et al. 2010). Groups II and III had a small grain size, so improve the surface resorption and increase the surface porosity, facilitating the implants' resorption process as the external and internal surface areas of the pores were exposed to the medium over the several microns distance beyond the graft body (as the results from the elemental mapping indicated), in turn facilitating osteoconduction. Analysis was carried out at a selection of different points, taking different points of inter-

Table 3. EDS analysis at the interface of the HA grafts after 60 days implantation. Values as Medians. Friedman test was applied for the comparison of the medians, assuming level of significance of 95% ($P < 0.05$)

Element	Group I		Group II		Group III		P values
	Weight%	Atomic%	Weight%	Atomic%	Weight%	Atomic%	
C K	21.93	43.17	7.77	13.69	28.00*	44.91	0.02
O K	16.14	23.86	45.07*	59.61	31.32	37.71	0.01
Na K			0.65	0.60	9.61*	5.98	0.03
P K	13.75	10.49	14.41	9.84	19.27*	9.26	0.02
Ca K	32.02*	18.89	30.01	15.84	11.80	2.14	0.01
Pd L	16.16*	3.59	2.09	0.42			0.03
Totals	100.00		100.00		100.00		
Ca/P	2.38*	1.8	2.08	1.60	0.61	0.23	0.01

*Significant differences.

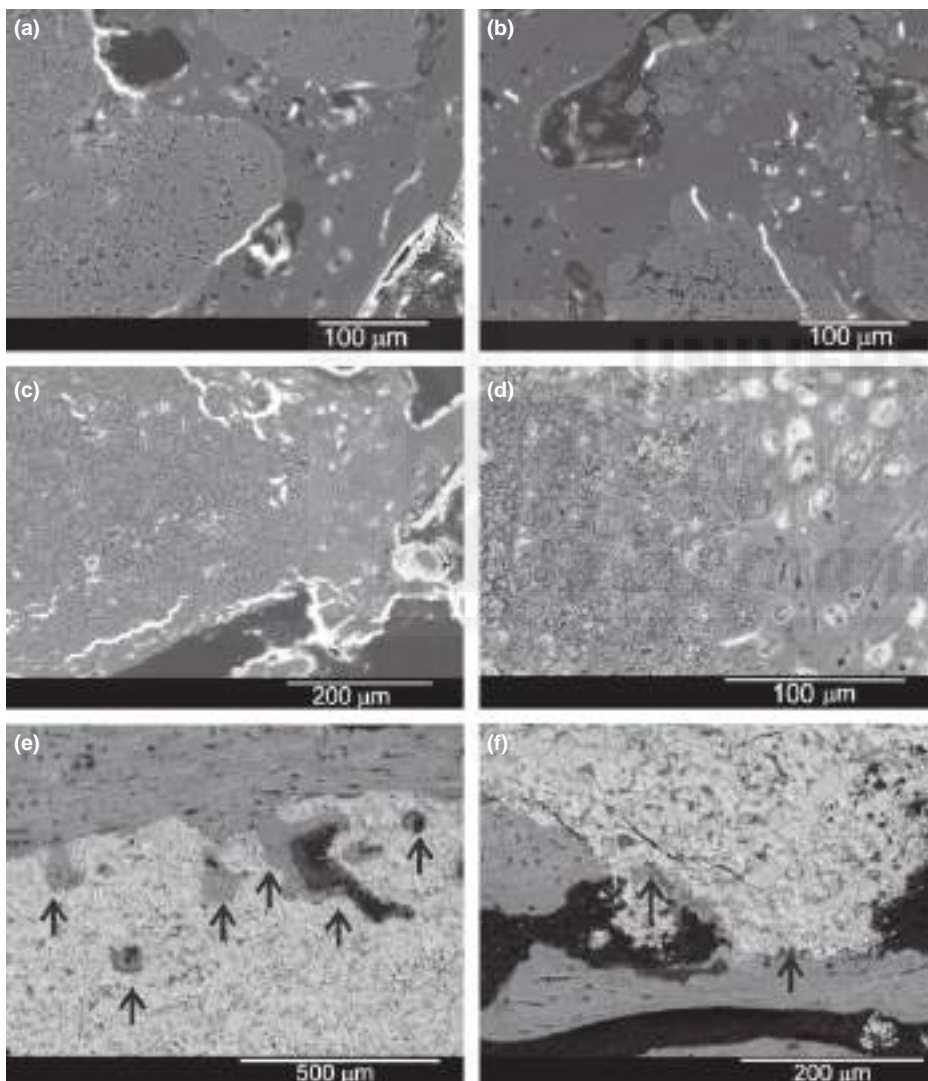


Fig. 5. SEM micrographs of the 60 days HA grafts implants. (a,b) at 1000°C, (c,d) at 800°C, and (e,f) at 600°C.

est from the middle and from the periphery of the samples to detect changes to Ca/P ratios. This element mapping revealed an

increase in the areas of Ca and P reaching from within the biomaterial graft toward its periphery. It could be that this ion increases

areas of biological apatite on the agglutinated Ca and P deposits and crystals, which in turn facilitate osteoconduction. In all cases, a decrease in the percentage of Ca and P was found in the residual biomaterial, with respect to the initial composition, whereas a gradual increase in the percentages of Ca and P ratio was found at the interface, suggesting an increase in the osteoinductive capacity of the material and replacement by new bone at its periphery.

Despite the New Zealand rabbit's rapid metabolic activity, other studies have established its validity as an experimental model for testing biomaterials used for bone replacement (Calvo-Guirado et al. 2012). In view of this, the results in this study were enhanced through the creation of critical defects of 6 mm diameter, which will not close spontaneously and therefore demonstrate the regenerative potential of the biomaterials under observation (Sharifi et al. 2012).

In conclusion, the data from this study show that changing the size, porosity, and crystallinity of one HA-based bone substitute material can influence positively the integration of the biomaterial within the implantation site and the new bone formation.

Acknowledgement: Part of this work has been supported by a Spanish Ministry of Economy and Competitiveness (MINECO); contract grant number: MAT2013-48426-C2-2-R.

Conflict of interest

The authors declare that they have no conflict of interest.

References

- Alsberg, E., Hill, E.E. & Mooney, D.J. (2001) Craniofacial tissue engineering. *Critical Reviews in Oral Biology & Medicine* **12**: 64–75.
- Araújo, M.G., Liljenberg, B. & Lindhe, J. (2010) Dynamics of Bio-Oss Collagen incorporation in fresh extraction wounds: an experimental study in the dog. *Clinical Oral Implants Research* **21**: 55–64.
- Barrère, F., van Blitterswijk, C.A. & de Groot, K. (2006) Bone regeneration: molecular and cellular interactions with calcium phosphate ceramics. *International Journal of Nanomedicine* **1**: 317–332.
- Berger, C.E., Rathod, H., Gillespie, J.I., Horrocks, B.R. & Datta, H.K. (2001) Scanning electrochemical microscopy at the surface of bone-resorbing osteoclasts: evidence for steady-state disposal and intracellular functional compartmentalization of calcium. *Journal of Bone and Mineral Research* **16**: 2092–2102.
- Betz, M.W., Yeatts, A.B., Richbourg, W.J., Caccamese, J.F., Coletti, D.P., Falco, E.E. & Fisher, J.P. (2010) Macroporous Hydrogels Upregulate Osteogenic Signal Expression and Promote Bone Regeneration. *Biomacromolecules* **11**: 1160–1168.
- Byrne, E.M., Farrell, E., McMahon, L.A., Haugh, M.G., O'Brien, F.J., Campbell, V.A., Prendergast, P.J. & O'Connell, B.C. (2008) Gene expression by marrow stromal cells in a porous collagen-glycosaminoglycan scaffold is affected by pore size and mechanical stimulation. *Journal of Materials Science: Materials in Medicine* **19**: 3455–3463.
- Calvo-Guirado, J.L., Delgado-Ruiz, R.A., Ramírez-Fernández, M.P., Maté-Sánchez, J.E., Ortiz-Ruiz, A. & Marcus, A. (2012) Histomorphometric and mineral degradation study of Ossceram: a novel biphasic B-tricalcium phosphate, in critical size defects in rabbits. *Clinical Oral Implants Research* **23**: 667–675.
- Carvalho, A.L., Faria, P.E., Grisi, M.F., Souza, S.L., Taba, M.J., Palioto, D.B., Novaes, A.B., Fraga, A.F., Ozyegin, L.S., Oktar, F.N. & Salata, L.A. (2007) Effects of granule size on the osteoconductivity of bovine and synthetic hydroxyapatite: a histologic and histometric study in dogs. *The Journal of Oral Implantology* **33**: 267–276.
- Chou, Y.F., Huang, W., Dunn, L.C., Miller, T.A. & Wu, B.M. (2005) The effect of biomimetic apatite structure on osteoblast viability, proliferation and gene expression. *Biomaterials* **26**: 285–295.
- Ebrahimi, M., Pripattanont, P., Monmaturoj, N. & Suttapreyasri, S. (2012) Fabrication and characterization of novel nano hydroxyapatite/ β -tricalcium phosphate scaffolds in three different composition ratios. *Journal of Biomedical Materials Research Part A* **100**: 2260–2268.
- Gauthier, O., Boulter, J.M., Aguado, E., LeGeros, R.Z., Pilet, P. & Daculsi, G. (1999) Elaboration conditions influence physicochemical properties and *in vivo* bioactivity of macroporous biphasic calcium phosphate ceramics. *Journal of Materials Science: Materials in Medicine* **10**: 199–204.
- Habibovic, P. & de Groot, K. (2007) Osteoinductive biomaterials—properties and relevance in bone repair. *Journal of Tissue Engineering and Regenerative Medicine* **1**: 25–32.
- Habibovic, P., Kruyt, M.C., Juhl, M.V., Clyens, S., Martinetti, R., Dolcini, L., Theilgaard, N. & van Blitterswijk, C.A. (2008) Comparative *in vivo* study of six hydroxyapatite-based bone graft substitutes. *Journal of Orthopaedic Research* **26**: 1363–1370.
- Hing, K.A., Wilson, L.F. & Buckland, T. (2007) Comparative performance of three ceramic bone graft substitutes. *The Spine Journal* **7**: 475–490.
- Hollister, S.J., Maddox, R.D. & Taboas, J.M. (2002) Optimal design and fabrication of scaffolds to mimic tissue properties and satisfy biological constraints. *Biomaterials* **23**: 4095–4103.
- Hulbert, S.F., Morrison, S.J. & Klawitter, J.J. (1972) Tissue reaction to three ceramics of porous and non-porous structures. *Journal of Biomedical Materials Research* **6**: 347–374.
- Julien, M., Khairoun, I., LeGeros, R.Z., Delplace, S., Pilet, P., Weiss, P., Daculsi, G., Boulter, J.M. & Guicheux, J. (2007) Physico-chemical-mechanical and *in vitro* biological properties of calcium phosphate cements with doped amorphous calcium phosphates. *Biomaterials* **28**: 956–965.
- Karageorgiou, V. & Kaplan, D. (2005) Porosity of 3D biomaterial scaffolds and osteogenesis. *Biomaterials* **26**: 5474–5491.
- Kasten, P., Beyen, I., Niemeyer, P., Luginbühl, R., Bohner, M. & Richter, W. (2008) Porosity and pore size of beta-tricalcium phosphate scaffold can influence protein production and osteogenic differentiation of human mesenchymal stem cells: an *in vitro* and *in vivo* study. *Acta Biomaterialia* **4**: 1904–1915.
- Khan, Y., Yaszemski, M.J., Mikos, A.G. & Laurencin, C.T. (2008) Tissue engineering of bone: material and matrix considerations. *The Journal of Bone and Joint Surgery (American Volume)* **90**: 36–42.
- Kim, K., Dean, D., Mikos, A.G. & Fisher, J.P. (2009) Effect of initial cell seeding density on early osteogenic signal expression of rat bone marrow stromal cells cultured on cross-linked poly(propylene fumarate) disks. *Biomacromolecules* **10**: 1810–1817.
- Klenke, F.M., Liu, Y., Yuan, H., Hunziker, E.B., Siebenrock, K.A. & Hofstetter, W. (2008) Impact of pore size on the vascularization and osseointegration of ceramic bone substitutes *in vivo*. *Journal of Biomedical Materials Research Part A* **85**: 777–786.
- Lazáry, A., Balla, B., Kósa, J.P., Bácsi, K., Nagy, Z., Takács, I., Varga, P.P., Speer, G. & Lakatos, P. (2007) Effect of gypsum on proliferation and differentiation of MC3T3-E1 mouse osteoblastic cells. *Biomaterials* **28**: 393–399.
- Le Nihouannen, D., Duval, L., Lecomte, A., Julien, M., Guicheux, J., Daculsi, G. & Layrolle, P. (2007) Interactions of total bone marrow cells with increasing quantities of macroporous calcium phosphate ceramic granules. *Journal of Materials Science: Materials in Medicine* **18**: 1983–1990.
- LeGeros, R.Z., Lin, S., Rohanizadeh, R., Mijares, D. & LeGeros, J.P. (2003) Biphasic calcium phosphate bioceramics: preparation, properties and applications. *Journal of Materials Science: Materials in Medicine* **14**: 201–209.
- Mistry, A.S. & Mikos, A.G. (2005) Tissue engineering strategies for bone regeneration. *Advances in Biochemical Engineering/Biotechnology* **94**: 1–22.
- Moyle, D.D., Klawitter, J.J. & Hulbert, S.F. (1973) Mechanical properties of the bone-porous biomaterial interface: elastic behavior. *Journal of Biomedical Materials Research* **7**: 363–382.
- Murphy, C.M., Haugh, M.G. & O'Brien, F.J. (2010) The effect of mean pore size on cell attachment, proliferation and migration in collagen-glycosaminoglycan scaffolds for bone tissue engineering. *Biomaterials* **31**: 461–466.
- Patterson, A.L. (1939) The Scherrer formula for X-ray particle size determination. *Physical Review* **56**: 978.
- Petrie Aronin, C.E., Sadik, K.W., Lay, A.L., Rion, D.B., Tholpady, S.S., Ogle, R.C. & Botchwey, E.A. (2009) Comparative effects of scaffold pore size, pore volume, and total void volume on cranial bone healing patterns using microsphere-based scaffolds. *Journal of Biomedical Materials Research Part A* **89**: 632–641.
- Ramírez-Fernández, M.P., Calvo-Guirado, J.L., Maté-Sánchez Del Val, J.E., Delgado-Ruiz, R.A., Negri, B. & Barona-Dorado, C. (2013) Ultrastructural study by backscattered electron imaging and elemental microanalysis of bone-to-biomaterial interface and mineral degradation of porcine xenografts used in maxillary sinus floor elevation. *Clinical Oral Implants Research* **24**: 523–530.
- Schwartz, C., Liss, P., Jacquemaire, B., Lecestre, P. & Frayssinet, P. (1999) Biphasic synthetic bone substitute use in orthopaedic and trauma surgery: clinical, radiological and histological results. *Journal of Materials Science: Materials in Medicine* **10**: 821–825.
- Schindler, O.S., Cannon, S.R., Briggs, T.W. & Blunn, G.W. (2008) Composite ceramic bone graft substitute in the treatment of locally aggressive benign bone tumors. *Journal of Orthopaedic Surgery* **16**: 66–74.
- Sharifi, D., Khoushkerdar, H.R., Abedi, G., Asghari, A. & Hesarak, S. (2012) Mechanical properties of radial bone defects treated with autogenous graft covered with hydroxyapatite in rabbit. *Acta Cirurgica Brasileira* **27**: 256–259.
- Shull, C.G. (1946) The determination of X-ray diffraction line widths. *Physical Review* **70**: 679–684.
- Sundelacruz, S. & Kaplan, D.L. (2009) Stem cell and scaffold-based tissue engineering approaches to osteochondral regenerative medicine. *Seminars in Cell and Developmental Biology* **20**: 646–655.
- Yamauchi, K., Takahashi, T., Funaki, K., Hamada, Y. & Yamashita, Y. (2010) Histological and histomorphometrical comparative study of β -tricalcium phosphate block grafts and periosteal expansion osteogenesis for alveolar bone augmentation. *International Journal of Oral Maxillofacial Surgery* **39**: 1000–1006.
- Yang, S., Leong, K.F., Du, Z. & Chua, C.K. (2001) The design of scaffolds for use in tissue engineering. Part I. Traditional factors. *Tissue Engineering* **7**: 679–689.

- Yuan, H., de Bruijn, J.D., Li, Y., Feng, J., Yang, Z., de Groot, K. & Zhang, X. (2001) Bone formation induced by calcium phosphate ceramics in soft tissue of dogs: a comparative study between porous alpha-TCP and beta-TCP. *Journal of Materials Science: Materials in Medicine* **12**: 7–13.
- Zaidi, M., Moonga, B.S. & Huang, C.L. (2004) Calcium sensing and cell signaling process in the local regulation of osteoclastic bone resorption. *Biological Reviews of the Cambridge Philosophical Society* **79**: 79–100.



Comparison of three hydroxyapatite/ β -tricalcium phosphate/collagen ceramic scaffolds: An *in vivo* study

José Eduardo Maté-Sánchez de Val,¹ Patricia Mazón,² José Luis Calvo Guirado,¹ Rafael Arcesio Delgado Ruiz,³ María Piedad Ramírez Fernández,¹ Bruno Negri,¹ Marcus Abboud,³ Piedad N. De Aza⁴

¹Implantology and Biomaterials, the University of Murcia, Murcia, Spain

²Department of Materials Science, Optics and Electronic Technology, Miguel Hernandez University, Elche, Alicante, Spain

³Prosthodontics and Digital Technologies, Stony Brook University, New York, New York

⁴Institute of Bioengineering, Miguel Hernández University, Elche, Alicante, Spain

Received 22 August 2012; revised 23 April 2013; accepted 29 April 2013

Published online 3 June 2013 in Wiley Online Library (wileyonlinelibrary.com). DOI: 10.1002/jbm.a.34785

Abstract: Calcium–phosphate ceramics, which have a composition similar to bone mineral, represent a potentially interesting synthetic bone graft substitute. In the present study, three porous hydroxyapatite (HA)/ β -tricalcium phosphate (β -TCP)/collagen ceramic scaffolds were developed, characterized, and tested for their bone repairing capacity and osteoinductive potential in a New Zealand Rabbit model. The ratio of the ceramic components HA-/TCP/collagen varied from 40/30/30 to 50/20/30 and 60/20/20 (in wt %), respectively. None of the ceramic scaffolds succeeded in completely bridging the 6 mm calvarian defect with new bone after 60 days implantation. 60/20/20 ceramic scaffolds showed significantly more bone formation in the pores and in the periphery of the graft than the other two materials. Histomorphometric

analysis revealed that the 40/30/30 scaffold produced best bone-to-implant contact ($67.23 \pm 0.34\%$ with higher quality, closer contact) in comparison with 50/20/30 ($54.87 \pm 0.32\%$), and 60/20/20 ($48.53 \pm 0.31\%$). Both physicochemical and structural properties of the ceramic composites affected their *in vivo* behavior, either dependently or independently, emphasizing the importance of assessing bone repair parameters individually. The scaffolds may offer clinical applications in reconstructive surgery for treating bone pathologies. © 2013 Wiley Periodicals, Inc. *J Biomed Mater Res Part A*: 102A: 1037–1046, 2014.

Key Words: bioceramics scaffolds, collagen, tricalcium phosphate, hydroxyapatite, histomorphometry, SEM

How to cite this article: de Val JEM-S, Mazón P, Guirado JLC, Ruiz RAD, Fernández MPR, Negri B, Abboud M, De Aza PN. 2014. Comparison of three hydroxyapatite/ β -tricalcium phosphate/collagen ceramic scaffolds: An *in vivo* study. *J Biomed Mater Res Part A* 2014;102A:1037–1046.

INTRODUCTION

Bone replacement materials have been used for decades in maxillofacial surgery and for filling defects, even when the bone surface is inadequate.^{1–4} The most common biomaterials in use are calcium–phosphate (Ca–P)-based bioceramics. Ca–Ps have a composition and structure similar to the mineral phase of bone and are osteoconductive. Among the various materials used in recent years tricalcium phosphate (TCP) has shown promising results in tissue culture, animal experiments and clinical studies.^{5–7}

A bone substitute material should present “bimodal” behavior that, in the early stages of differentiation, will allow osteoblasts to build bridges between its grains of different sizes and integrate with other osteoblasts, supporting both proliferation and differentiation. Intrinsic stimulation of new bone formation will be supported by the activation and absorption of mesenchymal stem cells into surfaces with nanoscale topographic features.^{8–10} The ultimate goal is the union of fully differentiated osteoblasts that will support

bone matrix production. This requires a porous structure with nanopores, micropores, and macropores, all involved in different stages of absorption, adhesion, and bone material deposition on and between the bone substitute material.^{11,12} Initial regeneration of the bone defect is favored by the presence of Ca–P in the bone replacement material.¹³

The physicochemical properties of bone substitutes based on tricalcium phosphates influence their mechanical stability. They also undergo rapid degradation and have a volume instability that does not allow new bone formation to retain the original volume.¹⁴ Ca–Ps are now in common use in the medical field because of their biocompatibility, safety, unlimited availability, and cost effectiveness. However, the Ca–P bioceramics also have some disadvantages: poor mechanical properties, time-consuming fabrication, and low-yield production, lack of an organic phase, presence of impurities, nonhomogenous particle size, and shape.^{15,16}

The use of biphasic calcium phosphates (BCP) is promising as conceptually it could overcome the disadvantages of

Correspondence to: J. E. Maté-Sánchez de Val; e-mail: jmsosont@hotmail.com/josemate@um.es

single-phase ceramics by combining two or more ceramic phases. BCP ceramics offer controlled bioactivity and balanced biodegradation. They are osteoconductive and offer the possibility of acquiring osteoinductive properties. The conventional synthetic porous Ca-P ceramics have been composed of microscale grain size, but recent studies have focused on producing bioceramics at the nanoscale. Nanohydroxyapatite (nano-HA) can promote osteoblast cell activity and facilitate osteointegration better than microcrystalline HA and so enhance new bone tissue formation.¹⁷ However, the superiority of biological calcified tissues is also due to the presence of bioorganic polymers (proteins, mainly collagen type I), which influence the material's strength and elasticity. Therefore, the development of organic/inorganic hybrid BCP scaffolds could provide excellent possibilities for optimizing conventional bone substitutes.^{18,19}

The incorporation of collagen into BCP ceramics might represent a convenient way of improving the organic phase of these materials and procuring the organic properties of biological calcified tissues. There are various studies of BCP compounds in the literature but little of this research has been applied clinically, due to the controversy concerning their optimum composition for clinical application. Furthermore, research so far has failed to confirm the beneficial effects of collagen coating on composite BCP scaffolds.^{20,21}

The objective of this study was to fabricate and characterize HA/ β -TCP/collagen ceramic scaffolds of various components' ratios, and compare their physical and *in vivo* behavior. The effect of the collagen incorporation was also evaluated. The hypothesis was that the utilization of a simple method of collagen incorporation may improve the physical properties of HA/ β -TCP scaffolds and increase their biocompatibility. In addition, histological and histomorphometric analyses were performed in order to evaluate the osseointegration of each composition. Radiological analysis was performed to further determine the clinical behavior and resorption of these materials.

MATERIALS AND METHODS

Raw materials and composition

The raw materials used in the present study were commercial collagen, synthesized HA, and synthesized TCP.

HA synthesis

HA was synthesized by solid-state reaction from a stoichiometric mixture of calcium hydrogen phosphate anhydrous (CaHPO₄, Sigma), and calcium carbonate (CaCO₃, Sigma) with an average particle size of <15 μ m and a Ca/P ratio of 1.72. The mixture of CaHPO₄ and CaCO₃ was heated in a platinum crucible to 1200°C for 6 h at a heating rate of 10°C/min followed by cooling to room temperature at a rate of 6.5°C/min. The obtained material was ground to an average particle size of 2 μ m (Mastersizer2000E device-Malvern) and then characterized by X-ray diffraction (XRD).

TCP synthesis

TCP was synthesized by solid-state reaction from a stoichiometric mixture of calcium hydrogen phosphate anhydrous

(CaHPO₄, Panreac) and calcium carbonate (CaCO₃, Fluka) with an average particle size of <15 μ m and a Ca/P ratio of 1.60. The mixture of CaHPO₄ and CaCO₃ was heated in a platinum crucible to 1000°C for 12 h followed by slow cooling. The obtained material was ground to an average particle size of 5 μ m and then characterized by XRD.

Collagen: Collagen type I of porcine origin (Sigma-Aldrich), a particle size of 80–120 μ m, was used in the study.

Ceramic scaffold preparation

The chosen constituents (Table I) were weighed out and thoroughly dry mixed in a mixing miller with partially stabilized zirconia balls. After the milling process, the powder mixture was cold isostatically pressed at 200 MPa. The pressure was maintained for 30 min, after which it was slowly depressurized to 1 atm. The whole process took 1 h.

Ceramics characterization

XRD (Bruker-AXS D8Advance) analyses of the raw materials and the ceramic composites were performed to determine crystallography and phase identification using Cu-K α radiation at 40 kV and 30 mA. The scans were performed at 2 θ values varying from 20° to 55° at a rate of 0.05°/min.

The morphology of the porous ceramic composites was studied using a scanning electron microscope (HITACHI S-3500N, Japan). Quantitative analyses were made by an electron dispersive X-ray spectroscopy (EDX) system coupled to the electron microscope using ZAF (atomic number, absorption, and fluorescence) correction software and Bayer standards. Microanalysis data were obtained from 10 independent determinations. The samples were precoated with palladium for scanning electron microscopy (SEM) images and carbon coated for EDX analysis, under an argon atmosphere using a sputtering machine (Polaron K550X Sputter Coater, Germany).

Apparent density measurement was performed on each sample using Archimedes' method by immersion in Hg. Sample mass was determined using an electronic balance and relative density (RD) was calculated with the following equation:

$$RD = \frac{\rho_a}{\rho_t} \times 100$$

where ρ_t and ρ_a are the samples' theoretical density and apparent density, respectively.

The relative total porosities (P) of sintered scaffolds were calculated by the gravimetric method using the following equation:

$$\%P = ((\rho_t - \rho_s) / \rho_t) \times 100$$

TABLE I. Composition of HA/TCP/Collagen Scaffolds

Compound	Group A	Group B (%)	Group C (%)
HA	40	50	60
B-TCP	30	20	20
Collagen	30	30	20

where ρ_t is the theoretical density of materials, and ρ_s is the density of the dried samples, which was calculated by the following equation:

$$\rho_s = m_s / V$$

where m_s is the total mass, and V is the volume, calculated by Archimedes method. In the above calculations, the theoretical density of HA and TCP was considered as 3.156 and 3.07 g/cm³, respectively.

The three-point bending strength (σ_f) was measured with a Microtest universal testing machine set at a cross-head speed of 0.33 mm s⁻¹ and a span of 40.0 mm. Fracture toughness (K_{1C}) was also obtained in the 3-point bending test as a function of loading rate by the single edge precracked-beam method.²² Measurements were performed at room temperature using the rectangular-shaped samples (3 mm × 4 mm × 45 mm) with a notch width of <0.5 mm. The ratio between notch depth and sample thickness was 0.4. Young's modulus (E) was evaluated from the stress-strain curves obtained with the flexural strength test. Seven replicates were determined for each material and the results were expressed as mean ± standard deviation.

Material properties

Three groups of 20 implants were tested, each of cylindrical shape (6 ± 0.01 mm in diameter and 2 ± 0.01 mm in length). The ratios of three constituents HA-/TCP/collagen (in wt % varied as follows: group A: 40/30/30; group B: 50/20/30; and group C: 60/20/20). A fourth group, group D (unfilled critical size defect), acted as control. These were distributed randomly amongst critical size defects in rabbit calvariae by means of random number generator software, SPSS v.18.0. (IBM Corporation, New York, NY).

Animal experimentation

Main protocol. The study protocol was approved by the Animal Ethics Committee of the University of Murcia, following Spanish Government and European Community Guidelines for animal care. Fifteen male New Zealand rabbits of 3.5–4.5 kg in weight were used. The three materials were implanted into the animals' calvariae. General anesthesia

included ketamine plus chlorbutol (5–8 mg/kg intravenously), 0.5–1 mg/kg acepromazine maleate as a coadjuvant, and 0.05 mg/kg atropine. Amoxicillin (0.1 mL/kg intramuscularly) was administered at the end of surgery. The total sample size was 20 rabbits with two defects in each, a total of 40 defects, randomized in four groups of 10 for each material composition.

Surgical procedure. Two critical defects (6 mm Ø) were created in each calvaria. The surgical approach was in the proximal-medial area of the calvaria, several millimeters below the frontal tuberosity. Bone tissue was removed with spherical surgical drills of 6 mm in diameter at low rotation speed with constant irrigation [Fig. 1(a–c)].

Histological and histomorphometric analysis

After the elapse of the 60-day implantation time, the implants together with the surrounding tissues were removed and fixed in 10% neutral buffered formalin and decalcified. The decalcification method utilized Osteomoll Merck KbaA (Germany) containing HCl (10%) and CH₂O (4%), immersing samples for 17 days and renewing the solution every 24 h. Subsequently, all samples were paraffin embedded, sectioned at 5 µm depth and stained using hematoxylin–eosin. The entire circumference of each section (containing bone, graft, and connective tissue) was traced manually to create an individual region of interest.

Histomorphometric evaluations consisted of measurements of the area of graft material in relation to the total area of interest. These were carried out using Image J software [developed by the National Institute of Health (NHS), Bethesda, MD]. Examinations were performed under a Nikon Elipse 80i microscope (Teknootik AB, Huddinge, Sweden), equipped with an Easy Image 2000 system (Teknootik AB) using 10× to 40× lenses for descriptive evaluation and morphometric measurement. Images were generated using a Leica Z6 APO microscope connected to a Leica DC 500 (Barcelona, Spain) digital camera, enlarged 23×. After calibrating the system and digitalizing images, interactive measurements of the areas of interest were obtained using image analysis software Leica QWin V3 (Barcelona, Spain). Histomorphometric analysis produced one



FIGURE 1. Surgical procedure: surgical approach (a), defect preparation (b), and graft placement (c). [Color figure can be viewed in the online issue, which is available at wileyonlinelibrary.com.]

bone-to-implant contact (BIC) measurement, measured as the percentage of the circumference and length of the cylinder in contact with new bone.

Resorption analysis

The image analysis program Image J (NIH) was used to calculate the resorption rate of the scaffolds. This was done by measuring the perimeter of the biomaterial at the time of implantation and comparing it with the residual material after 60 days.

Scanning electron microscopy

Twenty samples of each material (A: 40/30/30; B: 50/20/30; and C: 60/20/20) were studied after 60 days implantation comparing variations in Ca/P ratios. The samples were fixed by immersion in 4% formalin solution, dehydrated in a graded ethanol series and embedded in plastic resin (Technovit A 7210VCL; Kulzer & Co, Hanau, Germany). They were then polished using a manual grinder with 800 grit silicon carbide paper, mounted on an aluminum stub and carbon coated (using a Polaron sputter coater). Samples were examined using the scanning electron microscope (Hitachi S-3500N) at a working distance of 19 mm, an acceleration voltage of 15 kV and 15 \times magnification, fitted with an Oxford Instruments INCA 300 EDX Analytical System (Abingdon, Oxfordshire, UK). The areas of interest were outlined by the inner cortical walls and reached into the medullary core. Elemental mapping was performed to determine

the chemical degradation process and changes to medullary composition in all four study groups.

Radiological study

Digital radiographs were taken (using a Kodak 6100; Eastman Kodak, Rochester, NY) after sample removal using a custom-made acrylic support in order to ensure reproducibility of the technique. Exposure parameters were standardized. Each radiograph was studied using image analysis software Image J.

Statistical analysis

Statistical analysis was performed using PASW Statistics v.18.0.0 software (SPSS). Values were recorded as mean \pm standard deviation. One-way analysis of variance was applied for the comparison of the means, assuming level of significance of 95% ($p < 0.05$). Equal means were regarded as the null hypothesis, while the existence of significant differences between means acted as an alternative hypothesis. As significant differences between the means existed, the null hypothesis was rejected.

RESULTS

Preoperative material characterization

Figure 2 shows the XRD patterns of the synthesized TCP and HA powders, as well as the composite ceramic compositions. The polymorphic form of the TCP corresponded to JCPDS card no. 9-0169 and HA data corresponded to JCPDS

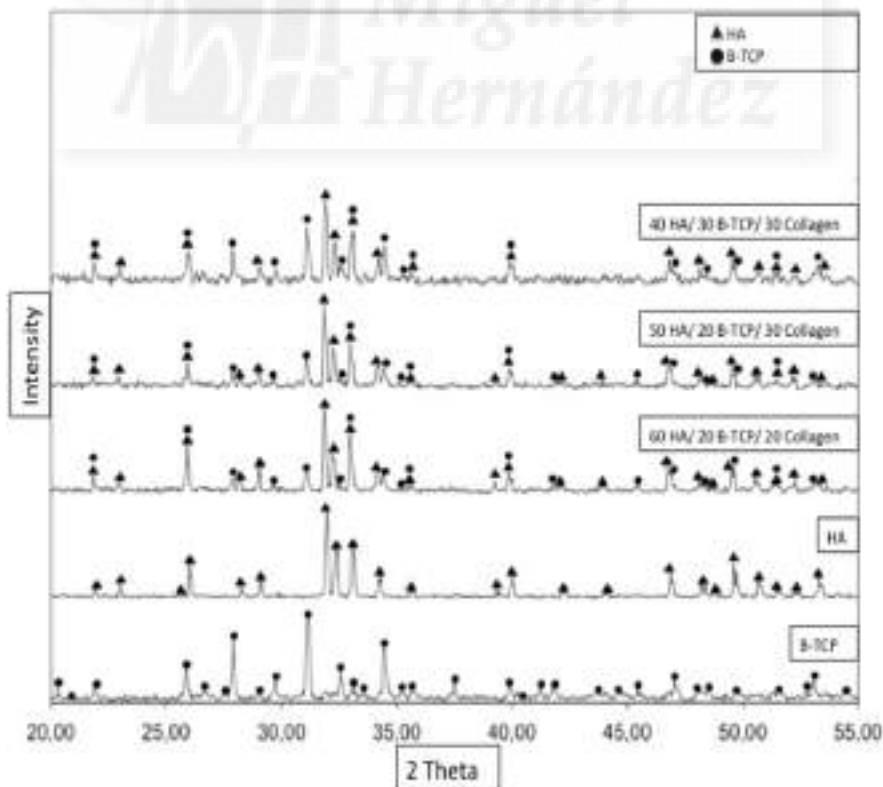


FIGURE 2. X-ray diffraction patterns of synthetic HA, TCP raw materials, and HA/TCP/collagen compositions.

TABLE II. Physical and Mechanical Properties of the Scaffolds

	Crystalline Phases	Porosity (%)	Density (g/cm ³)	RD (%)	Bending Strength, σ_f (MPa)	Young's Modulus, E (GPa)	Fracture Toughness, K_{1c} (MPa m ^{1/2})
Group A	HA/ β -TCP	32 \pm 1.23	2.18 \pm 0.56	76.25 \pm 2.34	7.76 \pm 1.02	3.15 \pm 1.12	0.34 \pm 0.03
Group B	HA/ β -TCP	27 \pm 1.07	2.20 \pm 0.67	78.12 \pm 2.56	8.21 \pm 0.99	3.18 \pm 0.89	0.40 \pm 0.12
Group C	HA/ β -TCP	23 \pm 0.98	2.35 \pm 0.38	85.25 \pm 3.01	7.92 \pm 1.76	3.16 \pm 1.02	0.37 \pm 0.07
Sintered HA	HA		99.2 \pm 0.98		115–200	80–110	1.0
Sintered TCP	β -TCP		99.7 \pm 0.87		140–154	33–90	
Cortical bone	CHA	5–12		1.8–2.0	60–147	11–19	2–11
Cancellous bone	CHA	46–95		0.09–1.0	0.5–8.0	0.06–1.5	

To facilitate comparison, sintered HA, sintered TCP, and cortical and cancellous bone data have also been included.

card no. 09-0432. No other secondary phases were detected. The XRD patterns of the composite ceramic compositions showed peaks corresponding with β -TCP and HA, regardless of the addition of collagen.

The physical and mechanical properties of the ceramic scaffolds are reported in Table II. As the collagen content increased (from 20 to 30 wt %), the porosity increased by about 4% for group B composition and about 9% for group A. Bending strengths ranged between 7.76 MPa for group A and 8.21 MPa for group B although this difference was statistically insignificant. Fracture toughness, the material's resistance to crack propagation, is an important parameter for assessing a material's susceptibility to failure and toughness was seen to be best for group B and lowest for group A, with statistically significant difference. For comparison, the properties of sintered HA, β -TCP, cortical, and cancellous bone are also included in Table II.

Figure 3 shows surface morphology of the three composites. The scaffold was composed of variable particle sizes ranging from 2–5 μ m.

Histological and resorption analysis

Analysis of the histological sections of each of the three materials was performed at 60 days post implantation. None of the grafted materials elicited a significant inflammatory reaction. In all samples, woven bone was identified around and in close contact with the material and, as might be expected in rabbit calvarial bone, small marrow spaces were observed in the perimaterial bone, which had reached

maturity over 60 days. The volume of the graft block in group A decreased progressively as bone formation increased at the periphery and within the block, leading to its virtual disappearance and almost complete closure of the cortex at 60 days. In group C, graft blocks showed slower resorption than the other groups; histological results showed that after implantation, changes to residual block content, peripheral bone resorption, new bone formation, and closure of the cortex were minimal in comparison with the other graft compositions (Fig. 4). In calvariae treated with group B blocks, there was intermediate block stability, much greater resorption than in group C, but lower than in group A and an intermediate rate of neoformation. In the control group, no spontaneous closure of the defect was seen, as might be expected of a critical defect [Fig. 4(a)]. The resorption pattern was variable across the groups. Group A samples [Fig. 4(b)] showed numerous resorption foci on block surfaces, which produced a much more irregular surface compared with other samples (peaked resorption pattern). Group B samples [Fig. 4(c)] presented intermediate behavior showing a moderate resorption pattern, with fewer unfilled regions and less irregularity, after a wavy resorption type across the surface. Finally, in group C, a linear pattern was observed with few resorption foci that were more regular and less active [Fig. 4(d)].

Histomorphometric analysis

Histomorphometric analyses were carried out to establish BIC data for the three materials, with group A showing best

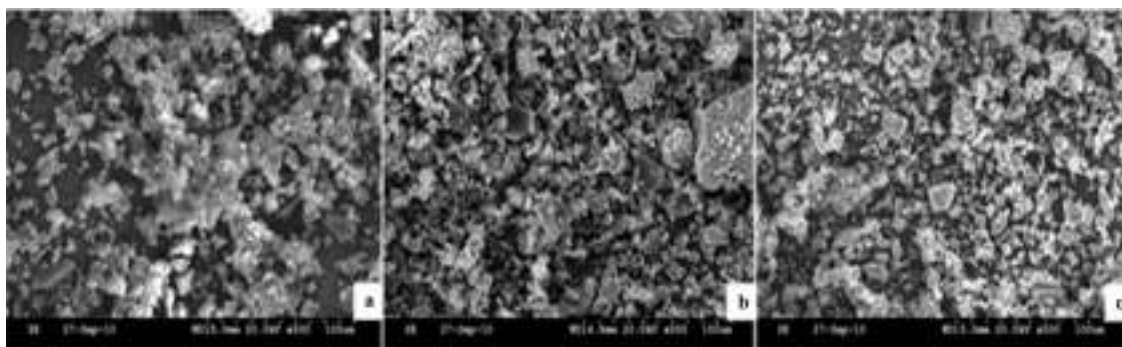


FIGURE 3. SEM morphology of the scaffolds' surfaces: (a) group A, (b) group B, and (c) group C.

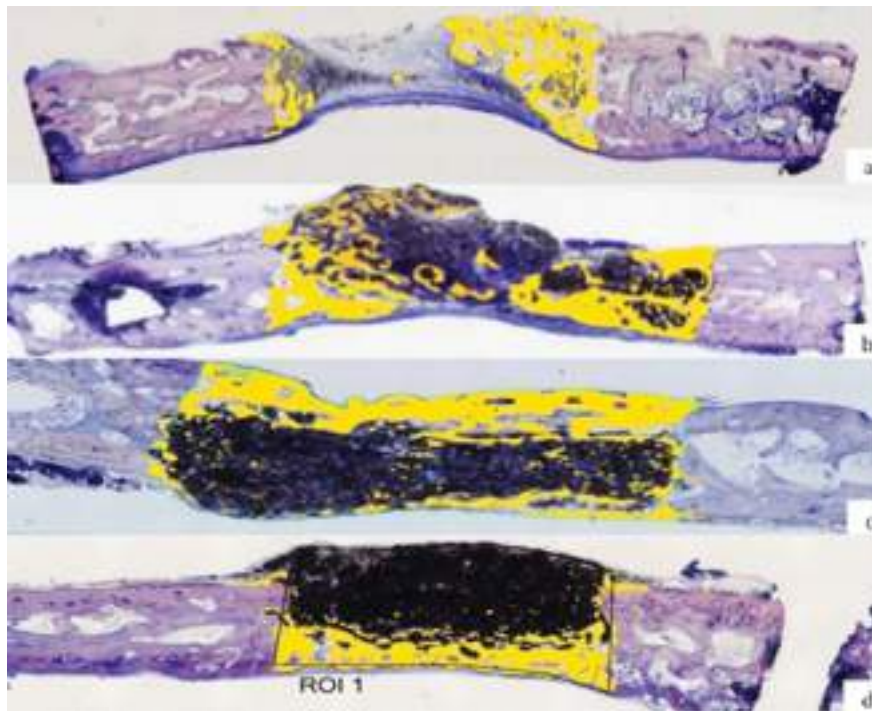


FIGURE 4. Histological cross sections at 60 days for each of the three materials: control (a), group A (b), group B (c), and group C (d). Black: residual scaffold. Yellow: bone remodeling site. (resorption foci). [Color figure can be viewed in the online issue, which is available at wileyonlinelibrary.com.]

BIC ($67.23 \pm 0.34\%$; with closer contact observed) than group B ($54.87 \pm 0.32\%$), followed by group C ($48.53 \pm 0.31\%$), in which close contact between bone and graft was significantly smaller. Moreover, new bone ingrowth, defect closure and residual biomaterial were recorded and analyzed, showing better results for group A samples in comparison with the other groups (Table III).

SEM and EDS analysis

SEM images showed complete integration of all specimens, without significant differences between the groups. In all cases, the cell growth was observed to be orderly and structured; there was cell attachment to the biomaterial and the establishment of an interface between the biomaterial and the old bone (Fig. 5). Examining the details of each panoramic image, group A showed integration of the graft in the calvarial bone [Fig. 5(a)], as well as cellular arrangement over the graft block [Fig. 5(b)]. In group B, integration existed in the surrounding bone [Fig. 5(c)] and an equally cellular arrangement

and growth over the graft [Fig. 5(d)]. In group C, a higher percentage of residual graft material was observed at 60 days [Fig. 5(e)], as well as cellular surface growth and integration. The interrelation with the peripheral bone was worse in comparison with the other two composites [Fig. 5(f)]. EDS analysis showed higher content of Ca and P in the new bone region for the composites of higher collagen content.

Radiological study

Radiographs were obtained after sample extraction, observing integration with the host bone in all study groups. The radiographic density varied with the chemical content of the samples, with group A showing correct integration and partial resorption that corresponded to the histological findings [Fig. 6(a)]; group B behaved similarly and was seen to be fully integrated with the surrounding bone [Fig. 6(b)]; group C showed a greater presence of residual biomaterial and correct integration [Fig. 6(c)]. There was no spontaneous closure of the defect, as expected for a critical defect [Fig. 6(d)].

TABLE III. Histomorphometric and BIC Measurements

	Group A	Group B	Group C	Control
BIC (%)	67.23 ± 0.34^a	54.87 ± 0.32	48.53 ± 0.31	0.00 ± 0.00
New bone ingrowth (%)	78.23 ± 2.65^a	74.12 ± 2.83	72.58 ± 2.49	37.38 ± 3.97
Defect closure (%)	63.34 ± 3.43^a	59.54 ± 3.32	70.43 ± 3.01^a	34.21 ± 2.34
Residual biomaterial (%)	59.34 ± 2.95	63.43 ± 2.90	79.39 ± 2.98^a	0.00 ± 0.00

^aSignificant differences $p < 0.05$.

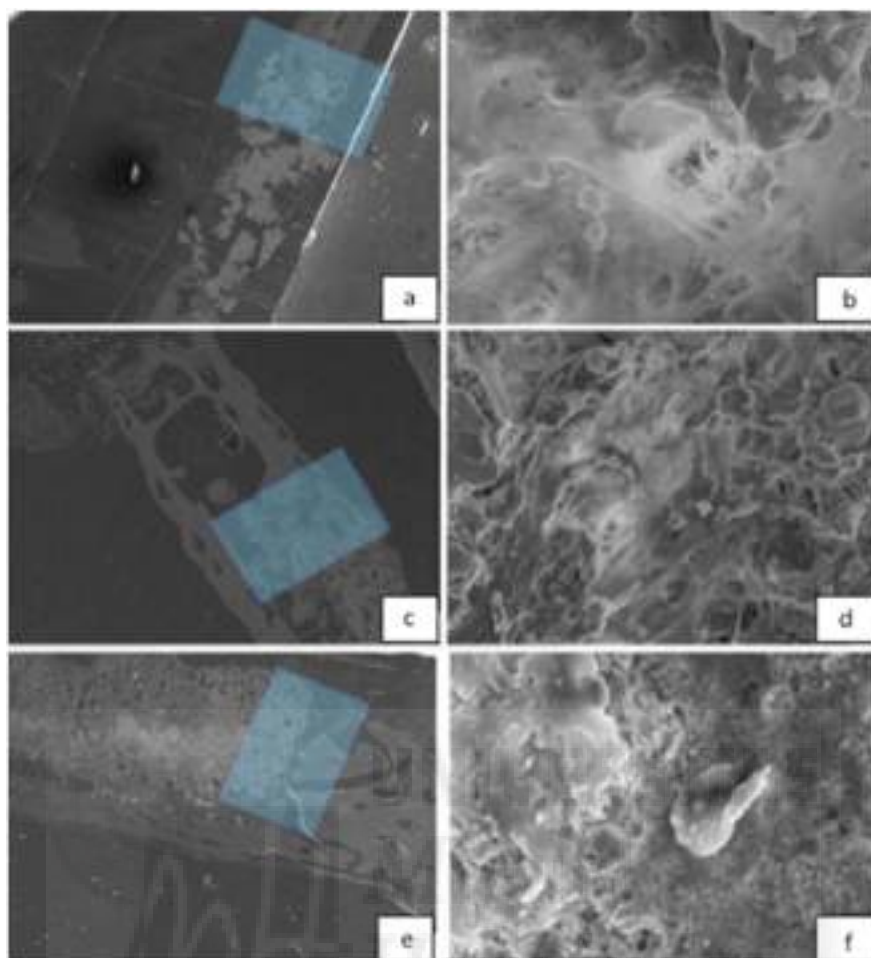


FIGURE 5. Postextraction SEM images of the cross sections. Group A (a and b), group B (c and d), and group C (e and f). a, c, and e, Panoramic views and (b, d, and f) higher magnifications. [Color figure can be viewed in the online issue, which is available at wileyonlinelibrary.com.]

DISCUSSION

In the present study, three newly developed porous Ca-P ceramic scaffolds were tested for their bone-healing capacity and osteoinductivity. Critical-sized calvarial wing defects were used to compare bone formation after the implantation of three ceramics. For bone tissue engineering, the design of Ca-P scaffolds should mimic the structure and properties of the bone extracellular matrices and this study set out to produce and test scaffolds with physical and biological properties similar to natural bone.²³

Different ratios of HA/ β TCP/collagen in the scaffolds can also produce different biological responses, so an ideal balance between these two phases should improve the physical and mechanical properties, as well as the biological behavior of Ca-P scaffolds. The effect of collagen can be understood as a facilitator of the early stages of cell anchorage to the biomaterial and as a vehicle to allow the bone cells to populate the biomaterial and bring about new bone substitution. Currently, several synthetic routes have been utilized for the preparation of Ca-P ceramic powders with different composition ratios. In this study, a solid-state reaction followed by cold isostatic pressing was used successfully for preparation

of porous Ca-P ceramic scaffolds. This technique is simple and economical.

The surface morphology of the phosphate-collagen scaffolds was rather rough and irregular and should favor the cell attachment after *in vivo* implantation. The surface porosities were indistinct and some cracks were present. Studies of the effects of collagen on the behavior of ceramic composite scaffolds have not found any significant differences in physicomechanical properties arising from different content of collagen.²⁰ Therefore, other factors such as porosity and density must play a major role in determining the physical, mechanical properties and biological behavior of HA/TCP/collagen ceramic scaffolds. When the present study data was compared with human bone (Table II), the materials' Young's modulus was quite different from that of cortical bone but matched cancellous bone more closely.²⁴

Brodie et al.²⁵ reported that collagen coating increases the strength of HA/TCP 50/50 (wt %), whereas it weakens HA/TCP 25/75 (wt %) and pure TCP discs. These inconsistent mechanical behaviors are in accordance with our results.

One of the main disadvantages of the cold isostatic method is the poor mechanical strength of the materials for

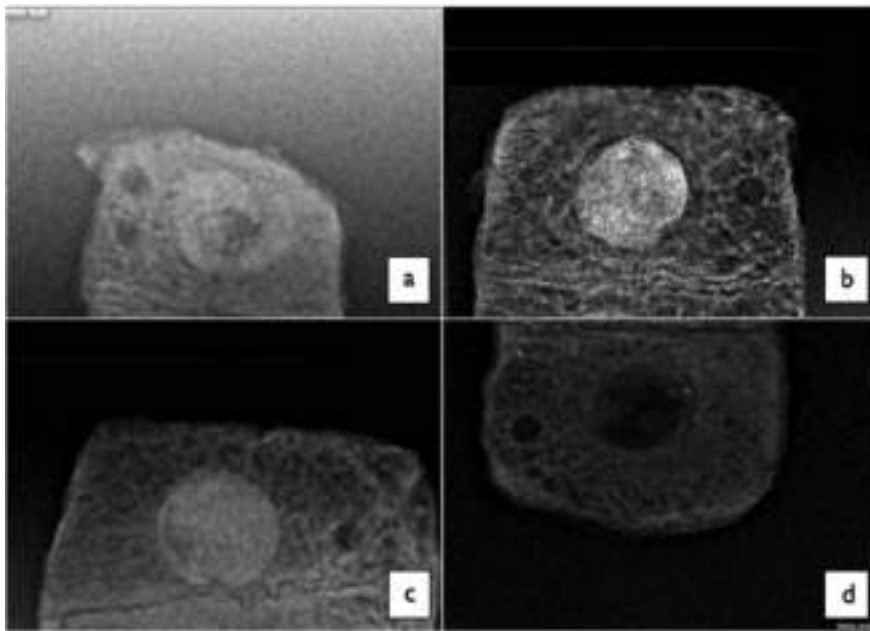


FIGURE 6. Radiological images of the implanted scaffolds showing density differences: group A (a), group B (b), group C (c), and control (d).

load bearing applications (Table II). Although a highly porous scaffold is preferred, as it favors bone cell adhesion and regeneration, this is at the expense of mechanical strength and resistance. However, the optimum physico-biological properties can be improved by incorporating collagen into the ceramic compositions (Table IV).

Multiple light microscopy and SEM evaluations of the implant–bone interface show how the same structure is represented differently according to the selected examination method.²⁶ The precision and reliability of a histomorphometric study of newly formed bone depends upon the correct identification and ultra structural characterization of all the cellular components that might play a role in the osseointegration process. Optical microscopy lacks the resolving power required for detailed structural analysis.^{27–29}

In the present study, SEM and EDX analysis revealed a close relation between the newly formed bone matrix and the graft surface. Elemental analysis of the bone tissue demonstrated the presence of calcium and phosphorus, pointing to the presence of mineralized bone. This observation suggests that the graft surface may provide an optimal stratum for bone tissue ingrowth.³⁰ The highest concentrations of calcium in the interface region was recorded for group A, due to the faster ion exchange rate in the interface area, resulting in highest levels of new bone formation. The

presence of extracellular Ca^{2+} resulting from resorption activity might be involved in the stimulation of osteoblasts.

Yamaguchi et al.³¹ showed that moderately high extracellular Ca^{2+} is a chemotactic and proliferating signal for osteoblasts and stimulates preosteoblast differentiation. Groups A and B had a high degree of porosity facilitating the implants' resorption process as the external and internal surface areas of the pores were exposed to the medium, over the several microns distance beyond the graft body, facilitating osteoconduction, as the results from the elemental mapping showed. The elemental point analysis was carried out from the middle to the periphery of the grafts. In the present study, this was made visible in element mapping, which revealed an increase in the areas of Ca and P reaching from within the graft body, facilitating osteoconduction, as the results from the elemental analyses showed. In all cases, a decrease in the percentage of Ca and P was found in the residual biomaterial, with respect to the initial composition, whereas a gradual increase in the percentages of Ca and P ratio was found in the interface, suggesting an increase in the osteoinductive capacity of the material and replacement by new bone at its periphery.

In agreement with an earlier study of the mineral degradation process of β -TCP using the SEM-backscattered electron technique,^{32,33} the present study found a release of Ca

TABLE IV. EDX Analysis Before and After 60 Days Implantation

	Initial Biomaterial			Residual Biomaterial			Interface		
	Group A	Group B	Group C	Group A	Group B	Group C	Group A	Group B	Group C
Ca/P ratio	2.26	2.23	2.49	2.23	2.08	2.45	2.70	2.06	2.20

and P ions, which was seen to promote new bone growth; it is possible that high levels of Ca and P stimulate osteogenesis due to their effects on osteoblast gene expression, as described by Lazáry et al.³⁴ In normal calcified bone, the Ca/P molar ratio increases with increasing calcification.

All the materials in this study were found to offer biocompatibility, sufficient mechanical strength and did not produce any adverse inflammatory reactions at the insertion site. The fact that the scaffolds were absorbable allowed their rapid replacement by the new bone without causing any reactions to foreign bodies. The fastest resorption rate of the material in group A > group B > group C was related to the percentage of HA and also collagen in the compositions. Rapid replacement by new bone allows a bone matrix to become established within the material, giving the host area physical properties similar to the bone.³⁵

A significant difference in resorption time and stability from the other scaffolds was found in group C, which showed greater stability and less resorption than the other groups.

The HA/ β -TCP scaffold in cylinder form allows a precise evaluation of resorption, dimensional stability and replacement by new bone.³⁶ It is known that an appropriate concentration of collagen in this biomaterial acts as an integration stimulant, promoting bone matrix and ion exchange with the implant environment.

According to Araújo et al.,³⁷ who studied an *in vivo* experimental model, the material produced appropriate bone replacement, cell differentiation and stimulated osteoblasts. The authors observed increased amounts of mineralized bone and osteoblast activity.

In spite of the New Zealand rabbit's rapid metabolic activity, other studies have established its validity as an experimental model for testing biomaterials used for bone replacement.³³ In view of this, the results in this study were enhanced through the creation of critical defects of 6 mm diameter, which did not close spontaneously and therefore demonstrated the regenerative potential of the biomaterials under observation.³⁸

Resorption patterns in the groups containing the highest percentage of collagen and less HA were more active than in the groups, which showed more irregular shapes and became smoother as the collagen content was reduced. This corresponds to collagen's proven osteogenic capacity, increasing foci of resorption, and new bone formation.

In the study of BIC, all the materials showed appropriate percentages of integration. Group A produced higher BIC values, with a much larger pattern of interdigitation in comparison with the other two groups. The composition of 30% of collagen, lower HA content but higher content of more soluble TCP, also improved the rate of new bone formation at the implant periphery.³⁹ The percentage of new bone formation for group A samples was significantly higher than in the other groups; the presence of higher collagen content allowed internal replacement of the material by new bone within a favorable time span, as demonstrated by the presence of new bone within the material and at its periphery.

CONCLUSIONS

The cold isostatic method was used successfully for fabricating HA/TCP/collagen ceramic scaffolds of desired shape and high porosity. The main shortcoming of these materials is their poor physical and mechanical properties, which were found to be similar, independently of the composition.

HA/TCP/collagen biomaterials proved to be biocompatible, bioresorbable and osteoconductive when used as a bone substitute material. SEM revealed that newly formed bone was closely attached to the synthetic materials. Elemental analysis showed that there was a gradual diffusion of Ca ions from the biomaterials into the newly forming bone at the interface.

Each of the studied compositions can be used in specific clinical applications in reconstructive surgery of bone pathology. Group A, with a faster resorption rate, can be used in situations requiring rapid replacement by autogenous bone. Group B, which represents the moderate resorption pattern, allows implementation in situations requiring partial replacement by autologous bone with matrix in place over the longer time. Group C, with a slow resorption pattern, is suitable when dimensional implant stability is required.

REFERENCES

1. Daculsi G, Laboux O, Malard O, Weiss P. Current state of the art of biphasic calcium phosphate bioceramics. *J Mater Sci Mater Med* 2003;14:195–200.
2. McAllister BS, Haghighat K. Bone augmentation techniques. *J Periodontol* 2007;78:377–396.
3. Browaeys H, Bouvry P, De Bruyn H. A literature review on biomaterials in sinus augmentation procedures. *Clin Implant Dent Relat Res* 2007;9:166–177.
4. Aghaloo TL, Moy PK. Which hard tissue augmentation techniques are the most successful in furnishing bony support for implant placement? *Int J Oral Maxillofac Implants* 2007;22 suppl:49–70.
5. Krekmanov L. The efficacy of various bone augmentation procedures for dental implants: A Cochrane systematic review of randomized controlled clinical trials. *Int J Oral Maxillofac Implants* 2006;21:696–710.
6. Esposito M, Grusovin MG, Kwan S, Worthington HV, Coulthard P. Interventions for replacing missing teeth: Bone augmentation techniques for dental implant treatment. *Cochrane Database Syst Rev* 2008;CD003607.
7. Chopra PM, Johnson M, Nagy TR, Lemons JE. Micro-computed tomographic analysis of bone healing subsequent to graft placement. *J Biomed Mater Res B Appl Biomater* 2009;88:611–618.
8. Fan H, Ikoma T, Tanaka J, Zhang X. Surface structural biomimetics and the osteoinduction of calcium phosphate biomaterials. *Nanosci Nanotechnol* 2007;7:808–813.
9. Zyman ZZ, Tkachenko MV, Polevodin DV. Preparation and characterization of biphasic calcium phosphate ceramics of desired composition. *J Mater Sci Mater Med* 2008;19:2819–2825.
10. Saldana L, Sanchez-Salcedo S, Izquierdo-Barba I, Bensiamar F, Munuera L, Vallet-Regi M, Vilaboa N. Calcium phosphate-based particles influence osteogenic maturation of human mesenchymal stem cells. *Acta Biomater* 2009;5:1294–1305.
11. Gauthier O, Bouler JM, Aguado E, Legeros RZ, Pilet P, Daculsi G. Elaboration conditions influence physicochemical properties and *in vivo* bioactivity of macroporous biphasic calcium phosphate ceramics. *J Mater Sci Mater Med* 1999;10:199–204.
12. Rivera-Munoz E, Diaz JR, Rogelio Rodriguez J, Brostow W, Castano VM. Hydroxyapatite spheres with controlled porosity for eye ball prosthesis: Processing and characterization. *J Mater Sci Mater Med* 2001;12:305–311.
13. Baksh D, Davies JE, Kim S. Three-dimensional matrices of calcium polyphosphates support bone growth *in vitro* and *in vivo*. *J Mater Sci Mater Med* 1998;9:743–748.

14. Wiltfang J, Merten HA, Schlegel KA, Schultze-Mosgau S, Kloss FR, Rupprecht S, et al. Degradation characteristics of alpha and beta tri-calcium-phosphate (TCP) in minipigs. *J Biomed Mater Res* 2002;63:115–121.
15. Fan H, Ikoma T, Tanaka J, Zhang X. Surface structural biomimetics and the osteoinduction of calcium phosphate biomaterials. *J Nanosci Nanotechnol* 2007;7:808–813.
16. Dorozhkin SV. Bioceramics of calcium orthophosphates. *Biomaterials* 2010;31:1465–85.
17. Huang Y, Zhou G, Zheng L, Liu H, Niu X, Fan Y. Micro-/nano-sized hydroxyapatite directs differentiation of rat bone marrow derived mesenchymal stem cells towards an osteoblast lineage. *Nano-scale* 2012;4:2484–2490.
18. Daculsi G, Laboux O, Malard O, Weiss P. Current state of the art of biphasic calcium phosphate bioceramics. *J Mater Sci Mater Med* 2003;14:195–200.
19. Dorozhkin SV. Calcium orthophosphate-based biocomposites and hybrid biomaterials. *J Mater Sci* 2009;44:2343–2387.
20. Zheng L, Yang F, Shen H, Hu X, Mochizuki C, Sato M, Wang S, Zhang Y. The effect of composition of calcium phosphate composite scaffolds on the formation of tooth tissue from human dental pulp stem cells. *Biomaterials* 2011;32(29):7053–7059.
21. Ebrahimi M, Pripatnanont P, Monmaturapoj N, Suttapreyasri S. Fabrication and characterization of novel nano hydroxyapatite/ β -tricalcium phosphate scaffolds in three different composition ratios. *J Biomed Mater Res A* 2012;100(9):2260–2268.
22. Fisher H, Marx R. Fracture toughness of dental ceramics: Comparison of bending and indentation method. *Dent Mater* 2002;18:12–19.
23. Dorozhkin SV. Calcium orthophosphates in nature, biology and medicine. *Materials* 2009;2:399–498.
24. Keaveny TM, Hayes WC. *Mechanical Properties of Cortical and Trabecular Bone*. Bone Growth. Boca Raton, FL: CRC Press; 1993. p 285–344.
25. Brodie JC, Merry J, Grant MH. The mechanical properties of calcium phosphate ceramics modified by collagen coating and populated by osteoblasts. *J Mater Sci Mater Med* 2006;17:43–48.
26. Orsini G, Traini T, Scarano A, Degidi M, Perrotti V, Piccirilli M, Piatelli A. Maxillary sinus augmentation with Bio-Oss particles: A light, scanning, and transmission electron microscopy study in man. *J Biomed Mater Res Part B: Appl Biomater* 2005;74:448–457.
27. Wierzechos J, Falcioni T, Kiciak A, Wolinski J, Koczorowski R, Chomici P, Poremska M, Ascaso C. Advances in the ultrastructural study of the implant–bone interface by backscattered electron imaging. *Micron* 2008;39:1363–1370.
28. Jasty M, Bragdon CR, Schutzer S, Rubash H, Haire T, Harris WH. Bone ingrowth into porous coated canine total hip replacements. Quantification by backscattered scanning electron microscopy and image analysis. *Scanning Microsc* 1989;3:1051–1057.
29. Skedros JG, Bloebaum RD, Bachus KN, Boyce TM. The meaning of gray levels in backscattered electron images of bone. *J Biomed Mater Res* 1993;27:47–56.
30. Skedros JG, Bloebaum RD, Bachus KN, Boyce TM, Constantz B. Influence of mineral content and composition on gray levels in backscattered electron images of bone. *J Biomed Mater Res* 1993;27:57–64.
31. Ramirez MP, Calvo JL, Mate JE, Delgado RA, Negri B, Barona C. Ultrastructural study by backscattered electron imaging and elemental microanalysis of bone-to-biomaterial interface and mineral degradation of porcine xenografts used in maxillary sinus floor elevation. *Clin Oral Implants Res* 2013;24:523–530.
32. Yamauchi K, Takahashi T, Funaki K, Hamada Y, Yamashita Y. Histological and histomorphometrical comparative study of β -tricalcium phosphate block grafts and periosteal expansion osteogenesis for alveolar bone augmentation. *Int J Oral Maxillofac Surg* 2010;39:1000–1006.
33. Calvo JL, Delgado RA, Ramirez MP, Maté JE, Ortiz A, Abboud M. Histomorphometric and mineral degradation study of Ossceram[®]: A novel biphasic B-tricalcium phosphate, in critical size defects in rabbits. *Clin Oral Implants Res* 2012;23:667–675.
34. Lazáry A, Balla B, Kósa JP, Bácsi K, Nagy Z, Takács I, et al. Effect of gypsum on proliferation and differentiation of MC3T3-E1 mouse osteoblastic cells. *Biomaterials* 2007;28:393–399.
35. Ono D, Jimbo R, Kawachi G, Ioku K, Ikeda T, Sawase T. Lateral bone augmentation with newly developed β -tricalcium phosphate block: An experimental study in the rabbit mandible. *Clin Oral Implants Res* 2011;22:1366–1371.
36. Ebrahimi M, Pripatnanont P, Monmaturapoj N, Suttapreyasri S. Fabrication and characterization of novel nano hydroxyapatite/ β -tricalcium phosphate scaffolds in three different composition ratios. *J Biomed Mater Res A* 2012;100:2260–2268.
37. Araújo MG, Liljenberg B, Lindhe J. Dynamics of Bio-Oss Collagen incorporation in fresh extraction wounds: An experimental study in the dog. *Clin Oral Impl Res* 2010;21:55–64.
38. Sharifi D, Khoushkerdar HR, Abedi G, Asghari A, Hesaraki S. Mechanical properties of radial bone defects treated with autogenous graft covered with hydroxyapatite in rabbit. *Acta Cir Bras* 2012;27(3):256–259.
39. Yin X, Stott MJ. Theoretical insights into bone grafting silicon-stabilized alpha-tricalcium phosphate. *J Chem Phys* 2005;122(2):024709.

Jose Eduardo Maté Sánchez
de Val
José Luis Calvo Guirado
Maria Piedad Ramírez
Fernández
Rafael Arcesio Delgado Ruiz
Patricia Mazón
Piedad N. De Aza

In vivo behavior of hydroxyapatite/ β -TCP/collagen scaffold in animal model. Histological, histomorphometrical, radiological, and SEM analysis at 15, 30, and 60 days

Authors' affiliations:

Jose Eduardo Maté Sánchez de Val, Professor of International Dentistry Research Cathedra, Universidad Católica San Antonio de Murcia (UCAM), Murcia, Spain

José Luis Calvo Guirado, Full Professor in Dentistry Chairman of International Dentistry Research Cathedra, University of Católica San Antonio de Murcia.(UCAM), Murcia, Spain
Maria Piedad Ramírez Fernández, International Dentistry Research Cathedra, Universidad Católica San Antonio de Murcia (UCAM), Murcia, Spain
Rafael Arcesio Delgado Ruiz, Prosthodontics and Digital Technologies, Stony Brook University, Stony Brook, NY, USA

Patricia Mazón, Departamento de Materiales, Óptica y Tecnología Electrónica, Universidad Miguel Hernández, Avda Universidad s/n, 03202, Elche, Alicante, Spain

Piedad N. De Aza, Bioengineering Institute, Miguel Hernandez University, Avda Universidad s/n, 03202 Elche, Spain

Corresponding author:

José Eduardo Maté-Sánchez de Val
Plaza los Luceros no 15 Bajo izq.
03004 Alicante

Spain
Tel.: +34 637 477 932
Fax: +34 965145695

e-mails: jmsodont@hotmail.com; jemate@ucam.edu

Key words: bioceramics, collagen, histomorphometry, hydroxyapatite, scaffolds, SEM, tricalcium phosphate

Abstract

Objective: The aim of this study was to fabricate and characterize HA/ β -TCP/collagen ceramic scaffolds of different composition ratios and compare their physical and *In vivo* mechanical behavior.

Materials and methods: Three groups of twenty samples each one of calcium-phosphate ceramic scaffold cylindrical implants (6 ± 0.01 mm in diameter and 2 ± 0.01 mm in length) were studied with varying wt % HA/wt % TCP/wt % Collagen composition: Group A: 40/30/30; Group B: 50/20/30; Group C: 60/20/20. A fourth group, Group D (unfilled critical size defect), acted as control. Three times of work were established 15, 30, and 60 days. Characterization, histological, histomorphometric, SEM, and radiological analysis were performed.

Results: Micrographs obtained on the different composites are comparable, it is possible observe that the materials revealed a microporous morphology formed by aggregated nanoparticles independently of the composition of the composite. BIC values for the three materials, with Group A showing best BIC at 15, 30, and 60 days (43.12 ± 0.14 ; 52.49 ± 1.08 and $67.23\% \pm 0.34$) (with closer contact observed) than Group B (38.84 ± 1.32 ; 47.64 ± 1.21 and 54.87 ± 0.32), followed by Group C (28.92 ± 2.41 ; 35.94 ± 1.92 and 48.53 ± 0.31).

Conclusions: The influence of time on the biological behavior of biomaterials studied has been demonstrated by varying the percentage of bone-implant contact and bone formation to obtain the best results at 60 days.

The use of biomaterials for bone regeneration is widely applied in the fields of bone reconstructive surgery, both in situations of bone atrophy, as in those where there are defects (Daculsi et al. 2003; Aghaloo & Moy 2007; Browaeys et al. 2007; McAllister & Haghigat 2007). An ideal material should have osteoinductive, osteoconductive, and osteogenic properties, which are achieved only by autologous bone regeneration, an ideal biomaterial should contain at least elements of conduction and induction to the formation of new bone. Within the group of synthetic biomaterials, formulations most commonly used are those composed of hydroxyapatite, tricalcium phosphate, and

combinations of both. Calcium phosphates have a composition and structure similar to the mineral phase of bone and are osteoconductive. Among the various materials used in recent years tricalcium phosphate (TCP) has shown promising results in tissue culture, animal experiments, and clinical studies (Krekmanov 2006; Esposito et al. 2008; Chopra et al. 2009).

Today, there are several types of commercially available calcium phosphate products for bone regeneration applications, including HA, β -TCP, and biphasic calcium phosphates (TCP/HA). With a similar composition to bone, HA ($\text{Ca}_{10}(\text{PO}_4)_6(\text{OH})_2$) is one of the most widely used chemistries for bioactive

Date:
Accepted 13 June 2015

To cite this article:

Maté Sánchez de Val JE, Calvo Guirado JL, Ramírez Fernández MP, Delgado Ruiz RA, Mazón P, De Aza PN. *In vivo* behavior of hydroxyapatite/ β -TCP/collagen scaffold in animal model. Histological, histomorphometrical, radiological, and SEM analysis at 15, 30, and 60 days. *Clin. Oral Impl. Res.* 00, 2015, 000-000
doi: 10.1111/clr.12656

materials (Ginebra et al. 2006). Due to its ability to promote osteoconduction, the presence of HA could enhance long-term performance of orthopedic implants. The combination of hydroxyapatite with tricalcium phosphate type B gets an ideal regeneration process material, with "bimodal" behavior; hydroxyapatite acts as a matrix for cell colonization and improves the mechanical properties of the material, with a long resorption times. Furthermore, the B-TCP act in the early stages of remodeling of the biomaterial, before being reabsorbed, and creating the ideal environment for the start of new bone medium (Mac-Millan et al. 2014). The ultimate goal was the union of fully differentiated osteoblasts that will support bone matrix production. This requires a porous structure with nanopores, micropores, and macropores, all involved in different stages of absorption, adhesion, and bone material deposition on and between the bone substitute material (Gauthier et al. 1999; Rivera-Munoz et al. 2001). Initial regeneration of the bone defect is favored by the presence of calcium phosphate in the bone replacement material (Baksh et al. 1998).

Bone substitutes based on calcium phosphates have differing physicochemical properties related to mechanical stability. They also undergo rapid degradation and have a volume instability, which does not allow new bone formation to retain the original volume (Wiltfang et al. 2002; Brogini et al. 2014).

Main advantages of using synthetic materials derived from the combination of B-TCP and hydroxyapatite are the absence of morbidity produced by obtaining autologous grafts, chemical similarity with the receiving medium and that it is fully compatible material that does not produce any anomalous inflammatory reaction during the regeneration process. Among the inconveniences, there is a lack of scientific basis related to the convergence of mechanical and physical properties between the biomaterial and the receiving area of the graft; besides the lack of organic content in the formulation of HA/B-TCP, which would get better adaptation to host bone (Fan et al. 2007; Dorozhkin 2010).

The use of biphasic calcium phosphates (BCP) is promising as conceptually it could overcome the disadvantages of single-phase ceramics by combining two or more ceramic phases. BCP ceramics offer controlled bioactivity and balanced biodegradation. They are osteoconductive and offer the possibility of acquiring osteoinductive properties. The conventional synthetic porous Ca-P ceramics have been composed of microscale grain size, but recent studies have focused on producing

bioceramics at the nanoscale. Nano-HA can promote osteoblast cell activity and facilitate osteointegration better than microcrystalline HA and so enhance new bone tissue formation. However, the superiority of biological calcified tissues is also due to the presence of bioorganic polymers (proteins, mainly collagen type I), which give strength and partial elasticity. Therefore, the development of organic/inorganic hybrid BCP scaffolds could provide excellent possibilities for optimizing conventional bone substitutes (Huang et al. 2012; Maté-Sánchez de Val et al. 2014a,b).

The incorporation of collagen during a biphasic ceramic synthesis is a suitable option to provide the organic part of the biomaterial, solving one of the main disadvantages of the completely inorganic ceramic. This addition of collagen improves the ability of cell attachment to the biomaterial and the beginning of the process of bone remodeling. There are various studies of BCP with different weight % in the literature but little of this research has been applied clinically. This is due to the controversy in the literature concerning the optimum weight % composition, and the ideal weight % composition of BCP for clinical application remains unclear. Furthermore, research has failed to confirm the beneficial effects of collagen coating on composite BCP scaffolds (Zheng et al. 2011; Maté-Sánchez de Val et al. 2014b).

The objective of this study was to fabricate and characterize HA/ β -TCP/collagen ceramic scaffolds of different composition ratios and compare their physical and *In vivo* mechanical behavior. The effect of collagen incorporation was also evaluated. The hypothesis was that the mechanical and physical properties would vary depending biomaterial implantation time and analysis. In addition, histological and histomorphometric analyses were performed to evaluate the osseointegration of each composition and by doing so, the influence of the HA/TCP/collagen ratio. Radiological analysis was performed to further determine the clinical behavior and resorption of these materials.

Material and methods

Raw materials and composition

The raw materials for this study were commercial collagen, hydroxyapatite (HA), and tricalcium phosphate (TCP). HA and TCP were obtained by solid-state reaction sintering. Details of the technique can be found in previous publications (Maté-Sánchez de Val et al. 2014a,b).

Table 1. Proportions of the constituents weighed out at the different biomaterials preparations

Compound	Group A	Group B (%)	Group C (%)
HA	40	50	60
B-TCP	30	20	20
Collagen	30	30	20

Ceramic scaffold preparation

The proportions of the constituents have been weighed out and thoroughly dry mixed in a mixing miller with PSZ-zirconia balls in a relation shown in Table 1. After the milling process, the powder mixture was cold isostatically pressed at 200 MPa. The pressure was maintained for 30 min, after which it was slowly depressurized to 101 325.00 Pa. The whole process took around 1 h.

Ceramics characterization

The mineralogical characterization of the powder material was performed by XRD (Bruker-AXS D8Advance, Bruker AXS GmbH, Karlsruhe, Germany) using Cu-K α radiation at 40 kV and 30 mA. Scans were performed with 2 θ values varying from 20 to 55° at a rate of 0.05°/min.

The morphology of the porous ceramic composites was studied using a scanning electron microscope (SEM, HITACHI S-3500N, Tokyo, Japan). Quantitative analyses were made by an Electronic Dispersive X-ray Spectroscopy (EDX) system coupled to the above-described electron microscope using ZAF (atomic number, absorption, and fluorescence) correction software and Bayer standards. Microanalysis data were obtained from the mean of ten independent determinations. The samples were precoated with palladium for SEM images and carbon coated for EDX analysis, under an argon atmosphere using a sputtering machine (Polaron K550X Sputter Coater, Berlin, Germany).

Apparent density measurement was taken on each sample using Archimedes' method by immersion in Hg. Sample mass was determined using an electronic balance, and relative density (RD) was calculated with the following equation:

$$RD = \frac{\rho_a}{\rho_t} 100,$$

where ρ_t and ρ_a are the samples' theoretical density and apparent density. The theoretical density of HA and β -TCP was considered as 3.156 and 3.07 g/cm³, respectively.

The pore size of different ceramic composites was evaluated using SEM micrographs.

Thirty readings for each composite were taken to calculate an average porosity value. Particle size distribution was measured by Laser scattering (Mod. Mastersize by Malvern). The specific surface area was measured by the chromatographic method (mod. Monosorb from Quantachrome Instruments, Boynton Beach, FL, USA) using BET model.

Three-point bending strength (σ_f) was measured with a Microtest universal testing machine set at a crosshead speed of 0.33 mm/s and a span of 40.0 mm. Fracture toughness (KIC) was also obtained in the 3-point bending test as a function of loading rate by the single edge precracked-beam method (Swab et al. 2015). Measurements were taken at room temperature using the rectangular-shaped samples ($3 \times 4 \times 45$ mm) with a notch width of less than 0.5 mm. The ratio between notch depth and sample thickness was 0.4. Young's modulus (E) was evaluated from the stress-strain curves obtained with the flexural strength test. Seven replicates were determined for each material, and the results were expressed as mean \pm standard deviation.

Material properties

Three groups of twenty samples each one of calcium-phosphate ceramic scaffold cylindrical implants (6 ± 0.01 mm in diameter and 2 ± 0.01 mm in length) were studied with varying wt% HA/wt% TCP/wt% collagen composition: Group A: 40/30/30; Group B: 50/20/30; Group C: 60/20/20. A fourth group, Group D (unfilled critical size defect), acted as control to verify that there was no interference in the process of regeneration. Three times of work were established, randomizing the four groups at each time by means of random number generator software, SPSSR

v.18.0. (IBM Corporation, New York, USA). The sample was divided into three periods of work, and in turn each time randomly for each study group.

Animal experimentation

Main protocol

The study protocol was approved by the Animal Ethics Committee of the University of Murcia, following Spanish Government and European Community Guidelines for animal care. Fifteen male New Zealand rabbits of 3.5–4.5 kg in weight were used. The three material variations were implanted in the animals' tibiae. General anesthesia included ketamine plus chlorbutol (5–8 mg/kg intravenously), 0.5–1 mg/kg acepromazine maleate as a coadjuvant, and 0.05 mg/kg atropine. Amoxicillin (0.1 ml/kg intramuscularly) was administered at the end of surgery. The total sample size was 15 rabbits with two defects in each tibia, a total of 60 defects, randomized in four groups of 15 for each material and control.

Surgical procedure

Two critical defects (6 mm \varnothing) were created in each tibia, making a total of 60. The surgical approach was in the proximal-medial area of the tibia, several millimeters below the frontal tuberosity. Bone tissue was removed with spherical surgical drills of 6 mm in diameter at low rotation speed with constant irrigation (Fig. 1a–d).

Histological and histomorphometric analysis

After the elapse of each period implantation time, the implants together with the surrounding tissues were removed and fixed in

10% neutral buffered formalin and decalcified. The decalcification method utilized Osteomoll Merck KbaA (Germany) containing HCl (10%) and CH_2O (4%), immersing samples for 17 days, and renewing the solution every 24 h. Subsequently, all samples were paraffin embedded, sectioned at 5 μm , and stained using hematoxylin–eosin. The entire circumference of each section (containing bone, grafted particles, and connective tissue) was traced manually to create an individual region of interest (ROI).

Histomorphometric evaluations consisted of measurements of the area of graft material in relation to the total measurement area. These were carried out using Image J software (developed by the National Institute of Health [NIH] of the United States of America). Examinations were performed under a Nikon Elipse 80i microscope (Teknooptik AB, Huddinge, Sweden), equipped with an Easy Image 2000 system (Teknooptik AB) using 10–40 \times lenses for descriptive evaluation and morphometric measurement. Images were generated using a Leica Z6 APO microscope connected to a Leica DC 500 (Barcelona, Spain) digital camera, enlarged 23 \times . After calibrating the system and digitalizing images, interactive measurements of the areas of interest were obtained using image analysis software Leica QWin V3 (Barcelona, Spain). Histomorphometric analysis produced one bone-to-implant contact (BIC) measurement, measured as the percentage of the circumference, and length of the cylinder in contact with new bone.

Resorption rate and pattern of surface resorption

The image analysis program Image J (National Institutes of Health, Bethesda, MD,

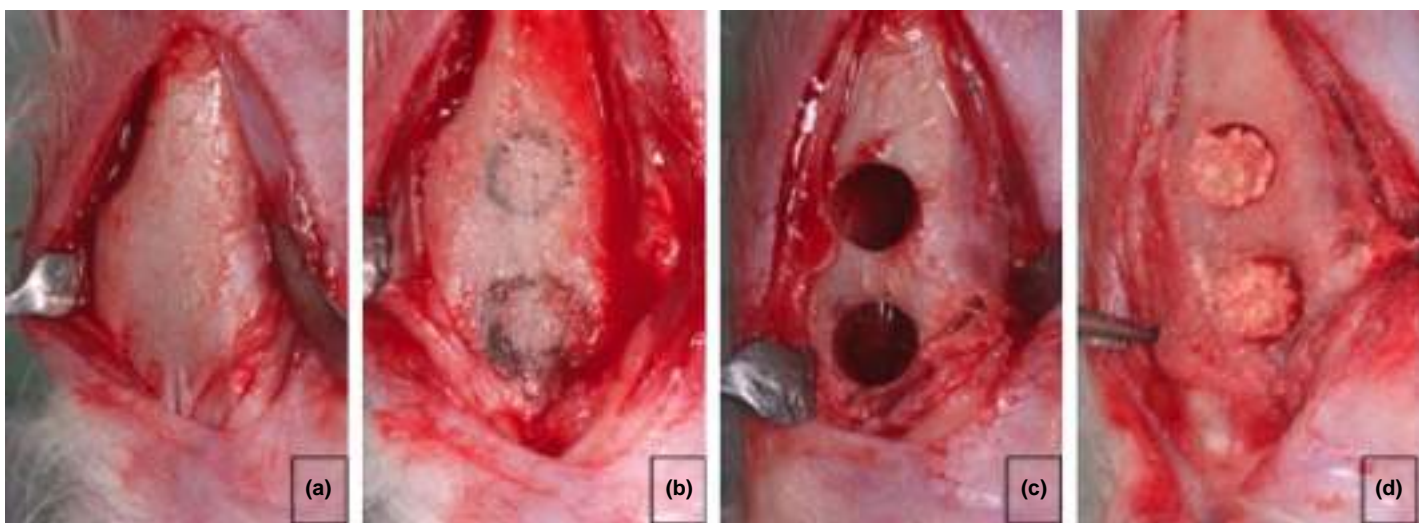


Fig. 1. Clinical images of surgical defect preparation and biomaterials placement.

USA) was used to calculate the resorption rate of the different material compositions. This was performed by demarcating the area of interest as the total biomaterial at the time of implantation, measuring its perimeter, and comparing this with the residual material after 15, 30, and 60 days.

Scanning electron microscope study

Twenty samples of each material (A: 40/30/30; B: 50/20/30; C: 60/20/20) were studied after 15, 30, and 60 days of implantation comparing variations in the ratios of Ca/P percentages. The samples were fixed by immersion in 4% formalin solution, dehydrated in a graded ethanol series, and embedded in plastic resin (Technovit A 7210VCL; Kulzer & Co, Hanau, Germany). They were then polished using a manual grinder with 800 grit silicon carbide paper, mounted on an aluminum stub and carbon coated (using a Polaron sputter coater). Samples were examined using the SEM-Hitachi S-3500N at a working distance of 19 mm, an acceleration voltage of 15 kv and 15× magnification, with an Oxford Instruments INCA 300 EDX System (Abingdon, Oxfordshire, UK), evaluating elemental composition of the graft material and bone in the medullary area. Areas of interest were delimited by the inner cortical walls and reached into the medullary core. Elemental mapping was performed in order to determine the chemical degradation process and changes to medullary composition in all four study groups.

Radiological study

Digital radiographs were taken (using a Kodak 6100, Eastman Kodak, Rochester, NY, USA) following sample removal using a custom-made acrylic support to ensure reproducibility of the technique. Exposure parameters were standardized. Each radiograph was studied using image analysis software Image J (National Institute of Health, Bethesda, MD, USA).

Statistical analysis

Statistical analysis was performed using PASW Statistics v.18.0.0 software (SPSS Inc). Values were recorded as mean ± standard deviation. Nonparametric Friedman test was applied to the comparison of medians and to quantify relationships between differences ($P < 0.05$). Equal means were regarded as the null hypothesis, whilst the existence of differences between means acted as an alternative hypothesis. As significant differences between the means existed, the null hypothesis was rejected.

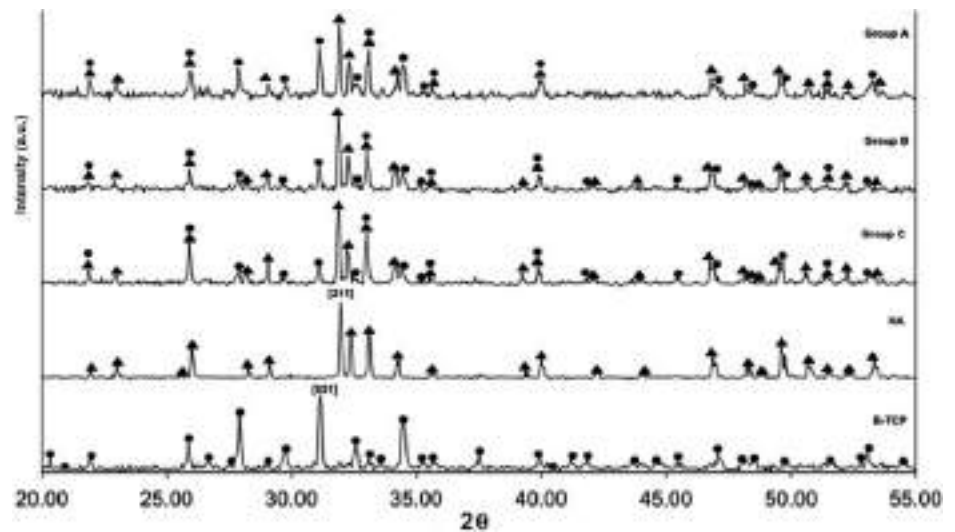


Fig. 2. X-ray diffraction patterns of the synthesized powder of TCP and HA as well as the composite ceramic powder materials.

Results

Preoperative material characterization

Fig. 2 shows the X-ray diffraction patterns of the synthesized powder of TCP and HA as well as the composite ceramic powder materials. It can be seen that the polymorphic form obtained was β -TCP in the rhomboedral crystalline system with main diffraction plan [021] and corresponded to JCPDS card no. 9-0169. On the other hand, the HA corresponded to JCPDS card no. 09-0432 and presents hexagonal system with main diffraction plan [211]. No other secondary phases were detected. The XRD patterns of the composite ceramic compositions showed peaks corresponding with β -TCP and HA.

The physical and mechanical properties of the ceramic scaffolds are reported in Table 2. As the collagen content increased (from 20 to 30 wt%), the porosity increased by about 4% for group B composition to about 9% for Group A. Bending strengths ranged between 7.76 and 8.21 MPa. Although there was almost no difference between the composites, it was obvious that the addition of collagen produced various responses among the different ratios in relation with porosity and mechanical properties of the compounds. Fracture toughness, the material's resistance to crack propagation, is an important parameter for assessing a material's susceptibility to failure. In general, toughness was seen to increase for Group B and decrease for Group A with the addition of collagen. When each group was compared, significant differences were recorded (to facilitate comparison, the properties of sintered HA, β -TCP, cortical, and cancellous bone are also included).

Table 3 shows the results of the specific surface on the nanostructured powders after milling β -TCP, HA, and the ceramic composites. The results show higher values for the HA matrix, getting to 10.4 m²/g. Also the HA powder present a morphology formed by clustered nanoparticles smaller in size by 50 nm, and the β -TCP powder shows nanoparticles bigger to those found for HA. The results found for the β -TCP, and HA nanostructured powder after the mill shows a change of the nanoparticles surface, generated by the process in the attrition mill. This superficial change of the nanoparticles has already been identified by other authors that have used the high-energy method of attrition milling in the development of ceramic powders (Camargo et al. 2012, 2014).

Fig. 3 shows surface morphology of the three composites. If the micrographs obtained on the different composites are comparable, it is possible observe that the materials revealed a microporous morphology formed by aggregated nanoparticles independently of the composition of the composite. The particles present an average diameter of ~50–60 nm. In addition, dense powder aggregates with sizes of ~2–5 μ m were observed.

Histological and resorption analysis

Analysis of the histological sections of each of the three materials was performed at 15, 30, and 60 days postimplantation. None of the grafted materials elicited a significant inflammatory reaction. In all samples, woven bone was identified around and in close contact with the material and, as might be expected in rabbit tibia bone, small marrow spaces were observed in the peri-material

Table 2. Microstructural characterization of materials. Physical and mechanical properties of the ceramic scaffolds

	Group A	Group B	Group C	Sintered HA	Sintered TCP	Cortical bone	Cancellous bone
Crystalline phases	HA/ β -TCP	HA/ β -TCP	HA/ β -TCP	HA	β -TCP	CHA	CHA
Porosity (%)	32 \pm 1.23	27 \pm 1.07	23 \pm 0.98			5–12	46–95
Density (g/cm ³)	2.18 \pm 0.56	2.20 \pm 0.67	2.35 \pm 0.38	99.2 \pm 0.98	99.7 \pm 0.87		
RD (%)	76.25 \pm 2.34	78.12 \pm 2.56	85.25 \pm 3.01			1.8–2.0	0.09–1.0
Bending strength, σ_f (MPa)	7.76 \pm 1.02	8.21 \pm 0.99	7.92 \pm 1.76	115–200	140–154	60–147	0.5–8.0
Young's modulus, E (GPa)	3.15 \pm 1.12	3.18 \pm 0.89	3.16 \pm 1.02	80–110	33–90	11–19	0.06–1.5
Fracture toughness, K_{1c} (MPam ^{1/2})	0.34 \pm 0.03	0.40 \pm 0.12	0.37 \pm 0.07	1.0		2–11	

Table 3. Specific surface of the presintered materials as well as the composites

	B-TCP	HA	Group A	Group B	Group C
Superficial area (m ² /g)	8.7 \pm 0.5	10.4 \pm 0.5	8.6 \pm 0.5	8.8 \pm 0.5	9.3 \pm 0.5

bone, which had reached maturity over 60 days. The volume of the graft block in Group A decreased progressively during the time of study, starting with minimal signs at 15 days until the material reabsorbed at 60 days and increased new bone formation surrounding and inside the biomaterials; bone formation increased at the periphery and within the block, leading to its virtual disappearance and almost complete closure of the cortex at 60 days. In Group C, graft blocks showed slower resorption than the other groups; histological results showed that following implantation, changes to residual block content, peripheral bone resorption, new bone formation and closure of the cortex were minimal in comparison with the other graft compositions (Fig. 4). In tibiae treated with Group B blocks, there was intermediate block stability, much greater resorption than in Group C, less than Group A, and an intermediate rate of neoformation. In the control group, no spontaneous closure of the defect was seen, as might be expected of a critical defect. The resorption pattern was variable across the groups being observed a progressive resorption during the time of study to

achieve greater resorption at 60 days. Thus, 15 days there is a partial resorption, being higher for group A, followed by group B and group C where finally reabsorption is partial. Similarly to 30 days resorption rates are higher with respect to the 15-day study and lower than those found at 60 days for the three study groups. Group A samples showed numerous resorption foci on block surfaces, which produced a much more irregular surface compared with other samples (peaked resorption pattern). Group B samples presented intermediate behavior showing a moderate resorption pattern, with fewer light areas and less irregularity, following a wavy resorption type across the surface. Finally, in Group C, a linear pattern was observed with few resorption foci that were more regular and less active (linear resorption pattern).

Histomorphometric analysis

Histomorphometric analysis was carried out to establish BIC values for the three materials, with Group A showing best BIC at 15, 30 and 60 days (43.12 \pm 0.14; 52.49 \pm 1.08 and 67.23% \pm 0.34) (without empty spaces) than Group B (38.84 \pm 1.32; 47.64 \pm 1.21 and

54.87 \pm 0.32), followed by Group C (28.92 \pm 2.41; 35.94 \pm 1.92 and 48.53 \pm 0.31), in which close contact between bone and graft was significantly less. Moreover, new bone ingrowth, defect closure, and residual biomaterial were recorded and analyzed, showing better values for Group A samples in comparison with the other groups (Table 4).

Scanning electron microscopy and EDS analysis

SEM images showed complete integration of all specimens, without significant differences between the groups. In all cases, the cell growth was observed to be orderly and structured; there was cell attachment to the biomaterial and the establishment of an interface between the biomaterial and the old bone (Fig. 5). Examining the details of each panoramic image, Group A showed integration of the graft in the tibial bone (5a), as well as cellular arrangement over the graft block (5b). In Group B, integration existed in the surrounding bone (5c) and an equally cellular arrangement and growth over the graft (5d). In Group C, a higher percentage of residual graft material was observed at 60 days (5e), as well as cellular surface growth, but integration arranged on the surface. The interrelation with the peripheral bone was worse in comparison with the other two composites (5f). EDS analysis showed higher content of Ca and P in the new bone region

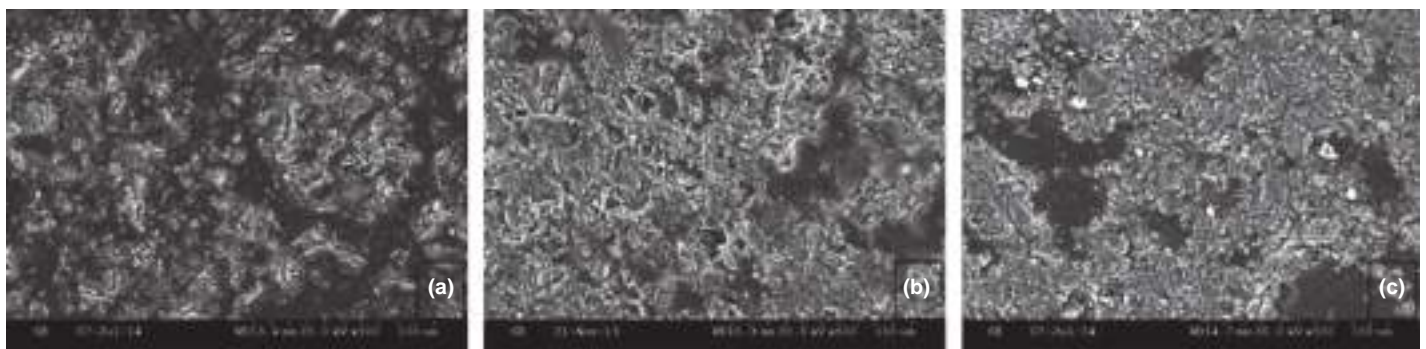


Fig. 3. Surface morphology of the three composites. SEM Images at 100 μ m.

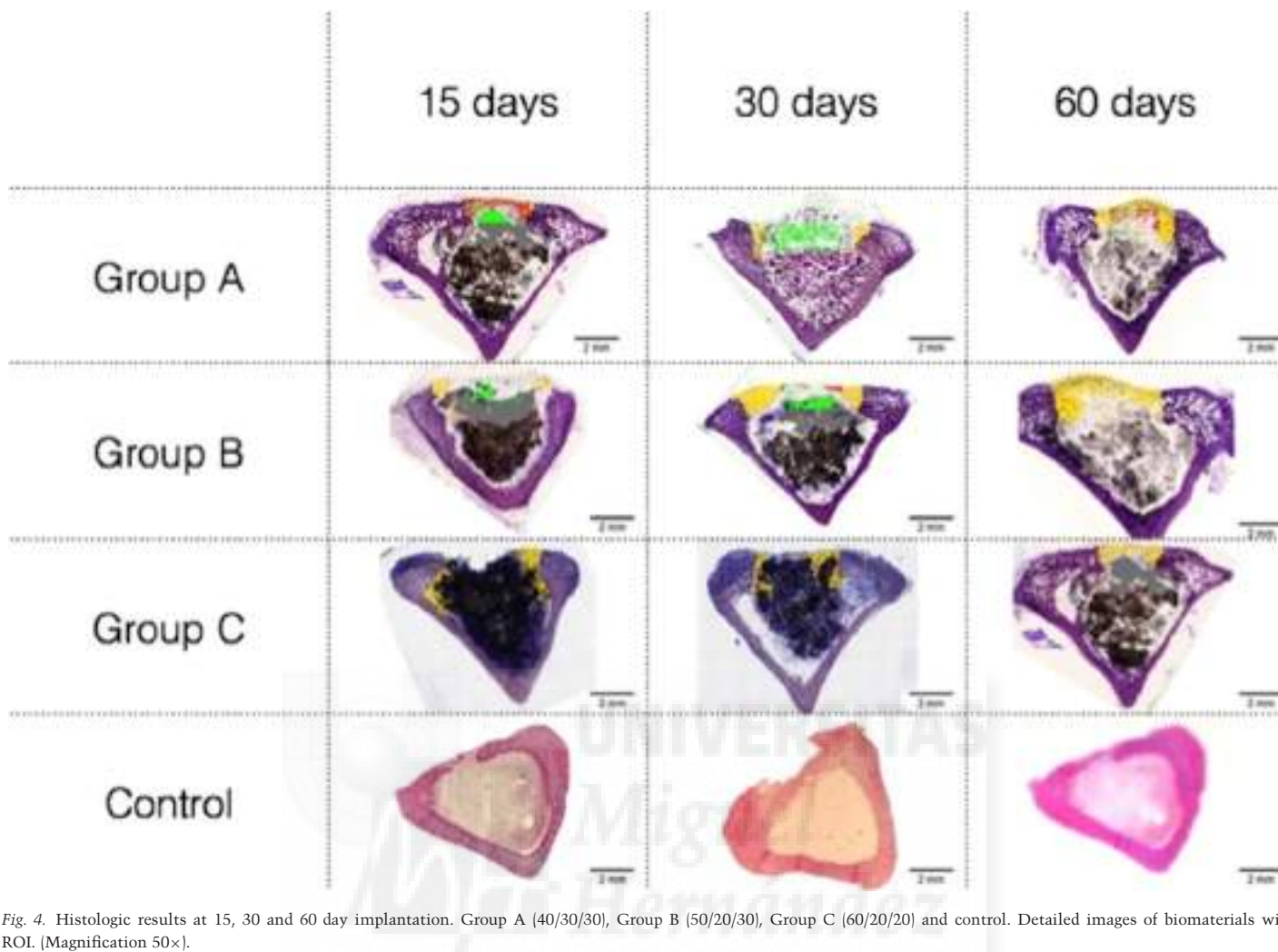


Fig. 4. Histologic results at 15, 30 and 60 day implantation. Group A (40/30/30), Group B (50/20/30), Group C (60/20/20) and control. Detailed images of biomaterials with ROI. (Magnification 50 \times).

for the composites of higher collagen content. The best results were recorded for Group A. The Ca/P ratio at the interface was best for Group A, as listed in Table 5.

The BSE imaging was used to highlight contrasts between resin, bone, and biomaterial. EDX was used to identify and evaluate the relative concentrations of all chemical elements present in the tissues, using point analysis to determinate mineral distribution. EDX spectra were collected at discrete points in each biopsy (* from Fig. 5). Elemental composition (atomic %) of the graft materials and bone were calculated from the spectra.

In BSE images, particles of HA/TCP/ collagen implant were seen to be a white-gray color due to low organic content and a relatively high Ca/P ratio (atomic %), whereas newly formed bone had a darker gray color because of the presence of collagen, marrow, and fat. SEM-BSE evaluation confirmed that the residual graft particles were surrounded by newly formed bone, which presented characteristics of mature bone with well-organized lamellae

and numerous small osteocytic lacunae (Fig. 5).

The bone-to-biomaterial interface was characterized by small numbers of projections of newly formed bone reaching into the graft particles. In many areas, much bigger regions containing exposed and partly loose parent implant particles were present, as a result of the material degradation in the physiological environment.

After 15 days of implantation, the implant was already well integrated into the host tissue, forming an irregular surface boundary caused by gradual degradation of the material, Fig. 4. The interface developed between the implant and the surrounded tissue was characterized by intermittent presence of calcium phosphate phase, which corresponded in structure and morphology to new bone tissue. The EDS analysis (Table 5) and histological studies backed up these findings. In many areas, much bigger regions containing exposed and partly loose parent implant particles were present, as a result of the material degradation

in the physiological environment. These particles are marked by arrows in Fig. 4.

At 30 days, the outside surface of the implant presented active regions, where the degradation process of the material originated. These observations led to the conclusion that interfacial activities at 60 days were already well in progress, remodelling the chemistry and morphology of the interface.

Radiological study

Radiographs were made following sample extraction, observing integration with the host bone in all study groups (Fig. 6). The radiographic density varied with the chemical content of the samples, with Group A showing correct integration and partial resorption that corresponded to the histological findings; Group B behaved similarly and was seen to be fully integrated with the surrounding bone; Group C showed a greater presence of residual biomaterial and correct integration. There was no spontaneous closure of the defect, as could be expected for a critical defect.

Table 4. Histomorphometric analysis to evaluate BIC for the three materials

Group A				
Time (days)	15	30	60	P values
BIC (%)	43.12 ± 0.14*(43.12)	52.49 ± 1.08* (52.50)	67.23 ± 0.34* (67.23)	0.012
New bone ingrowth	39.32 ± 3.01*(39.32)	58.38 ± 2.14* (58.38)	78.23 ± 2.65* (78.22)	0.026
Defect closure	18.64 ± 1.13 (18.64)	37.43 ± 2.41* (37.43)	63.34 ± 3.43* (63.34)	0.031
Residual biomaterial	78.32 ± 1.09* (78.32)	65.09 ± 0.94* (65.10)	59.34 ± 2.95 (59.34)	0.009
Resorption rate	21.68 ± 2.18 (21.68)	34.91 ± 3.21* (34.91)	40.66 ± 3.10* (40.66)	0.038
Group B				
Time (days)	15	30	60	
BIC (%)	38.84 ± 1.32 (38.84)	47.64 ± 1.21* (47.64)	54.87 ± 0.32* (54.87)	0.017
New bone ingrowth	34.73 ± 10.65 (34.73)	56.03 ± 1.74* (56.04)	74.12 ± 2.83* (74.12)	0.030
Defect closure	16.32 ± 2.01 (16.33)	34.63 ± 3.21* (34.63)	59.54 ± 3.32* (59.55)	0.025
Residual biomaterial	80.09 ± 1.05* (80.09)	72.52 ± 0.98* (72.52)	63.43 ± 2.90 (63.43)	0.006
Resorption rate	19.91 ± 0.39 (19.91)	27.48 ± 2.43* (27.49)	36.57 ± 2.64* (36.57)	0.041
Group C				
Time (days)	15	30	60	
BIC (%)	28.92 ± 2.41 (28.92)	35.94 ± 1.92 (35.94)	48.53 ± 0.31* (48.53)	0.029
New bone ingrowth	29.75 ± 1.10 (29.75)	68.48 ± 3.01* (68.48)	72.52 ± 2.49* (72.52)	0.003
Defect Closure	19.94 ± 2.01 (19.94)	32.24 ± 0.64 (32.24)	60.46 ± 3.01* (60.47)	0.015
Residual Biomaterial	83.32 ± 2.31* (83.32)	74.34 ± 0.64 (74.34)	79.39 ± 2.98 (79.40)	0.019
Resorption rate	16.68 ± 1.22 (16.67)	25.66 ± 1.18* (26.66)	20.61 ± 3.01 (20.61)	0.007
Control				
Time (days)	15	30	60	
BIC (%)	0.00 ± 0.00	0.00 ± 0.00	0.00 ± 0.00	
New bone ingrowth	24.84 ± 0.05 (24.84)	29.84 ± 2.13 (29.84)	37.38 ± 3.97 (37.38)	0.069
Defect Closure	10.21 ± 0.32 (10.21)	23.98 ± 3.10 (23.99)	34.21 ± 2.34 (34.20)	0.003
Residual Biomaterial	0.00 ± 0.00	0.00 ± 0.00	0.00 ± 0.00	
Resorption rate	0.00 ± 0.00	0.00 ± 0.00	0.00 ± 0.00	
Nonparametric Friedmann test. Significant differences *P < 0.05. Mean ± SD (Median).				

Discussion

The results obtained from the x-ray diffractometry on the ceramic composites powders show the presence of representative peaks from the β -TCP and HA phases for all the powder compositions, where only a slight variation in the intensities of the peaks between the compositions, which is related to the presence of the concentration of phases in % in each two phase powder composition.

The presence of a larger concentration of the matrix HA in the composites was prepared, which lead to a slight reduction of the specific surface for these compositions, if these results are associated with the HA matrix (Table 4). This small variation in the specific surface between the compositions can be explained by the slight variation of the morphological characteristics, previously observed through the micrographs represented by Fig. 3a–c, where there is a thin morphology of nanoparticles for the HA matrix. Morphological characterization has shown that the powder HA has a morphology that is more refined than the

powder β -TCP. It has been observed that this fine morphology of the powder HA has also influenced the values of the superficial area obtained by BET, showing slightly superior superficial area, for the compositions with a larger concentration of the matrix HA. These fine morphologies found can be a potential in the development of biomaterials for bone replacement and leads to innovative results in the microstructural level of microporosity and of surface grains and microporos. The literature shows that the developments of β -TCP/HA nanostructured powders and biphasic composites have two basic targets: improve physical characteristics as open porosity, superficial area of grains and microporus, and biomaterial solubility.

In this paper, three different compositions of the combination of hydroxyapatite, β -TCP and collagen are formulated. The differences in the proportions of the three synthesized materials must produce different reactions *In vivo* in animals which are implanted, as these variations of the composition will provide different resorption times, different mechanical, physical properties and therefore

a different *In vivo* behavior of the tested biomaterials. (Keaveny & Hayes 1993).

The adaptation of the properties of the biomaterial to the receiving area in relation to the physical, mechanical properties, their structural and biological behavior directly affects the remodeling process. So the greater convergence is achieved between the biomaterial and the receiving area, the better it will behave the biomaterial. The effect of collagen can be understood as facilitating the early stages of cell anchorage to the biomaterial and as a vehicle allowing the action of bone cells to initiate biomaterial substitution by new bone. Currently, several synthetic routes have been utilized for the preparation of calcium-phosphate ceramic powders with different composition ratios. In this study, a solid-state reaction followed by cold isostatic pressing was used successfully for preparation of porous calcium-phosphate ceramic scaffolds. This technique is simple and economical (Dorozhkin 2009).

Additionally, the integration of all HA/TCP/Collagen bone substitute materials within their implantation bed was observed, focusing on the pattern of tissue in-growth

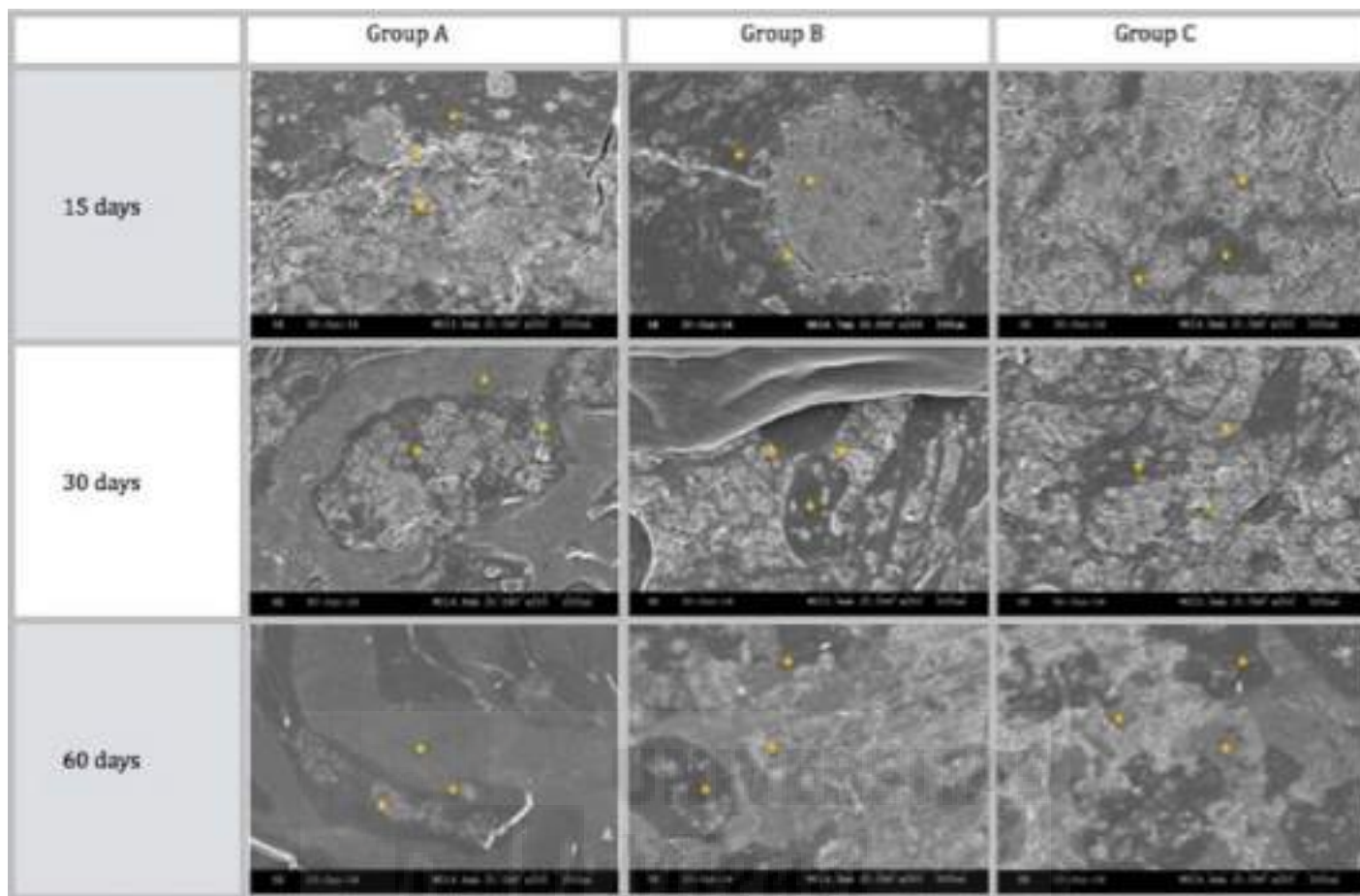


Fig. 5. SEM analysis of samples after 15, 30, and 60 days implantation showing biomaterials, interface, and new bone; Group A (40/30/30), Group B (50/20/30), and Group C (60/20/20), images show correct integration of the implant and the absence of peripheral gaps surrounding the materials. (Original magnification: 50×; 200 μm).

Table 5. EDS analysis with content of Ca and P in the new bone region, interface, and residual biomaterial for the composites at 15, 30, and 60 days

Ca/P Ratio	New Bone			P values
	Group A	Group B	Group C	
15 days	2.13 ± 0.23 (2.13)	2.19 ± 1.02 (2.19)	2.43 ± 0.10* (2.43)	0.005
30 days	2.23 ± 0.16 (2.23)	2.20 ± 0.65 (2.20)	2.46 ± 0.61* (2.46)	0.038
60 days	2.26 ± 0.64 (2.26)	2.23 ± 0.93 (2.23)	2.49 ± 1.23* (2.49)	0.012
Ca/P Ratio	Residual Biomaterial			P values
	Group A	Group B	Group C	
15 days	2.22 ± 1.2 (2.22)	2.06 ± 1.43 (2.06)	2.44 ± 0.45* (2.44)	0.021
30 days	2.19 ± 1.02 (2.18)	2.12 ± 0.54 (2.12)	2.48 ± 1.01* (2.49)	0.031
60 days	2.23 ± 0.88 (2.22)	2.08 ± 0.43 (2.08)	2.45 ± 0.98* (2.45)	0.001
Ca/P Ratio	Interface			P values
	Group A	Group B	Group C	
15 days	2.34 ± 0.99 (2.34)	2.23 ± 1.25 (2.23)	2.42 ± 0.59* (2.42)	0.047
30 days	2.29 ± 0.67 (2.29)	2.30 ± 1.11 (2.30)	2.41 ± 0.27 (2.41)	0.064
60 days	2.70 ± 1.02* (2.70)	2.06 ± 1.10 (2.06)	2.20 ± 0.75 (2.20)	0.024

Nonparametric Friedmann test. Significant differences *P < 0.05. Mean ± SD (median).

into the granules in relation to their particle size, porosity, and morphology. Group C present a slow resorption pattern according to the biggest particle size (Table 3). On the other

hand, group A with the smaller particle size presents the faster resorption pattern and group B with middle particle size presents a moderate resorption pattern (Tables 3 and 4).

Changes in particle size, porosity, and morphology of HA/TCP/Collagen implants induce not only different resorption pattern also the residual of biomaterial after the study.

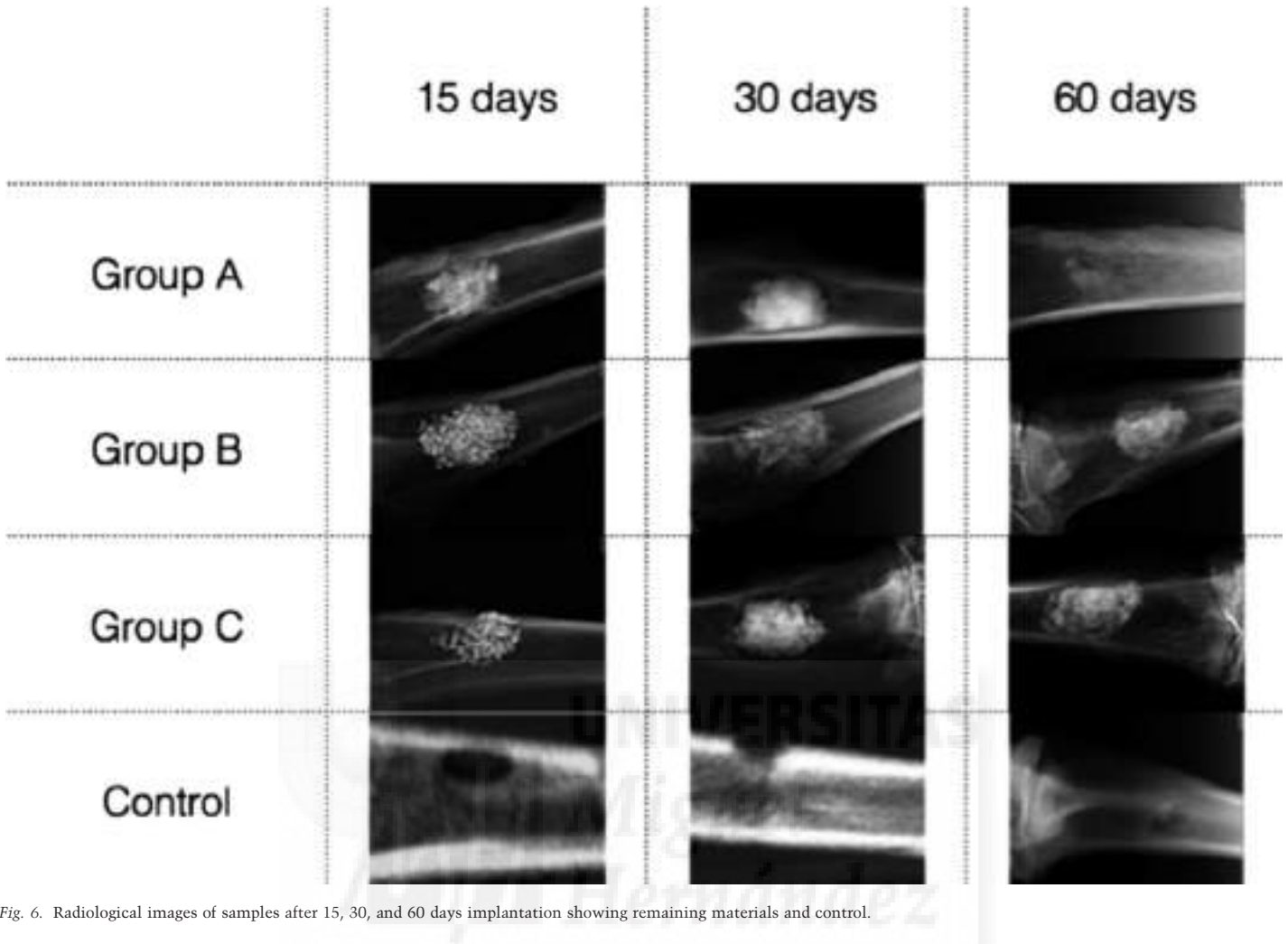


Fig. 6. Radiological images of samples after 15, 30, and 60 days implantation showing remaining materials and control.

Human cortical bone bears a total porosity of 5–12% depending on different anatomical sites with the pores in the range of nano to macroscale that are well interconnected (Table 2). However, the total porosity of HA/TCP/collagen implants in this study was much higher and in the range of 23–32% with high interconnectivity. Interconnections between pores must have a key influence on bone ingrowth and are necessary to promote body fluid circulation, angiogenesis, cell communication, and migration to the core of the implant. It is reported that the degree of interconnectivity of implants is more important than the size of pores as it greatly affects the vascularization for new bone penetration and formation.

The surface roughness of biomaterials directly influences the possibility to create a zone of facilitated cell anchorage. This synthesis process achieves a highly rough and irregular surface appearance with some micro-cracks, creating a favorable environment for the initial attachment of cells and the beginning of the process of bone remodel-

ing. Studies of the effects of collagen on the behavior of ceramic composite scaffolds have not found any significant differences in physical–mechanical properties arising from different ratios of collagen content (Maté-Sánchez de Val et al. 2014a,b). Therefore, other factors such as porosity and density must play a major role in determining the physical, mechanical properties, and biological behavior of HA/TCP/collagen ceramic scaffolds. When the present study data were compared with human bone (Table 2), the materials' Young's moduli were quite different from that of cortical bone but were closer to cancellous bone (Keaveny & Hayes 1993).

Brodie et al. (2006) reported that collagen coating increases the strength of HA/TCP 50/50 (wt%), whereas it weakens HA/TCP 25/75 (wt%) and pure TCP discs. These inconsistent mechanical behaviors are in accordance with our results.

One of the main disadvantages of the cold isostatic method is the poor mechanical strength of the materials for load bearing applications (Table 2). Although a highly por-

ous scaffold is preferred, as it will favor bone cell adhesion and regeneration, this is achieved at the expense of mechanical strength and resistance. However, the method can be improved by incorporating collagen into the composite material to achieve improved mechanical strength and optimum physico-biological properties.

Multiple light microscopy and SEM evaluations of the implant–bone interface show how the same structure is represented differently according to the examination method selected. The precision and reliability of a histomorphometric study of newly formed bone depends upon the correct identification and ultra structural characterization of all the cellular components that might play a role in the osseointegration process. Optical microscopy lacks the resolving power required for detailed structural analysis (Jasty et al. 1989; Orsini et al. 2005; Wierzbosch et al. 2008).

It is widely known that bone calcification is preceded by the formation of an extracellular organic matrix, primarily secreted by bone

cells. Bone-forming cells – active osteoblasts and osteocytes – control the synthesis of this extracellular matrix and regulate the exchange between ions present in bulk extracellular fluid and those present in calcified bone. In this way, only a detailed *in situ* study and precise visualization of all the components at the interface between the biomaterial surface and newly formed bone will provide an adequate assessment of the bone integration process.

In the present study, SEM and EDX analysis revealed a close relation between newly formed bone matrix and graft particle surface. Elemental analysis of the bone tissue demonstrated the presence of calcium and phosphorus, pointing to the presence of mineralized bone tissue on the particle surface. This observation suggests that the graft surface could provide an optimal stratum for bone tissue ingrowth. Furthermore, SEM analysis showed that a new bone matrix had developed over the graft surface.

SEM analysis of the samples studied, revealed intimate contact between biomaterials and bone receptor areas, with significant absences spaces that could lead to the conclusion that it is wrong the integration of biomaterials used. The three compositions behaved in a similar way, an increased mineral content observed in those samples where the hydroxyapatite content is higher (60%).

Elemental analysis of the bone tissue demonstrated the presence of calcium and phosphorus, pointing to the presence of mineralized bone tissue. This observation suggests that the graft surface may provide an optimal stratum for bone tissue ingrowth (Skedros et al. 1993a,b; Ramirez et al. 2013). The highest concentrations of calcium in the interface region were recorded for group A, indicating the highest levels of new bone formation, due to the faster ion exchange rate in the interface area. The presence of extracellular Ca^{2+} resulting from resorption activity might be involved in the stimulation of osteoblasts.

Yamauchi et al. 2010; showed that moderately high extracellular Ca^{2+} is a chemotactic and proliferating signal for osteoblasts and stimulates pre-osteoblast differentiation. Groups A and B had a high degree of porosity facilitating the implants' resorption process as the external and internal surface areas of the pores were exposed to the medium over the several microns distance beyond the graft body (as the results from the elemental mapping indicated), in turn facilitating osteoconduction. Analysis was carried out at a selection of different points,

taking different points of interest from the middle and from the periphery of the samples to detect changes to Ca/P ratios. This element mapping revealed an increase in the areas of Ca and P reaching from within the biomaterial graft towards its periphery. It could be that this ion increases areas of biological apatite on the agglutinated Ca and P deposits and crystals, which in turn facilitate osseointegration. In all cases, a decrease in the percentage of Ca and P was found in the residual biomaterial, with respect to the initial composition, while a gradual increase in the percentages of Ca and P ratio was found at the interface, suggesting an increase in the osseointegrative capacity of the material and replacement by new bone at its periphery.

In agreement with an earlier study of the mineral degradation process of β -tricalcium phosphate using the SEM-BSE technique (Calvo et al. 2012), the present study found a release of Ca and P ions, which was seen to promote new bone growth; it is possible that high levels of Ca and P stimulate osseointegration due to their effects on osteoblast gene expression, as described by Lazáry et al. (2007). In normal calcified bone, the Ca/P molar ratio increases with increasing calcification.

The three compositions studied were completely biocompatible with perfect mechanical properties to accommodate the environment in which they were implanted. All were gradually reabsorbed without producing any abnormal inflammatory reaction. This process of partial and progressive resorption, allowed creating an ideal location for the gradual replacement by new bone. The fastest resorption rate of the material was in Group A > Group B > Group C and was related to the percentage of HA in each material and also collagen in the composition (Ebrahimi et al. 2012). A significant difference in resorption time and in the stability of the material was found in Group C, which showed greater stability and less resorption than the other studied groups during 15, 30 and 60 days.

Despite the New Zealand rabbit's rapid metabolic activity, other studies have established its validity as an experimental model for testing biomaterials used for bone replacement (Ono et al. 2011). In view of this, the results in this study were enhanced through the creation of critical defects of 6 mm diameter, which will not close spontaneously and therefore demonstrate the regenerative potential of the biomaterials under observation.

In relation to the bone-implant contact, all materials present a high percentage of inte-

gration, increasing progressively during the study period from 15 to 60 days, where the percentages are highest. The results show that the presence of collagen increases the percentage of integration of biomaterials studied as well as better results for group A are seen most new bone formation both in the periphery and inside of biomaterials. These results are progressively increased throughout the study period (Calvo et al. 2012). Therefore the increased collagen produces a material with a faster resorption time, and controlled resorption inside and periphery pattern. The dimensional stability of biomaterials is directly related to the concentration of hydroxyapatite, being slower the reabsorption in group C compared to the other two study groups.

The percentage of new bone formation for Group A samples was significantly higher than in the other groups; the presence of collagen allows internal replacement of the material by new bone within a favorable period of time, as demonstrated by the presence of new bone within the material and at its periphery.

Conclusions

The development of calcium phosphates nanostructured powders is a current research topic and has generated new perspectives in the development of biomaterials for bone tissue replacements. These new biomaterials can be used in orthopedics, in traumatology and dentistry, as a matrix element in filling defects and regeneration of bone tissue. The results obtained by BET show that the nanostructured powders offer nanometric morphologies with a superficial area that promises wettability, adherence and cellular proliferation in these surfaces. The cold isostatic method was used successfully for fabricating HA/TCP/Collagen ceramic scaffolds of desired shape and high porosity. Biomaterials proved to be biocompatible, bioresorbable and osseointegrative. SEM and elemental analysis revealed that newly formed bone was closely attached to the synthetic material, there was a gradual diffusion of Ca ions from the biomaterial into the newly forming bone at the interface.

The influence of time on the biological behavior of biomaterials studied has been demonstrated by varying the percentage of bone-implant contact and bone formation to obtain the best results at 60 days. Group A, have a faster resorption rate, Group B presents a moderate resorption pattern and

Group C a slow resorption pattern. Each material should have different clinical applications in relation with its *In vivo* behavior and with its resorptions patterns.

References

- Aghaloo, T.L. & Moy, P.K. (2007) Which hard tissue augmentation techniques are the most successful in furnishing bony support for implant placement? *International Journal of Oral & Maxillofacial Implants* **22**(Suppl): 49–70.
- Baksh, D., Davies, J.E. & Kim, S. (1998) Three-dimensional matrices of calcium polyphosphates support bone growth *in vitro* and *in vivo*. *Journal Material Science Material Medicine* **9**: 743–748.
- Brodie, J.C., Merry, J. & Grant, M.H. (2006) The mechanical properties of calcium phosphate ceramics modified by collagen coating and populated by osteoblasts. *Journal Material Science Materials Medicine* **17**: 43–48.
- Broggini, N., Bosshardt, D.D., Jensen, S.S., Bornstein, M.M., Wang, C.C. & Buser, D. (2014) Bone healing around nanocrystalline hydroxyapatite, deproteinized bovine bone mineral, biphasic calcium phosphate, and autogenous bone in mandibular bone defects. *Journal Biomedical Materials Research B: Appl Biomaterials* **29**: doi: 10.1002/jbm.b.33319.
- Browaeys, H., Bouvry, P. & De Bruyn, H. (2007) A literature review on biomaterials in sinus augmentation procedures. *Clinical Implant Dentistry and Related Research* **9**: 166–177.
- Calvo, J.L., Delgado, R.A., Ramírez, M.P., Maté, J.E., Ortiz, A. & Abboud, M. (2012) Histomorphometric and mineral degradation study of Osseoram (®): A novel biphasic B-tricalcium phosphate, in critical size defects in rabbits. *Clinical Oral Implants Research* **23**: 667–675.
- Camargo, N.H., De Lima, S.A. & Gemelli, E. (2012) Synthesis and characterization of hydroxyapatite/TiO₂n nanocomposites for bone tissue regeneration. *American Journal of Biomedical Engineering* **2**: 41–47.
- Camargo, N.H., Franczak, P.F., Gemelli, E., Costa, B.D. & Moraes, A.N. (2014) Characterization of three calcium phosphate microporous granulated bioceramics. *Advance Materials Research* **936**: 687–694.
- Chopra, P.M., Johnson, M., Nagy, T.R. & Lemons, J.E. (2009) Micro-computed tomographic analysis of bone healing subsequent to graft placement. *Journal Biomedical Materials Research B Applied Biomaterials* **88**: 611–618.
- Daculsi, G., Laboux, O., Malard, O. & Weiss, P. (2003) Current state of the art of biphasic calcium phosphate bioceramics. *Journal Materials Science Materials Medicine* **14**: 195–200.
- Dorozhkin, S.V. (2009) Calcium orthophosphates in nature, biology and medicine. *Materials* **2**: 399–498.
- Dorozhkin, S.V. (2010) Bioceramics of calcium orthophosphates. *Biomaterials* **31**: 1465–1485.
- Ebrahimi, M., Pripatnanont, P., Monmatrapoj, N. & Suttapreyasri, S. (2012) Fabrication and characterization of novel nano hydroxyapatite/β-tricalcium phosphate scaffolds in three different composition ratios. *Journal Biomedical Materials Research A* **100**: 2260–2268.
- Esposito, M., Grusovin, M.G., Kwan, S., Worthington, H.V. & Coulthard, P. (2008) Interventions for replacing missing teeth: bone augmentation techniques for dental implant treatment. *Cochrane Database Systematic Review* CD003607.
- Fan, H., Ikoma, T., Tanaka, J. & Zhang, X. (2007) Surface structural biomimetics and the osteoinduction of calcium phosphate biomaterials. *Journal Nanoscience Nanotechnology* **7**: 808–813.
- Gauthier, O., Boulter, J.M., Aguado, E., Legeros, R.Z., Pilet, P. & Daculsi, G. (1999) Elaboration conditions influence physicochemical properties and *in vivo* bioactivity of macroporous biphasic calcium phosphate ceramics. *Journal Material Science Materials Medicine* **10**: 199–204.
- Ginebra, M.P., Traykova, T. & Planell, J.A. (2006) Calcium phosphate cements as bone drug delivery systems: a review. *Journal Control Release* **113**: 102–110.
- Huang, Y., Zhou, G., Zheng, L., Liu, H., Niu, X. & Fan, Y. (2012) Micro-/nano- sized hydroxyapatite directs differentiation of rat bone marrow derived mesenchymal stem cells towards an osteoblast lineage. *Nanoscale* **4**: 2484–2490.
- Jasty, M., Bragdon, C.R., Schutzer, S., Rubash, H., Haire, T. & Harris, W.H. (1989) Bone ingrowth into porous coated canine total hip replacements. Quantification by backscattered scanning electron microscopy and image analysis. *Scanning Microscopy* **3**: 1051–1057.
- Keaveny, T.M. & Hayes, W.C. (1993) Mechanical Properties of Cortical and Trabecular Bone. Bone Growth, 285–344. Boca Raton, FL: CRC Press.
- Krekmanov, L. (2006) The efficacy of various bone augmentation procedures for dental implants: a Cochrane systematic review of randomized controlled clinical trials. *International Journal of Oral & Maxillofacial Implants* **21**: 696–710.
- Lazáry, A., Balla, B., Kósa, J.P., Bácsi, K., Nagy, Z. & Takács, I. (2007) Effect of gypsum on proliferation and differentiation of MC3T3-E1 mouse osteoblastic cells. *Biomaterials* **28**: 393–399.
- MacMillan, A.K., Lamberti, F.V., Moulton, J.N., Geilich, B.M. & Webster, T.J. (2014) Similar healthy osteoclast and osteoblast activity on nanocrystalline hydroxyapatite and nanoparticles of tri-calcium phosphate compared to natural bone. *International Journal Nanomedicine* **9**: 5627–5637.
- Maté-Sánchez de Val, J.E., Calvo-Guirado, J.L., Delgado-Ruiz, R.A., Gómez-Moreno, G., Ramírez-Fernández, M.P. & Romanos, G.E. (2014a) Bone neo-formation and mineral degradation of 4Bone.® Part I: material characterization and SEM study in critical size defects in rabbits. *Clinical Oral Implants Research* doi: 10.1111/clr.12420.
- Maté-Sánchez de Val, J.E., Mazon, P., Guirado, J.L., Ruiz, R.A., Ramírez Fernández, M.P., Negri, B., (MINECO); contract grant number: MAT2013-48426-C2-2-R.
- Abboud, M. & De Aza, P.N. (2014b) Comparison of three hydroxyapatite/β-tricalcium phosphate/collagen ceramic scaffolds: an *in vivo* study. *Journal Biomedical Materials Research A* **102**: 1037–1046.
- McAllister, B.S. & Haghghat, K. (2007) Bone augmentation techniques. *Journal of Periodontology* **78**: 377–396.
- Ono, D., Jimbo, R., Kawachi, G., Ioku, K., Ikeda, T. & Sawase, T. (2011) Lateral bone augmentation with newly developed β-tricalcium phosphate block: an experimental study in the rabbit mandible. *Clinical Oral Implants Research* **22**: 1366–1371.
- Orsini, G., Traini, T., Scarano, A., Degidi, M., Perrotti, V., Piccirilli, M. & Piattelli, A. (2005) Maxillary sinus augmentation with Bio-Oss particles: a light, scanning, and transmission electron microscopy study in man. *Journal of Biomedical Materials Research. Part B, Applied Biomaterials* **74**: 448–457.
- Ramirez, M.P., Calvo, J.L., Mate, J.E., Delgado, R.A., Negri, B. & Barona, C. (2013) Ultrastructural study by backscattered electron imaging and elemental microanalysis of bone-to-biomaterial interface and mineral degradation of porcine xenografts used in maxillary sinus floor elevation. *Clinical Oral Implants Research* **24**: 523–530.
- Rivera-Munoz, E., Diaz, J.R., Rogelio Rodriguez, J., Brostow, W. & Castano, V.M. (2001) Hydroxyapatite spheres with controlled porosity for eye ball prosthesis: processing and characterization. *Journal Materials Science Materials Medicine* **12**: 305–311.
- Skedros, J.G., Bloebaum, R.D., Bachus, K.N. & Boyce, T.M. (1993a) The meaning of gray levels in backscattered electron images of bone. *Journal of Biomedical Materials Research* **27**: 47–56.
- Skedros, J.G., Bloebaum, R.D., Bachus, K.N., Boyce, T.M. & Constantz, B. (1993b) Influence of mineral content and composition on gray levels in backscattered electron images of bone. *Journal of Biomedical Materials Research* **27**: 57–64.
- Swab, J.J., Tice, J., Wereszczak, A.A., Kraft, R.H. (2015) Fracture Toughness of Advanced Structural Ceramics: Applying ASTM C1421. *Journal of The American Ceramic Society* **98**: 607–615.
- Wierzechos, J., Falcioni, T., Kiciak, A., Wolinski, J., Koczowski, R., Chomiczki, P., Poremska, M. & Ascaso, C. (2008) Advances in the ultrastructural study of the implant-bone interface by backscattered electron imaging. *Micron: the International Research and Review Journal for Microscopy* **39**: 1363–1370.
- Wiltfang, J., Merten, H.A., Schlegel, K.A., Schultze-Mosgau, S., Kloss, F.R., Rupprecht, S. & Kessler, P. (2002) Degradation characteristics of alpha and beta tri-calcium-phosphate (TCP) in minipigs. *Journal Biomedical Materials Research* **63**: 115–121.

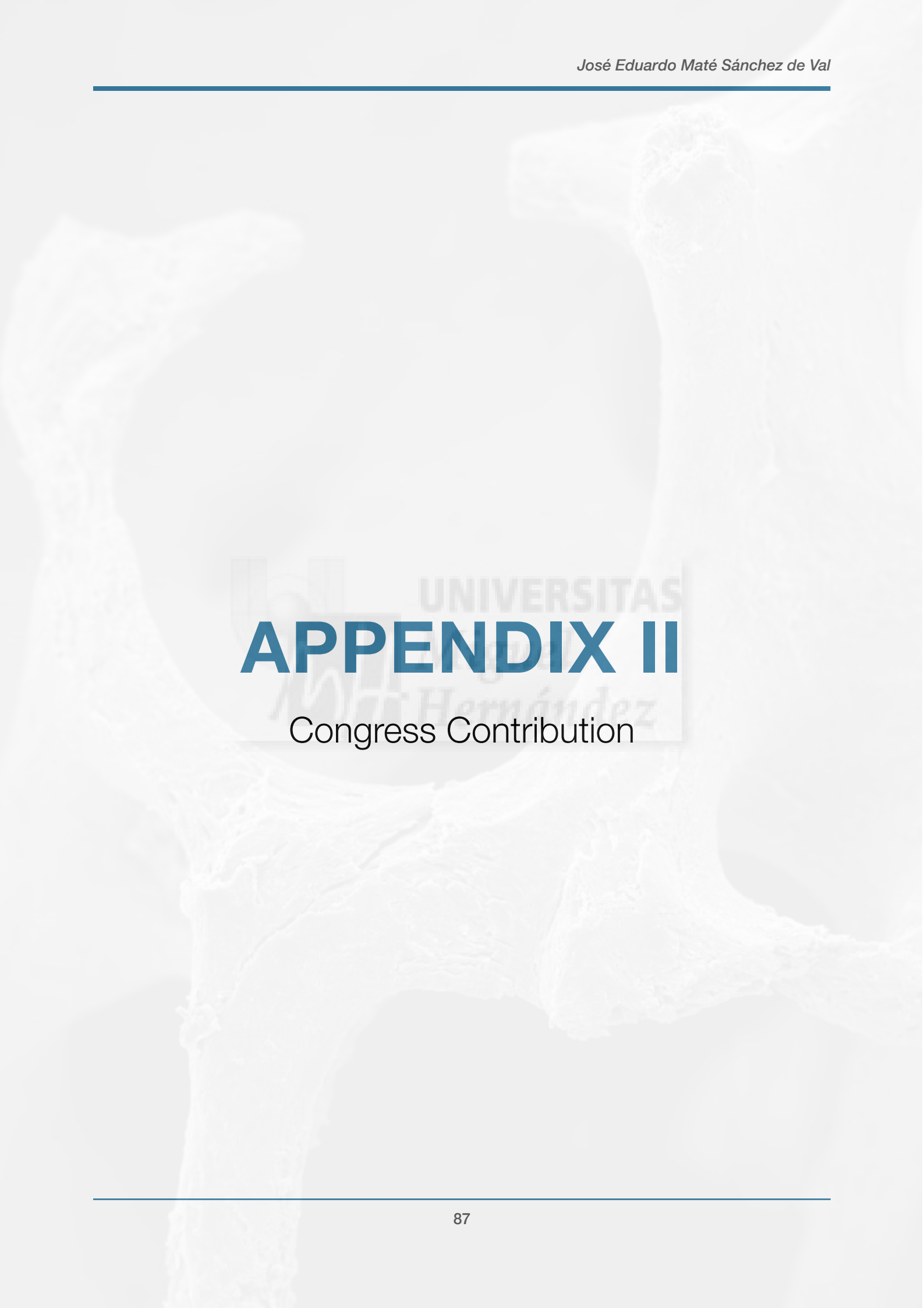
Yamauchi, K., Takahashi, T., Funaki, K., Hamada, Y. & Yamashita, Y. (2010) Histological and histomorphometrical comparative study of β -tricalcium phosphate block grafts and periosteal expansion osteogenesis for alveolar

bone augmentation. *International Journal of Oral Maxillofacial Surgery* **39**: 1000–1006.

Zheng, L., Yang, F., Shen, H., Hu, X., Mochizuki, C., Sato, M., Wang, S. & Zhang, Y. (2011) The effect of composition of calcium phosphate com-

posite scaffolds on the formation of tooth tissue from human dental pulp stem cells. *Biomaterials* **32**: 7053–7059.





UNIVERSITAS
APPENDIX II
Congress Contribution

In vivo behavior of hidroxiapatite/ β -TCP/ collagen scaffold in animal model. Histological, histomorphometrical, radiological and SEM analysis at 15, 30 and 60 days

J. Maté-Sánchez de Val,¹ J. Calvo Guirado,² P. De Aza,³ P. Mazon,⁴ A. Markovic,⁵ A. Aguilar-Salvatierra⁶

¹UCAM Universidad Católica San Antonio de Murcia, Alicante, Spain, ²Murcia University, Murcia, Spain, ³Bioengineering Institute. Miguel Hernandez University. Avda. Universidad s/n, 03202 Elche., Elche, Spain, ⁴Miguel Hernandez University, Elche, Spain, ⁵Belgrade University, Belgrade, Serbia, ⁶Granada University, Granada, Spain

Background: The use of biomaterials for bone regeneration is widely applied in the fields of bone reconstructive surgery, both in situations of bone atrophy, as in those where there are defects. (Daculsi et al. 2003; McAllister et al. 2007; Browaeys et al. 2007; Aghaloo et al. 2007). Within the group of synthetic biomaterials, formulations most commonly used are those composed of hydroxyapatite, tricalcium phosphate and combinations of both. The incorporation of collagen during a biphasic ceramic synthesis is a suitable option to provide the organic part of the biomaterial, solving one of the main disadvantages of the completely inorganic ceramic. This addition of collagen improve the ability of cell attachment to the biomaterial and the beginning of the process of bone remodeling.

Aim/Hypothesis: The aim of this study was to fabricate and characterize HA/ β -TCP/ collagen ceramic scaffolds of different composition ratios and compare their physical and *in vivo* mechanical behavior.

Material and methods: Three groups of twenty samples each one of calcium-phosphate ceramic scaffold cylindrical implants (6 ± 0.01 mm in diameter and 2 ± 0.01 mm in length) were studied with varying wt% HA/ wt% TCP/ wt% Collagen composition: Group A: 40/30/30; Group B: 50/20/30; Group C: 60/20/20. A fourth group, Group D (unfilled critical size defect), acted as control. Three times of work were established 15, 30 and 60 days. Characterization, histological, histomorphometric, SEM and Radiological analysis were performed.

Results: Micrographs obtained on the different composites are comparable, it is possible observe that the materials revealed a microporous morphology formed by aggregated nanoparticles independently of the composition of the composite. BIC values for the three materials, with Group A showing best BIC at 15, 30 and 60 days (with closer contact observed) than Group B, followed by Group C. (Table 4). SEM images showed complete integration of all specimens, without significant differences between the groups. The radiographic density varied with the chemical content of the samples, with Group A showing correct integration and partial resorption that corresponded to the histological findings; Group B behaved similarly and was seen to be fully integrated with the surrounding bone; Group C showed a greater presence of residual biomaterial and correct integration.

Conclusions and clinical implications: The influence of time on the biological behavior of biomaterials studied has been demonstrated by varying the percentage of bone-implant contact and bone formation to obtain the best results at 60 days.

Parameters	Group A			Group B			Group C			Control		
	15	30	60	15	30	60	15	30	60	15	30	60
BIC (%)	41.1 ± 0.24	55.4 ± 0.38	67.2 ± 0.34	30.4 ± 0.22	47.4 ± 0.21	54.0 ± 0.22	24.3 ± 0.42	34.4 ± 0.33	46.1 ± 0.33	5.0 ± 0.00	5.0 ± 0.00	5.0 ± 0.00
Bone loss (mm)	0.11 ± 0.01	0.12 ± 0.01	0.13 ± 0.01	0.11 ± 0.01	0.12 ± 0.01	0.13 ± 0.01	0.11 ± 0.01	0.12 ± 0.01	0.13 ± 0.01	0.11 ± 0.01	0.12 ± 0.01	0.13 ± 0.01
Defect Closure	15.4 ± 1.43	27.4 ± 0.42	47.3 ± 0.42	15.2 ± 1.42	24.2 ± 0.21	33.2 ± 0.21	15.4 ± 1.42	22.4 ± 0.21	32.4 ± 0.21	15.2 ± 1.42	22.4 ± 0.21	32.4 ± 0.21
Resorption (mm)	1.14 ± 0.04	1.14 ± 0.04	1.14 ± 0.04	1.14 ± 0.04	1.14 ± 0.04	1.14 ± 0.04	1.14 ± 0.04	1.14 ± 0.04	1.14 ± 0.04	1.14 ± 0.04	1.14 ± 0.04	1.14 ± 0.04